Fall 2013

Preparation and characterization of oxidized cellulose beads by extrusion/spheronization for chemoembolization

Jinzhou Zhang
University of Iowa

PREPARATION AND CHARACTERIZATION OF OXIDIZED CELLULOSE BEADS BY EXTRUSION/SPHERONIZATION FOR CHEMOEMBOLIZATION

by

Jinzhou Zhang

A thesis submitted in partial fulfillment
of the requirements for the Doctor of
Philosophy degree in Pharmacy (Pharmaceutics)
in the Graduate College of
The University of Iowa

December 2013

Thesis Supervisor: Professor Dale Eric Wurster

Graduate College
The University of Iowa
Iowa City, Iowa

CERTIFICATE OF APPROVAL

_____

PH.D. THESIS

_____

This is to certify that the Ph.D. thesis of

Jinzhou Zhang

has been approved by the Examining Committee for the thesis requirement for the Doctor of Philosophy degree in Pharmacy (Pharmaceutics) at the December 2013 graduation

Thesis Committee: _____
Dale Eric Wurster , Thesis Supervisor

_____
Maureen D. Donovan

_____
Douglas R. Flanagan

_____
Jennifer Fiegel

_____
Aliasger K. Salem

To my family

ACKNOWLEDGEMENTS

I would like to express my sincere appreciation to the following people because they were essential to me, fulfilling my academic and professional goals during my doctorate studies: First my first adviser, Dr. Vijay Kumar, I express to him my deepest gratitude for his teaching, philosophy and wise counseling. His guidance, support and availability were crucial in my studies, especially in times of discouragement and frustration. His enthusiasm, passion and encouragement will definitely influence my career. His valuable advices, from professional to personal levels, will never be forgotten. I am very grateful to have had the opportunity to learn under his guidance. I would like to thank Dr. Wurster, Dr. Donovan and Dr. Flanagan for taking over my thesis providing the final changes, comments and scientific critique to promote this document. I am very pleased and honored by their presence and the quality time they spent in evaluating the results here by presented.

I also want to thank the committee members of my thesis: Dr. Fiegel and Dr. Salem. I appreciate their time and commitment provided to this thesis.

I also express my gratitude to Dr. Raghavan for his kind help and support whenever it was needed during my graduate study.

I also thank not only all the members of my research group, but my friends in the College of Pharmacy, especially Yinjian, Ross, Nan, Hong-guan, Peng, Jhon and Dan for their friendship, discussions, cooperation, support and for making all those graduate years more alive and fun.

TABLE OF CONTENTS

LIST OF TABLES

LIST OF FIGURES

LIST OF ABBREVIATIONS

TACE	transarterial chemoembolization
HCC	hepatocellular carcinoma
MBA	N,N9-methylene-bis-acrylamide
AMPS	acrylic monomer 2-acrylamido-2-methylpropane sulfonate
dox	doxorubicin hydrochloride
QSMs	Quadrasphere microspheres
DMF	dimethylformamide
HMD	hexamethylene diisocyanate
E-L-S	expanding-loading-shrinking
HPMC	hydropropylmethylcellulose
DEB	drug eluting beads
MCC	microcrystalline cellulose
OC	oxidized cellulose
DAC	dialdehyde cellulose
ORC	oxidized regenerated cellulose
DP	degree of polymerization
HPLC	high performance liquid chromatography
PAD	pulsed amperometric detection
CPT	camptothecin
MTX	Methotrexate
PLGA	poly-lactide co-glycolide
MRT	mean resident time
DPPC	1,2-dipalmitoyl-sn-glycero-3-phosphocholine
SLNs	solid lipid nanoparticles
EAC	Ehrlich ascites carcinoma
DSC	differential scanning calorimeter
DC	degree of Crystallinity
PXRD	powder X-ray diffraction
FT-IR	Fourier-Transform Infrared
PVA	poly(vinyl alcohol)

CHAPTER I

INTRODUCTION

Transcatheter arterial chemoembolization (TACE)

The technology of transarterial chemoembolization (TACE) was introduced by Yamada et al. in the late 1970s. Dr. Yamada first embolized a hepatic artery which supplied nutrition to a hepatocellular carcinoma (HCC) to deliver antitumor therapy without damaging the surrounding liver parenchyma (*1, 2*). TACE is an interventional radiology procedure, and although there is no worldwide standard for the technique, chemotherapeutics may be emulsified with Lipiodol®, which is a radiopaque contrast agent composed of iodinated ethyl esters of fatty acids from poppyseed oil (37 wt% iodine). The TACE infusion is normally performed by accessing tumor feeding arteries with a catheter under radiographic imaging guidance (Fig I-1). (*3-5*) When a vessel supplying blood to a tumor has been identified, appropriate doses of a chemotherapeutic agent incorporated within an embolic material is injected through the catheter. The total chemotherapeutic dose may be given through one vessel or divided among several vessels supplying the tumor (*6*). There are two benefits of this approach: first, arterial embolization interrupts the blood supply and postpones tumor growth; and second, focused administration of chemotherapy allows a higher drug dose administrated directly to the tissue while simultaneously reducing systemic exposure. The chemotherapeutic agent is not cleaned rapidly from the tumor bed after drug associated of embolization.

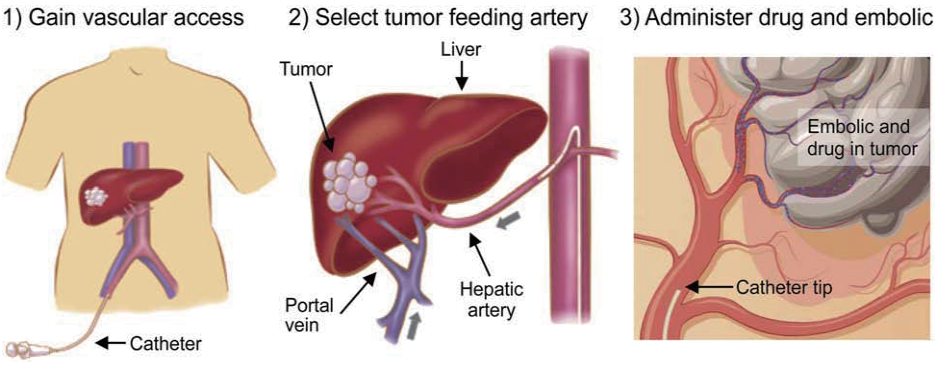

Figure I-1. Schematic describing transarterial chemoembolization(TACE) for liver tumor. Access is gained in the femoral artery (left) and a hepatic artery is selected by use of a guidewire and a catheter (middle). A microcatheter is then often positioned in a tumor feeding artery (right). From this location, TACE is performed by infusing a mixture of chemotherapeutics and embolic agents (right).(*5*)

Compared to systemic chemotherapy, the therapeutic effect of TACE is focused directly in the liver and reduces the systemic side effects of the chemotherapy agents (*3*).

Several drug-delivery systems for TACE have been recently tested. These include biodegradable and non-biodegradable materials.

Biodegradable & non-biodegradable drug-delivery systems for TACE

Tris-acryl cross-linked with gelatin is an entirely synthetic, hydrophilic, and non-biodegradable material, and its beads, ranging in size from 40-1200 μm, are currently commercially available ("Embogold®" and "Embosphere®" microspheres, Biosphere Medical Incorporated, Rockland, MA). These beads have been tested for compatibility with several chemotherapeutic agents (*7*). The tris-acryl gelatin microspheres were obtained by the following technique (*8*). A solution of N-acryloyl-2-amino-2-hydroxymethylpropane-1,3 diol (hydrophilic trisacryl monomer) and of N,N'-methylene-bis-acrylamide (MBA) was heated to 57 °C with pH adjusted to 6.5, following by adding a peroxide (ammonium persulfate) and a polymerization initiator (N,N,N',N'-tetramethylenediamine). Subsequently, gelatin was added to the solution of trisacryl monomer. The solution was then emulsified in paraffin oil and incubated at 25 °C for 18 hours with addition of glutaraldehyde. Neutralization was obtained by continuously incubating the solution at 25 °C in the presence of sodium borohydride. Two sizes of Embosphere microspheres, 100–300 μm and 700–900 μm, were tested in this study (*7*). The cytotoxic drugs used for the tests were carboplatin, mitomycin C, 5-fluorouracil and pirarubicin. The addition of a two-milliliter samples containing Embosphere® microspheres were mixed with 5 mL of carboplatin, mitomycin C, 5-fluorouracil, or

pirarubicin at 37 °C for 24 h and then washed with 0.9% saline solution at least five times. The concentration of carboplatin was 7.15 mg/mL, the concentration of mitomycin C was 0.71 mg/mL, the concentration of 5-fluorouracil was 35.72 mg/mL, and the concentration of pirarubicin was 1.43 mg/mL. Twenty-five mg of carboplatin, 2.5 mg of mitomycin C, 125 mg of 5-fluorouracil, or 5 mg of pirarubicin were loaded per milliliter of beads. The respective distributions of large and small diameters, surface area, sphericity index, or surface regularity index of the microspheres were not significantly different between the experimental samples containing carboplatin, mitomycin C, 5-fluorouracil, or pirarubicin and the control sample of microspheres with similar diameters. Embosphere® microspheres can be mixed with carboplatin, mitomycin C, 5-fluorouracil, or pirarubicin for chemoembolization therapy without any risk of damaging their morphology, dimensions or geometric characteristics.

LC® Beads (outside United States marketed as DC® Beads; Biocompatibles International, Farnham, Surrey, UK; distributed by AngioDynamics, Queensbury, NY) are non-biodegradable poly(vinyl alcohol) (PVA) hydrogel beads prepared by modifying PVA with a sulfonic acid-functional group. They are available in 100-300, 300-500, 500-700, 700-900 μm size ranges (*9-12*). The PVA is chemically modified to react with acrylic monomers by free radical polymerization. An inverse suspension polymerization was used to prepare microspheres of the PVA–acrylic hydrogel by additional of acrylic monomer 2-acrylamido-2-methylpropane sulfonate (AMPS). Anionic functional groups are pendent to the polymer chains (Fig I-2). The presence of negative charges in the sulphonate groups of DC® Bead enables the beads to interact with positively charged drugs, such as doxorubicin (dox) and irinotecan. Dox or irinotecan molecules bind

ionically to the sulphonate groups where the positively-charged drug binds to the negatively-charged polymer-bound sulfonate groups within the poly(vinyl alcohol)-based hydrogel (Fig I-3) (*13*). Dox or irinotecan were sequestered from solution in a time dependent on the concentration of drug solution and size of the beads. The DC beads could load a maximum of ~ 40 mg dox/ml of hydrated beads with 99% drug loading efficiency (*10*) and ~ 50-60 mg irinotecan/ml of hydrated beads with 99% drug loading efficiency (*12*). The release kinetics and the prediction of the vivo behavior of DC beads have been assessed using an in vitro T-apparatus, where the drug releases by both convection and diffusion in a flow through system (Fig I-4). This method was developed to simulate the in vivo conditions of embolization procedures. Slow release of dox from DC beads with half-lives over 1,500 h were predicted for all size ranges and only 50% and 65% of irinotecan was released from the 700-900 μm and 100-300μm size beads, respectively. A linear relationship was found between the release data from the T-apparatus and from pharmacokinetic data obtained from in vivo studies.

Doxorubicin hydrochloride loading in Quadrasphere® microspheres (QSMs) (BioSphere Medical Inc., South Jordan, Utah) was also reported recently (*14*). QSMs are non-biodegrable poly(vinyl alcohol-sodium acrylate) copolymer microspheres. The size of QSMs ranges from 50 μm to 200 μm. QSMs can expand to 4 times their dry-state diameter and 64 times their volume within 10 min when in contact with blood. The negatively charged acrylate groups of QSMs interact with the positively charged doxorubicin. Approximately 5 mg of doxorubicin can be loaded into one milliliter of QSMs. In vitro testing of QSM doxorubicin loading and release over time showed 82–94%

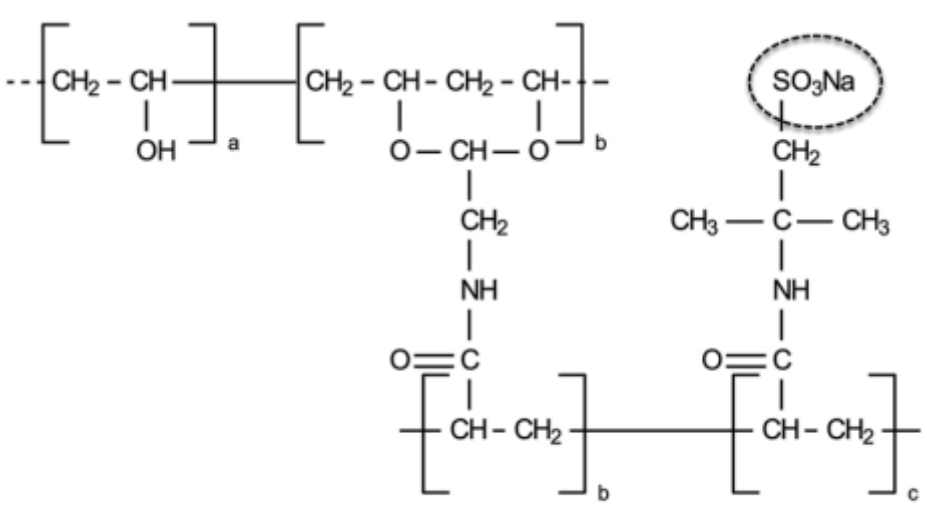

Figure I-2. Chemical structure of the sulfonate-modified polyvinyl alcohol hydrogel polymer used in the fabrication of DC® Beads.

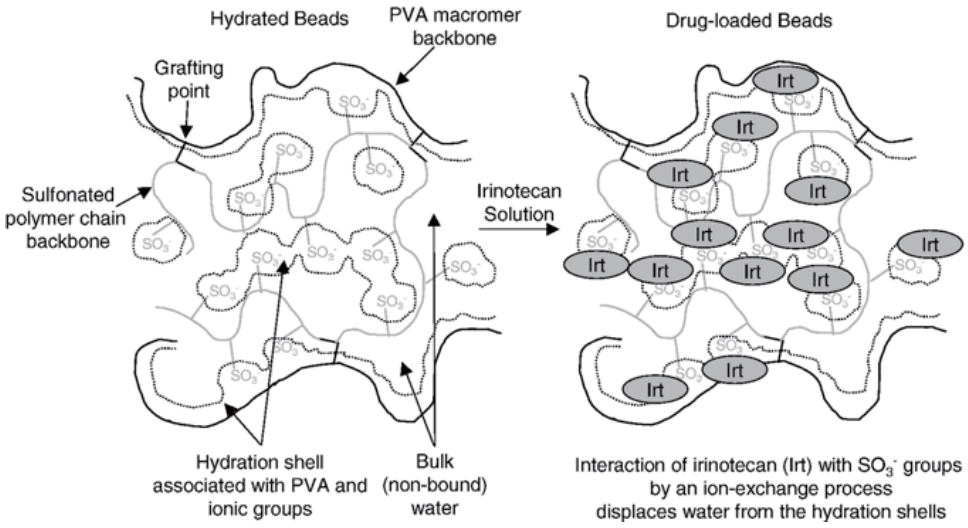

Figure I-3: Schematic depiction of irinotecan (Irt) loading with sulfonated hydrogel beads.(*12*)

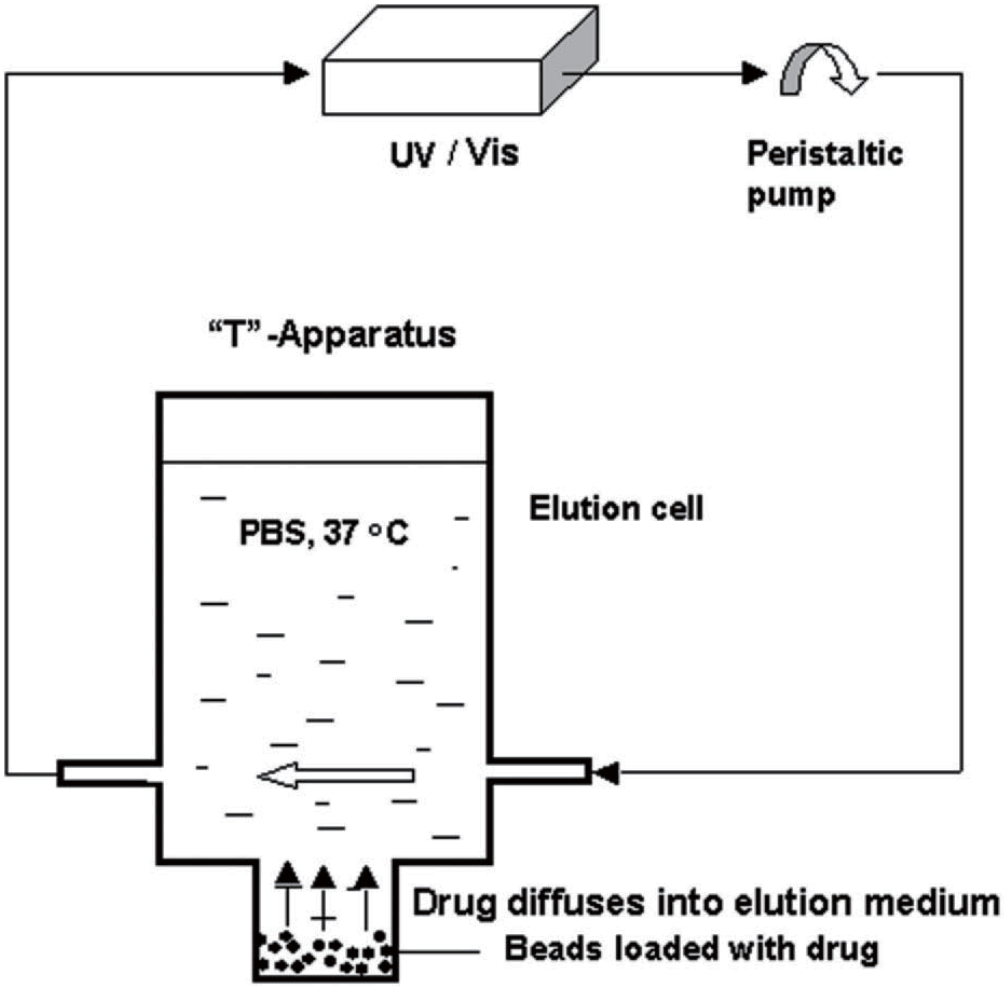

Figure I-4: Schematic representation of a T-apparatus.(*12*)

doxorubicin loading within 2 h with about 6% of doxorubicin release within the first 6 h after loading, and then a slow release pattern.

Biodegradable polymers such as chitosan (*15*) and alginate (*16*) have also been used to prepare microspheres for TACE. Doxorubicin–containing chitosan beads for TACE of hepatocellular carcinoma were reported by Kim. (*15*) These cross-linked chitosan beads were prepared by dissolving chitosan in 4% acetic acid and was dropping the solution into an alkaline coagulant to obtain chitosan beads by using a custom-made microsphere producer. The chitosan beads were soaked in distilled water, then in ethanol, and then 100 ml dimethylformamide (DMF). A 0.1 molar ratio of hexamethylene diisocyanate (HMD) to the amino groups of chitosan was added in the chitosan beads-DMF mixtures at room temperature for 4 h to cross-link the chitosan molecular network (Fig I-5). The product was washed by ethanol to remove the unreacted HMD and DMF and then by distilled water. The cross-linked chitosan microspheres were then freeze-dried. Doxorubicin-containing chitosan beads were prepared by employing an expanding-loading-shrinking (E-L-S) process (Fig I-6). The chitosan beads were placed in ethanol under reduced pressure to fully expand at room temperature (the expanding process). Then doxorubicin hydrochloride was added into the chitosan following by solvent evaporating under reduced pressure for 5 hours at room temperature (the loading process). The beads were freeze-dried (the shrinking process). As a result of this E-L-S process, 10% (w/w) doxorubicin-containing chitosan beads were prepared with a bead size between 45 μm and 100 μm. The percentage of doxorubicin released over a period of 7 days was 22.6% based on an in vitro release study.

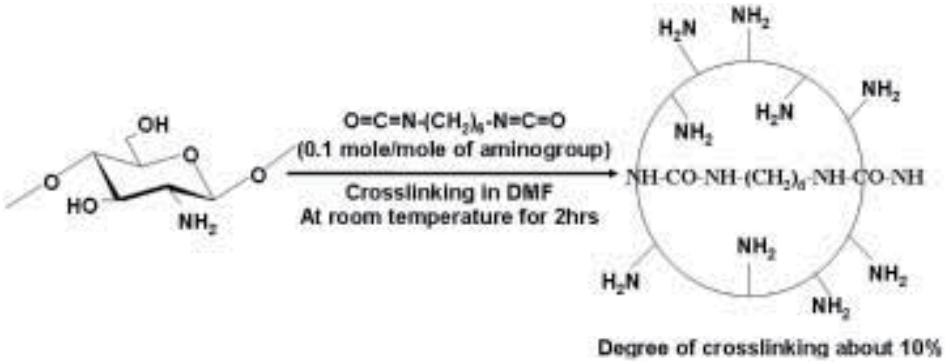

Figure I-5. Schematic of cross-linking of chitosan microspheres by hexamethylene diisocyanate (HMD). (*15*)

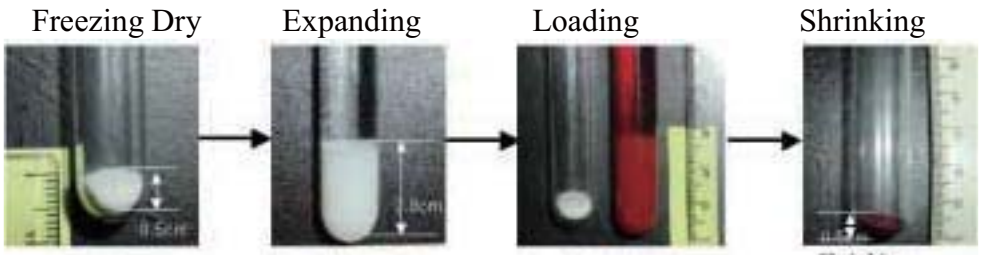

Figure I-6. Expanding-loading-shrinking method for doxorubicin hydrochloride trapping in chitosan microspheres. (*15*)

In another study, mitomycin-C loaded chitosan-coated alginate beads were prepared for use in chemoembolization studies (*16*). In a typical procedure, a 4.0% solution of sodium alginate containing 5.0% hydropropylmethylcellulose (HPMC) was used as the water phase. Mitomycin-C was dissolved in the water phase. An oil phase was composed of petroleum ether, mineral oil and Tween 80. The water phase was sprayed into the oil phase using an extrusion device with a small orifice. $CaCl_2$ solution was used as a cross-linker for the alginate microspheres. Chitosan-coating onto the alginate microspheres was achieved by polyionic complex formation between alginate and chitosan. The chitosan-coated alginate beads obtained were spherical in shape and varied in size from 100 to 400 μm. The swelling ratio varied from 50% to 280%, depending on the chitosan molecular weight and concentration. The equilibrium swelling was achieved in ~30 min, and the maximum drug loading ratio was ~65% was achieved for has high molecular weight chitosan, and chitosan solution has the highest concentration and shortest coating time with chitosan. Over the first 12 hours, 60-80% of the drug was released and then the release rate was decreased. Totally, almost 90% of drug was released in 10 days.

One problem with current drug eluting bead (DEB) technology is a limit to the amount of drug in the beads since the maximum of drug loading for current DEB is 10%. Based on the loading techniques used, drugs are restricted to water soluble small molecules. The other problem is the methods used to prepare the primary beads are too complex. Other methods of bead/pellet preparation are needed to overcome these problems. There is also a question frequently raised by physicians about what options there are once all of drug has eluded if treatment is not complete or if the tumor recurs?

Numerous clinical studies have demonstrated multiple repeat DEB-TACE procedures per patient. (*4*) Physicians would like to be able to access a tumor on multiple occasions in order to administer additional DEB-TACE treatments as needed; the non-biodegradable beads may not be able to re-enter the feeding artery once the artery had been occluded. There is an opinion that DEB evolution will eventually move in this biodegradable direction as an essential feature (*5*).

Pellet preparation method

Pellets are spherical or nearly spherical granules that can be produced by several methods. Pellets usually range in size varying from 500 to 1500 μm. The most frequently used pelletization processes include extrusion/spheronization, solution/suspension layering, powder layering, and direct pelletization. Each method is introduced below.

Solution/suspension layering

Solution/suspension layering involves the application of solutions and/or suspensions of drug substances and binders on solid cores. Solid cores can be inert materials or crystals/granules of the same drug. (17) Conventional coating pans (18, 19), fluid bed centrifugal granulators, Wurster coaters or rotor tangential spray (20) have been used successfully to manufacture pellets. Evaporative efficiency has been a significant problem with conventional coating pans. The fluidized bed is more suited for producing pellets by layering. Bottom spray and rotary tangential spray are better methods than top spray to conduct layer. Solution/suspension layering is usually used when the desired

drug loading of the pellets is low because production of high drug loading pellets from a low solids content formulation is not economically feasible.

Powder layering

Powder layering comprises the deposition of successive layers of dry powder which can be drug, excipient, or both on a solid core with the help of a binding liquid. The requirement for a powder-layering process includes the need for a reactor with solid walls with no holes to avoid powder loss beneath the product chamber (*17*). Drum/pan coaters and rotor tangential spray fluid-bed granulators have been used used to produce pellets (*21*). Pan coaters have been used for a long time to manufacture pellets by the powder layering method. However, pan coaters have some significant limitations, such as poor mixing and inefficient drying. To overcome the limitations of a pan coater, a rotor tangential spray fluid-bed granulator was used (*21*). Centrifugal force, fluidization air velocity, and gravitational force generate a rope-like motion of the particles in the product bed during the layering process. The radial velocity of the disk, spray method, and powder and binder liquid delivery rates are critical parameters that must be carefully evaluated. Serious problems can arise during powder layering, however, such as caking, generating large amount of fines and content uniformity problems.

Direct pelletization

Direct pelletization processes are mainly performed in high shear mixers and rotor tangential spray fluid-bed equipment (*22*). Unlike solution/suspension layering and powder layering methods, seeds are not necessary. The pelletization is accomplished by

the addition of a binding liquid and allowing a suitable movement of the wetted powders.(*23, 24*) According to the nature of the liquid binder, direct pelletization can be described as wet or melt pelletization. In the wet pelletization process, the binder is liquid at room temperature, but in the melt pelletization process, a high temperature is needed to melt the binder. The solidification of pellets is achieved by evaporation of the binding liquid for wet pelletization or cooling the binding liquid for melt pelletization. Rotor speed is the key factor for the direct pelletization (*25*). A low rotor speed is used during mixing and early wet-massing stage; the high rotor speed is used at the liquid addition stage to obtain a uniform liquid distribution, and low rotor speed is used again during wet-massing stage. The low-high-low rotor speed variation during the pelletization processing may be used to produce spheroids with a narrow size distribution and with minimal oversized particles.

Extrusion/spheronization

Extrusion-spheronization is a multistep process. The first step involves mixing the drug and excipients. The second step involves wet massing of the uniformly mixed powders to produce a wet mass that can be easily extruded. The extrusion process involves pressing the moistened mass through a screen. The extrudate thus obtained is then transferred into a spheronizer, where it is first broken into short cylindrical rods and then converted into spherical particles. Drying and sieving are then performed to obtain the desired sizes of spherical particles.

Extrusion/spheronization processing

Production of pellets via extrusion/spheronisation was not widely recognized until about the process were published by Conine and Hadley (*26*) and Reynolds(*27*). The pellets or beads produced by the extrusion spheronization possess the following advantages over other pelletization methods (*28-33*): 1) Ability to produces spheroids with high loading capacity of active ingredient without producing very large particles; 2) High process yields with narrow size distributions, good sphericity, low material waste and low friability; 3) Different drugs can be blended and formulated in a single unit dosage form. As mentioned previously, extrusion/spheronisation is a multi-step process (Fig.I-7) (*33*). Each production step is a distinct process and each has a number of process parameters. The end product from each of the steps is shown in Figure I-8.

Dry mixing and wet granulation

A dry powder mix of an active pharmaceutical ingredient(s) (API) and excipient(s) is prepared to obtain a uniform blend in the first step of the extrusion-spheronization process. The uniformity of the dry mix is very important, since it can affect the quality of the granulation and, in turn, the spherical nature of the particles produced. An uneven distribution of materials or wide differences in properties can result in localized overwetting during the granulation step. Overwet regions can have adverse effects during the extrusion and spheronization steps, including a broadening of the size distribution(*34*). Dry mixing and granulation are usually performed in the same equipment. Batch-type mixer/granulators include planetary mixers (*35*), vertical or horizontal high shear mixers

(*36-38*), and sigma blade mixers(*39*). Continuous mixer/granulators include the Nica M6 instant mixer (*40*) and high-shear, twin-screw mixer/extruders(*41-46*). The wet granulation step is similar to conventional granulation techniques used to produce products for compression, but it requires much higher amounts of liquid than those required for conventional granulation(*47*). The amount of granulation liquid is critical to successfully achieve pellets by using extrusion and spheronization(*44*). The amount of mixing time required to achieve sufficient granulating fluid uniformity is also important. In addition, the temperature generated during wet granulation can result in a more water evaporation or in an increase in the solubility of some of the solids(*38*). A reduction in fluid will reduce the plasticity of the granulation and in turn, significantly influence pellet properties(*48*).

Extrusion

The third step of extrusion/spheronization is the extrusion step, which comprises forcing the wet mass through a small orifice to form small cylindrical particles of uniform diameter(*49*). The extrudate particles will break into similar lengths under their own weight. The extrudate must have enough plasticity to deform but not so much as to adhere to other particles when collected or rolled in the spheronizer. Extruders come in many types, but they can generally be divided into different classes based on several criteria. Rowe divided them into screw-, gravity- and piston-type extruders (Figure I-9) based on their feeding mechanism(*50*). Hicks and Freese classified them into four types: screw; sieve and basket; roll; and ram extruders(*49*), and Wilson and Rough divided them into extruders with pumping (ram, axial screw) and wiping action (sieve and basket, roll,

radial screen)(*51*). Screw extruders consist of either one (single) or two (twin) augers that push the wet mass from the material feed zone to the extrusion zone. During the transport process, the screws compress the wet mass, removing most of the entrapped air. The major advantages of screw feed extruders are a higher throughput rate, ease of changing different screen types and ease of cleaning(*30*). The wet mass is fed by gravity into the nip area and forced through the dies in gravity feed extruders. Gravity-fed extruder types include cylinder, gear, and radial designs. The major difference between the gravity fed and the screw-fed radial extruders is no compression prior to extrusion. In piston feed extruders or ram extruders, a piston displaces and forces the material through a die at the end. Piston feed extruders or ram extruders are designed to allow for measurement of the rheological properties of formulations, which asserts in for formulation development (*52, 53*). The production of small size pellets using wet extrusion/ spheronization is challenging and scarcely reported in the literature. Previous studies with extrusion showed difficulties because the pressure on the screen increases when orifice size decreased(*54*).

Spheronization

The fourth step in the extrusion/spheronization process is the spheronization step. A spheronizer consists of a bowl having a stationary cylindrical wall and a rapidly rotating bottom plate or disk with a grooved surface. The transformation from cylinder-shaped extrudate to a sphere occurs in various stages during the spheronization step. Extrudates are broken into small cylinders at the beginning, which are then drawn to the walls of the extruder due to centrifugal forces, followed by collision, movement up the

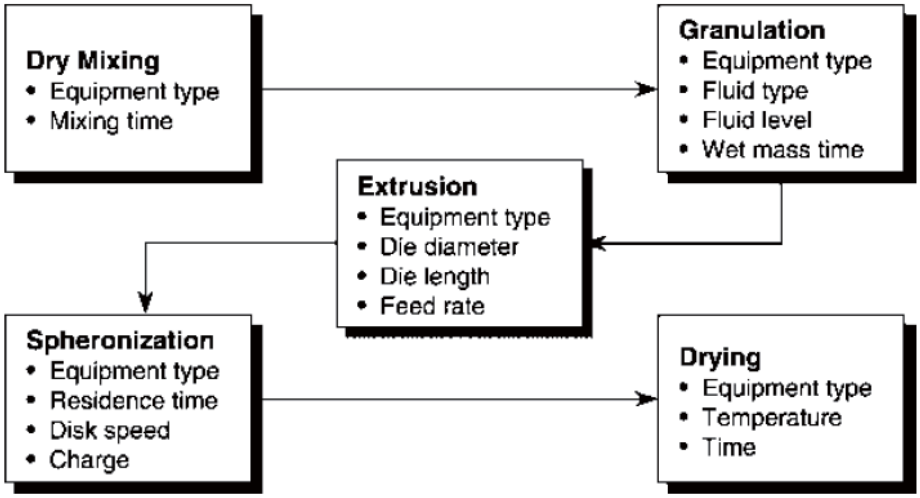

Figure I-7: Process flow chart of the extrusion/spheronization process showing the process variables for each individual step(*33*).

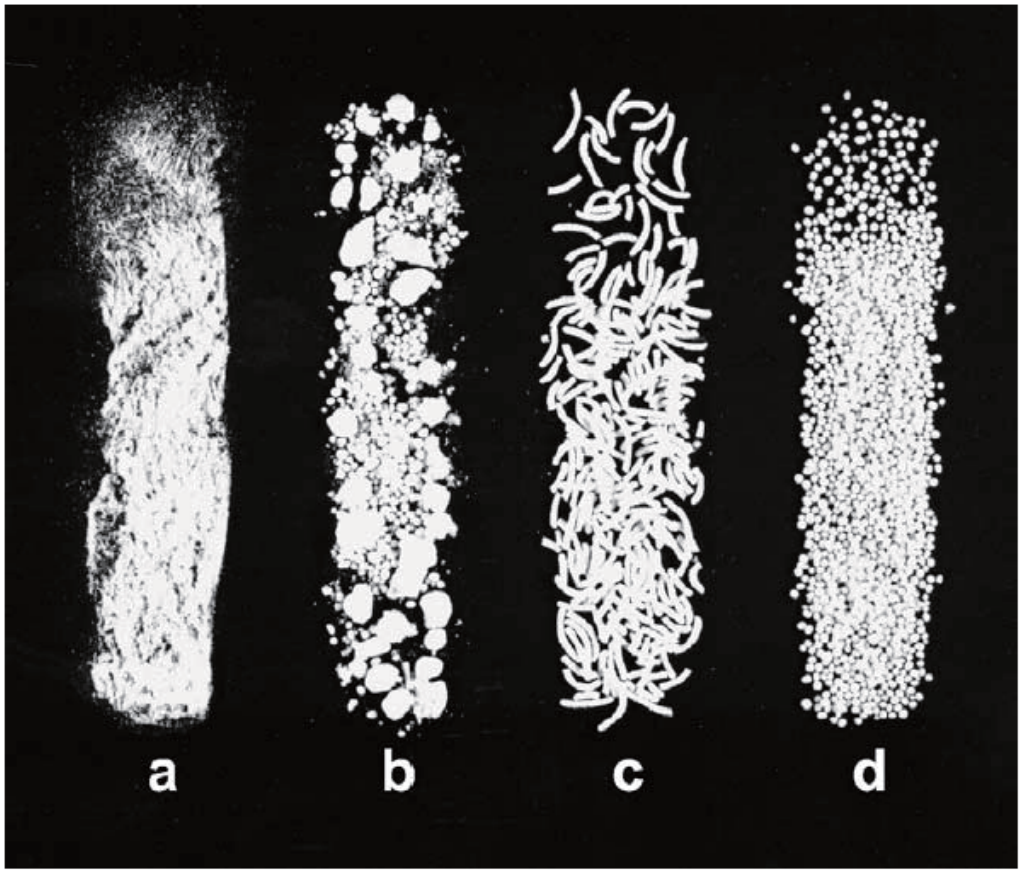

Figure I-8: Product produced by the first four extrusion process steps: (a) powder from dry mixing, (b) granules from granulation, (c) extrudate from extrusion, and (d) spheres from spheronization(*33*).

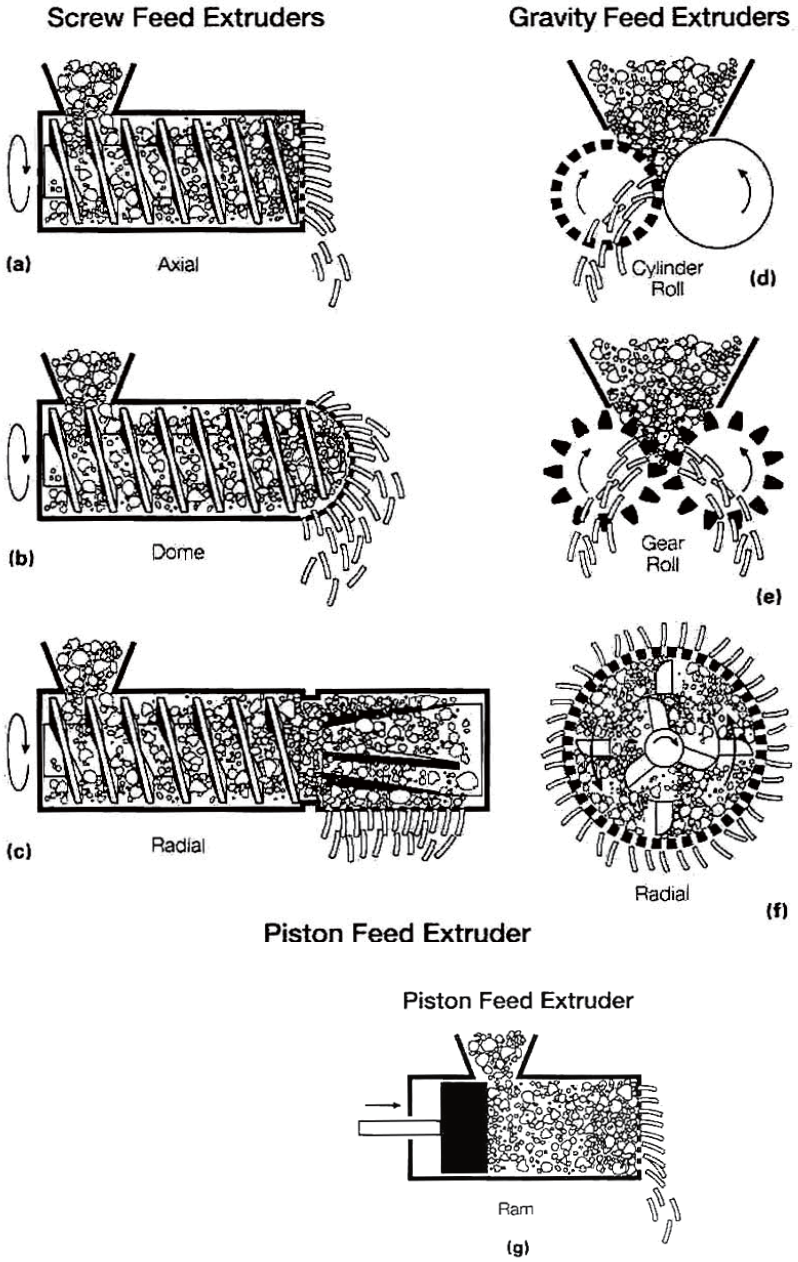

Figure I-9: Schematic diagram of extruder types used in extrusion/spheronization: screw feed (a. axial-, b. dome- and c. radial-type), gravity feed (d. cylinder-, e. gear- and f. radial-type) and piston feed (g. ram) extruders(*50*).

wall and falling back onto the rotating bed. This results in a typical “rope-like” formation (Fig. I-10).(*27*) The mechanism of spheronization is complex, and two models have been proposed to describe the mechanism (Fig. I-11). Rowe describes a model where the extrudates are first broken into small cylinders and then are rounded off into cylindrical particles with rounded edges, followed by forming dumbbell-shaped particles and ellipsoids, and finally spheres are obtained(*50*). Alternately, Baert et al. proposed cylindrical particles with round edges form into bent rope-shaped particles, and then form a dumbbell with a twisted middle(*55*). The twisted dumbbells are broken into two spherical particles with a flat side having a hollow cavity which is further round into spheres. Besides the requirements of the extrudates, the spheronization process is mainly dependent on three factors: spheronization speed, residence time and loading. Major factors influencing the shape of the pellets are disk speed and residence time. A faster disk speed and a longer residence time increase the coarse fraction and the mean diameter to result in a smaller fine fraction, but also increase the moisture loss during the process. The moisture loss can reduce the plasticity of the particle so that the particles may not round off into pellets and instead to stay as deformed cylinders or dumbbells. There are no significant changes in the shape of extrudates using low disk speeds(*40, 56-58*).

Drying

Drying is the final step in the process. This can be accomplished by different drying methods, with oven and fluid-bed drying being the most commonly used. The main differences between oven and fluid-bed drying are the rate of fluid removal and the way the material is handled during drying. Oven drying is a slow drying process in a

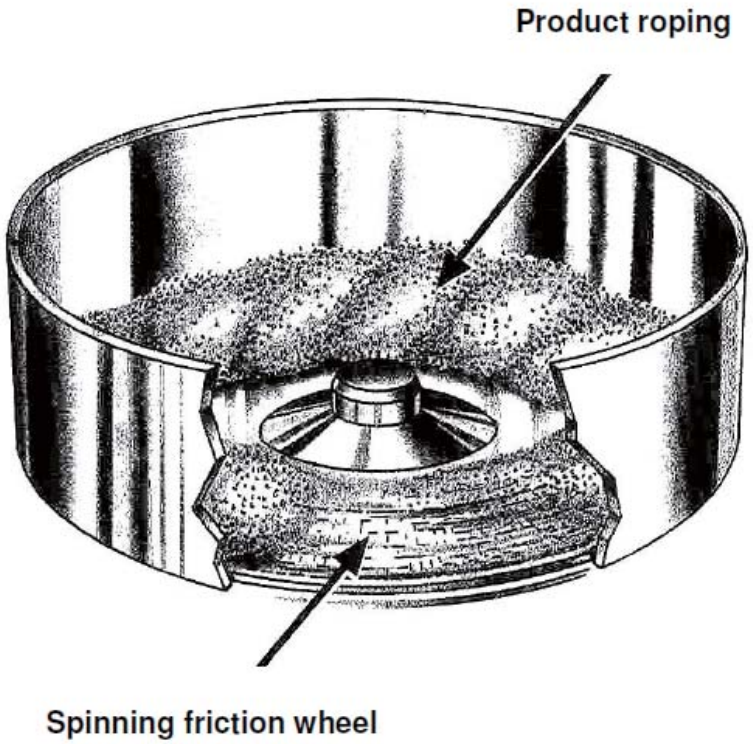

Figure I-10: A representation of the characteristic rope-like formation in a spheronizer bowl during operation(*27*).

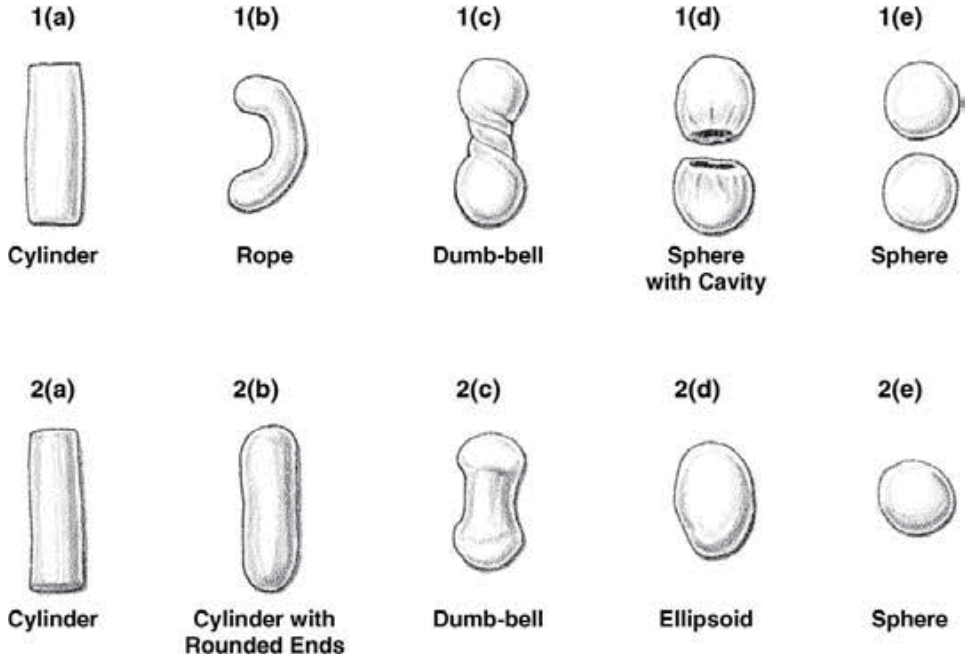

Figure I-11: A graphic representation of the two models proposed to describe the mechanism of spheronization. The model proposed by Rowe describes a transition from cylindrical particles (2a) into cylindrical particles with rounded edges (2b), dumbbells (2c), ellipsoids (2d), and spheres (2e). The model proposed by Baert et al. describes a transition from initial cylindrical particles (1a) into a bent rope (1b), dumbbell (1c), two spherical particles with a hollow cavity (1d), and spheres (1e)(*50, 55*).

static bed, while fluidized bed drying is a much more rapid drying process because of the turbulent motion of the dried material in a heated air stream(*59-62*).

Extrusion–spheronization excipients

It should be noted that not every moistened powder mixture can be successfully extruded and spheronized. For effective extrusion, the requirements include i) a homogeneous cohesive plastic mass must be produced during extrusion; ii) the wetted mass should have inherent fluidity and self-lubricating properties, permitting flow during extrusion; and iii) the extruded mass should not be too adhesive or cohesive.
The requirements for spheronization of the cylindrical extrudate are: i) the extrudate should be brittle enough to be broken down to short lengths in the spheronizer, ii) the extrudate should be sufficiently plastic so that the cylindrical rods can be rolled into spheres in the spheronizer, and iii) the extrudates should not adhere to each other to avoid aggregation during spheronization(*47*). Due to these requirements, a limited number of excipients are suitable to act as pelletization aids in the extrusion/ spheronization process. Microcrystalline cellulose (MCC) (Figure I-12) has been considered the most common extrusion–spheronization excipient. Research in recent years has been directed towards the evaluation of spheronization excipients with the intention to reduce or eliminate MCC from the formulation. Biopolymers or synthetic polymers, singly or in mixtures along with different granulation liquids have been studied recently(*63-66*). In this work, a single excipient with water used as the granulation liquid will be evaluated.

Microcrystalline cellulose

Microcrystalline cellulose (MCC) was the first excipient used as a pelletization aid. MCC is able to absorb and retain a large quantity of water like a sponge due to its large surface area and high internal porosity(*67-69*). A MCC wet mass has the ideal rheological properties for extrusion and spheronization. During extrusion, a MCC wet mass is compressed and the water which is squeezed from the internal structure lubricates the particles flowing through the extruder. After extrusion, the volume of the cylinders increases and they appear dry and brittle, allowing them to be chopped into short lengths during the initial phase of spheronization. During the spheronization phase, the force of spheronization compresses the excudates and deforms the short cylinders to obtain spherical pellets. MCC is able to form good quality pellets with water soluble and water insoluble drugs while allowing a high level of drug content(*70*). MCC pellets have good sphericity, low friability, high density and smooth surfaces. The lack of disintegration of MCC pellets, however results in prolonged drug release for poorly soluble drugs(*71-73*).

Starch

Starch is a polysaccharide, composed of two types of alpha-glucans: amylose and amylopectin (Fig I-13). Amylose is a long, mostly linear polymer, containing α-D-glucose units linked together with σ(1→4)-D-glycosidic bonds. Amylopectin is a highly branched polymer, containing about 95 % of σ(1→4)-D bonds and about 5% of branching σ(1→6)-D bonds(*74*). A modified starch was reported to be better to prepare pellets by extrusion-spheronization(*75*). This modified starch is a crystalline, high-amylose starch formed by gelatinization of amylose-rich starches, followed by enzymatic

debranching of amylopectin and retrogradation of linear amylose chain(*76*). This starch grade is insoluble in cold water and does not swell, but freely disperses in cold water. Pellets with good sphericity are obtained only after the addition of a binder. A narrow concentration range for water is allowed for starch pellet preparation during extrusion–spheronization. Modified starch pellets show immediate release of poorly soluble model drugs due to rapid pellet disintegration(*66*).

Chitosan

Chitosan is a polysaccharide comprising copolymers of glucosamine and N-acetylglucosamine, which is obtained by partial deacetylation of chitin (Figure I-14). Chitosan has a pH-dependent solubility in water due to its cationic character. It is soluble in acidic media and insoluble in basic media(*77*). Chitosan used as a pure spheronization excipient to produce pellets via extrusion–spheronization has been reported by several authors (*65, 78*). In a recent study, Charoenthai et al. investigated two molecular weights of chitosan as pelletization excipients for extrusion–spheronization using water as a granulating liquid(*65*). Paracetamol was used as a model drug, while lactose monohydrate was used as a filler. Pellets could be produced with 60% chitosan, 2.5% sodium alginate, 20% paracetamol, and the remainder was anhydrous lactose using water as the granulating liquid. The most probable reason for this successful production of good pellets was the formation of a polyelectrolyte complex between chitosan and sodium alginate. Chitosan pellets show fast drug release. In a recent study, Jess and Steckel have studied the effect of the degree of deacetylation of different chitosan grades on the properties of pure chitosan pellets(*78*). It was found that chitosan with the highest degree

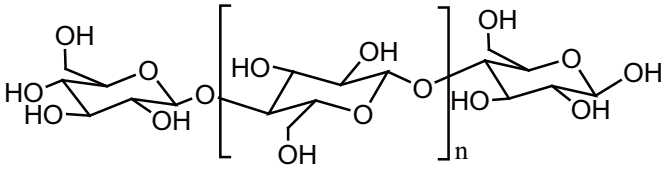

Figure I-12: Structure of cellulose.

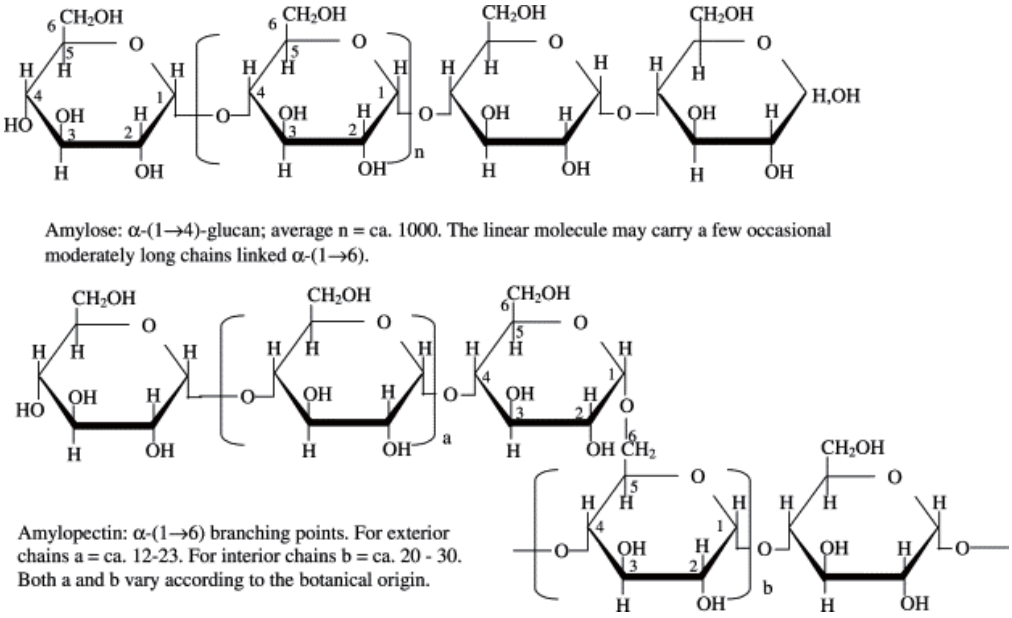

Figure I-13: Chemical structure of starch.

of deacetylation (99.9%) and 0.2 N acetic acid as a granulation liquid provided the best wet mass plasticity to obtain pellets. Budesonide was used as a model drug and it was observed that the drug release was sustained in a zero-order fashion over 9 hours.

Kappa-Carrageenan

Carrageenans are a group of acid polysaccharides, consisting mainly of potassium, sodium, calcium, magnesium and ammonium salts of sulfate esters of galactose and 3,6-anhydrogalactose, which are alternately linked with α-1,3 and β-1,4 linkages in the polymer (Figure I-15). The three commercial types of carrageenans are iota-, kappa-, and lambda-carrageenan. They differ in their solubility and swellability in cold water and thus differ in extrusion– spheronization properties. Kappa-carrageenan is insoluble in cold water and iota-, and lambda-carrageenan are soluble in cold water. In 2005, Bornhöft et al. introduced carrageenan as a pelletization excipient for extrusion–spheronization(*64*). Many carrageenans were screened for pelletization behavior, but only kappa-carrageenan was found to be suitable for preparation of pellets via extrusion/spheronization. Higher levels of water content were required for kappa-carrageenan formulations compare to MCC formulations and the kappa-carrageenan pellets disintegrated rapidly with resulting rapid drug release.

Pectinic acid

Pectins are a family of polysaccharides in which the polymer backbone mainly comprises σ-(1→4)-D-galactouronic acid residues. It consists chiefly of partially methoxylated polygalacturonic acids (Fig I-16). Due to polymer swelling and partial

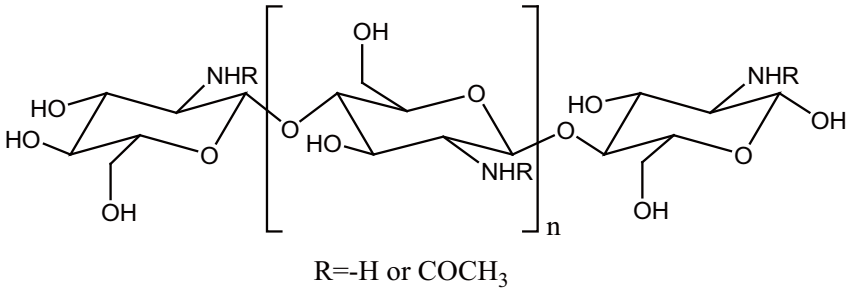

Figure I-14: Chemical structure of chitosan.

Kappa-carrageenan

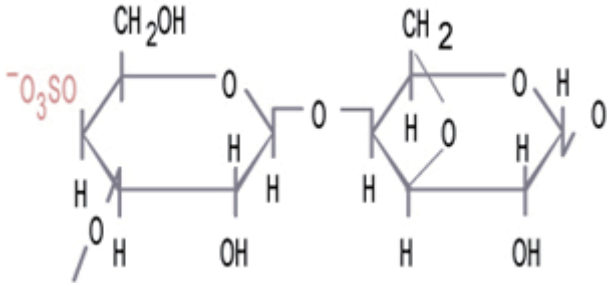

Iota-carrageenan

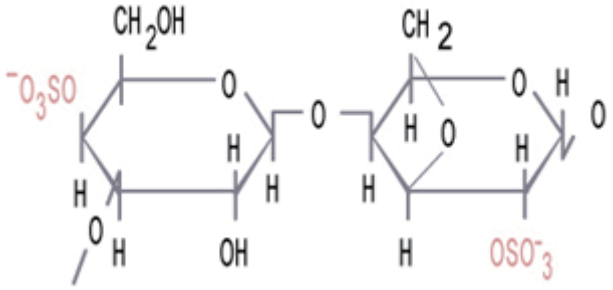

Lambda-carrageenan

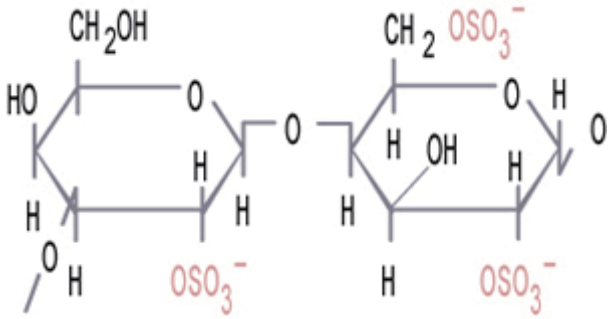

Figure I-15: Structures of carrageenans.

water-solubility, most pectin types are not suitable for pelletization if processed with pure water as a wet-massing liquid(*79*). Only pectinic acid which is a low-methoxylated (4%) pectin derivative was successfully pelletized because pectinic acid is insoluble in water(*80, 81*). Compared to MCC formulations, pectinic acid formulations required less water and the acceptable water content range was narrower. Pectinic acid had a high drug loading capacity (up to 80% drug loading) and produced rapidly disintegrating pellets. Pectinic acid pellets showed immediate drug release.

Biodegradable oxidized cellulose

Cellulose is considered to be a functional, low cost and renewable raw material. It can be converted into a wide range of derivatives with desired properties for a variety of biomedical applications. Among many cellulose derivatives, only oxidized cellulose is biodegradable. Oxidized cellulose can be obtained by treating cellulose with an oxidant under controlled conditions(*82*). The oxidation conditions, such as the nature of oxidant, temperature, pH and reaction duration, all influence the chemical and physical properties of the resulting oxidation products. Depending on the oxidation conditions, oxidized celluloses containing aldehyde, ketone, and/or carboxylate groups are produced. The possible oxidized anhydroglucose units that may be introduced in the cellulose structure are shown in Figure I-17 (*83*). In this research, 6-carboxycellulose (Figure I-17) was produced, and the discussion below is limited to only 6-carboxycellulose (structure I).

Preparation of oxidized cellulose

6-Carboxycellulose commonly called oxidized cellulose (OC) has been extensively studied. Shorygin and Khait firstly prepared OCs from cellulose by using nitrogen dioxides as oxidizing agents(*84*). Since then, nitrogen dioxide has been shown to produce OC as the major product. Nitrogen dioxide can be used directly during the oxidation of cellulose, but only low degrees of oxidization to OC were obtained(*85*). Other researchers used chemicals to produce nitrogen dioxide during oxidation to obtain high degrees of oxidization to OC. Wanleg et al. used a mixture of HNO_3-H_2SO_4-$NaNO_2$ as the oxidizing agent, and OC containing 16% (w/w, 3.6 mmol/g) carboxylic acid groups was produced(*86*). Painter used phosphoric acid as a solvent and sodium nitrite as an oxidizing agent to prepare OC which contained 22.5-24.0% (w/w, 5.0-5.3 mmol/g) carboxylic acid groups. The carboxylic acid content depends on reaction time and degree of polymerization of cellulose(*87*). Walimbe et al. reported a two-stage method: first, $K_2Cr_2O_7/H_2SO_4$ was used as oxidizing agent; second, nitrogen dioxide was used(*88*). Compared to nitrogen dioxide alone, the reaction period for vapor phase oxidation is reduced considerably. OC with a 6-18% carboxylic content was obtained by this method. Bertocchi et al. developed a H_3PO_4/NO_2 method which involves soaking cellulose in phosphoric acid at low temperature and then reacting with NO_2 below 0 ^oC (*89*). The initial soaking in H_3PO_4 helps to obtain a high degree of oxidation and high yield. Kumar and Yang reported a new method to prepare OC by using a mixture of H_3PO_4-$HNO_3/NaNO_2$ at room temperature(*90*). Good yields of product and a high degree of oxidation of OC were obtained with this method. OC with different carboxylic acid contents can be easily prepared by their method.

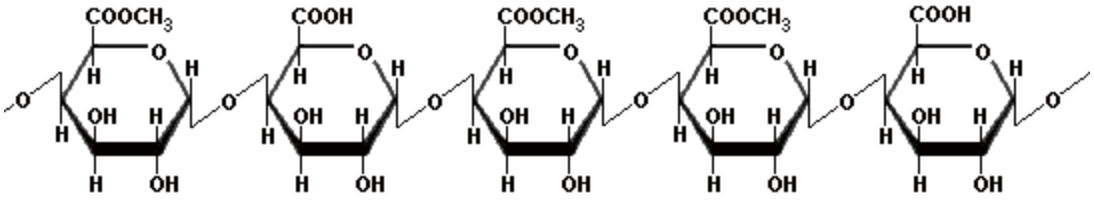

Figure I-16: Structure of pectinic acid.

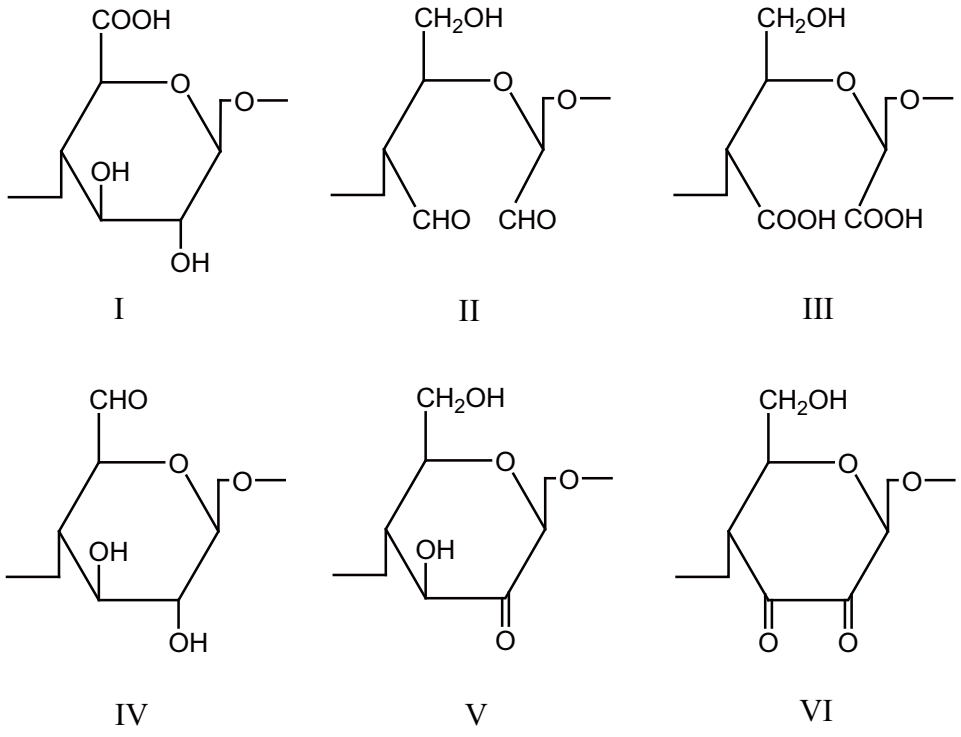

Figure I-17: Possible oxidized anhydroglucose units in an oxidized cellulose product. Structure I is 6-carboxycellulose.

Dialdehyde cellulose (2,3-DAC) and 6-carboxy cellulose are the only cellulose derivatives that are biodegradable(*91*). Currently, however, only 6-carboxy cellulose is accepted for use in humans. It is listed in the United States Pharmacopoeia (USP) as oxidized cellulose (OC) and oxidized regenerated cellulose (ORC) containing 16-24% and 18-24% carboxylic acid groups, respectively(*92*). Eastman Chemical Co. (Kingsport, Tennessee) was the first to introduce OC in the market place. In the early 1960s, Johnson & Johnson (Princeton, NJ) started manufacturing and marketing OC. Currently, OC is commercially available from Johnson & Johnson Medical Inc. (Division of Ethicon, Inc., Arlington, Texas), Normaco, Inc. (Athens, Georgia) and Beckton Dickinson Co. (Sparks, Maryland).

Biodegradation and biocompatibility of oxidized cellulose

Modified celluloses are utilized increasingly in the biomedical field for a variety of purposes, in part, because of their potential ease of degradation to non-toxic materials. Asthon reported that OC containing as low as 3% (w/w) carboxyl groups is bioabsorbable, and the rate of absorption of OC increases with an increase in the carboxyl level or a decrease in the degree of polymerization (DP).(*93*) Dimitrijevich et al. investigated the biodegradation/solubilization of oxidized regenerated cellulose (ORC) *in vitro* and *in vivo*(*94, 95*). ORC contains 18-24% (w/w) carboxyl groups at carbon-6 and 15% (w/w) ketone groups at carbon-2. Products of the solubilization and degradation processes were examined by high performance liquid chromatography (HPLC) with pulsed amperometric detection (PAD). It was found that the ORC readily undergoes chain shortening to give oligomers, which are further hydrolyzed to smaller fragments

including glucuronic acid and glucose, when ORC was exposed to serum and plasma(*94*). *In vivo*, degradation was found to be rapid, and oligometric products were evident primarily in the peritoneal fluid of the implantation site. No accumulation in the serum and urine was noted(*95*). The mechanism of degradation consists of an initial chemical depolymerization steps followed by an enzymatic hydrolysis reaction mediated by glycosidases endogenous to peritoneal macrophages. It was suggested that the degradation of ORC to oligomers occurred due to the presence of the carboxyl group at C-6 position. By analogy to the hydrolysis mechanism reported by Dimitijevich for ORC(*94, 95*), the OC probably involves nucleophilic attack by the hydroxide ion on C-5 of the glucuronic acid unit, causing the cleavage of the anhydroglucopyranose linkage and the formation of a terminal glucuronic acid unit with a double bond between C4 and C5 atoms (Figure I-18)(*96*).

Applications of oxidized cellulose

Oxidized cellulose (OC) has been extensively used as an adhesion barrier to prevent or reduce the frequency of postoperative adhesion formation. The barriers have been shown to be safe and effective in human clinical trials(*97*). The commercially available OC for this purpose is Interceed® (TC7), manufactured by Johnson & Johnson. Oxidized cellulose (OC) can be used as a hemostat during surgical procedures. It is directly applied to the surface of a surgical trauma site after wound closure and becomes saturated with blood by the local hemorrhage, and subsequently swells into a gelatinous mass that aids in the formation of a clot. Biodegradation of the OC at the surgical site has

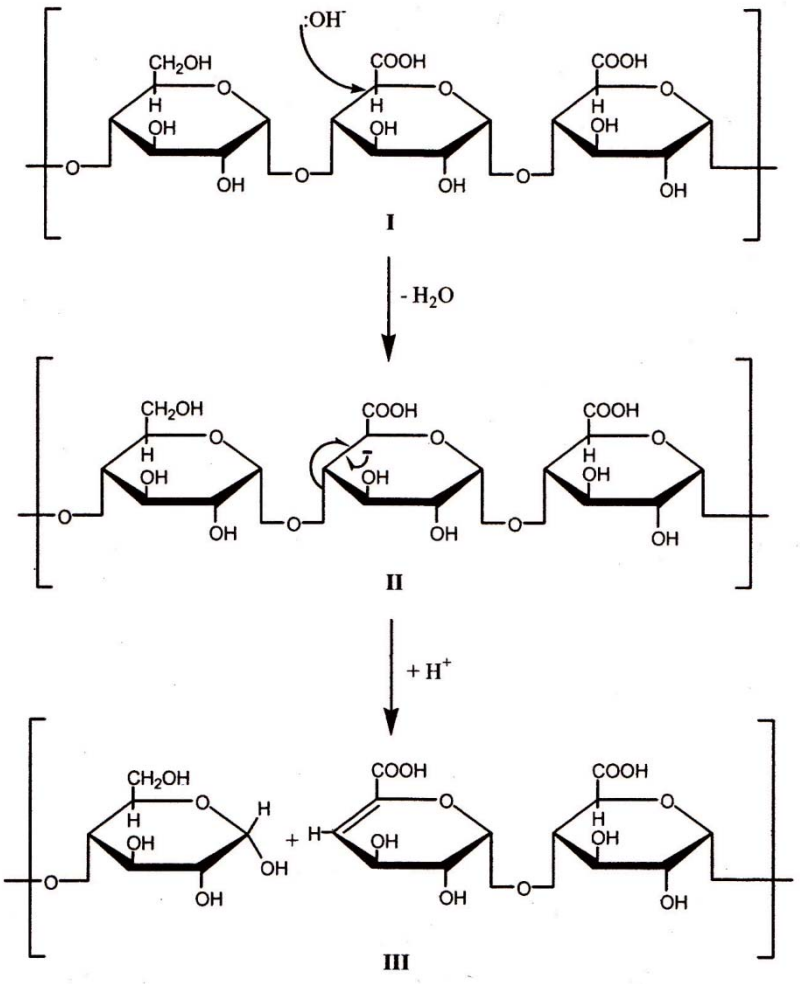

Figure I-18: Possible degradation mechanism of OC in neutral or basic solution.(*96*)

been reported to occur within several days(*95*). Commercially, the OC hemostat is under the trade name Surgical® NU-KIT from Johnson & Johnson.Owing to the presence of carboxylic acid functional groups, OC and ORC have also been used as drug carriers. Zhu et al. studied OC as a macromolecular pro-drug carrier using phenylpropanoamine as a model amine drug. Aqueous OC dispersions can be used to molecularly entrap amine drugs to produce an ionically-linked OC-drug complex. Their results showed the conjugate to be more susceptible in the presence of rat liver homogenate.(*98*) Dolberg et al. prepared a salt of OC with kanamycin sulfate which had a prolonged antibacterical activity in tissue for 20 days after implantation.(*99*) Frisov and coworkers conducted pharmacokinetic studies on OC/ORC-gentamicin implants and their results showed 4 days of sustained release of gentamicin. OC microspheres containing camptothecin (CPT), a highly potent antineoplastic agent, have been prepared by spray drying.(*100*) The release studies in pH 7.4 buffer revealed the dissolution of CPT to be faster from the microsphere formulations than from physical mixtures and free CPT.

Methotrexate (MTX)

Methotrexate (MTX) is a common anticancer drug used for chemotherapy (Figure I-19). MTX is a bright yellow-orange, odorless powder and it is practically insoluble in water, alcohol, chloroform, and ether. It is freely soluble in dilute solutions of alkaline hydroxides and carbonates; it is slightly soluble in dilute hydrochloric acid. The solubility changes from ~38 mg/mL in pH 7.4 buffer to ~ 2 mg/mL in pH 5.5 buffer (*101*). MTX has four pK_a values due to the two amino groups and two carboxylic acid groups. The

basic pK_a values for the 2,4-diaminopteridine sections are less than 0.5 and 5.32. The acidic pK_a values for the p-aminobezoylglutamic acid are 4.83 and 3.76. It decomposes upon melting at a temperature of 185-204 ^{o}C (*102*).

As a chemotherapeutic agent, MTX has been used in the treatment of several forms of cancer and it is administered in high doses. The administration of large doses of MTX results in systemic toxicity. Upon intravenous administration, the drug disappears from the circulation in a triphasic fashion; the first phase has a half-life of 45 min, the second phase a half-life of 2.5 h, and the final phase a half-life of 7 h.

MTX was chosen as an antineoplastic drug for this study because it is a cell-cycle phase specific drug whereby prolonged exposure of the drug to the cancer cells is necessary for optimal efficacy. Thus, sustained- release of a drug like MTX over a long time period would improve its efficacy. In order to improve bioavailability, reduce adverse effects, maximize clinical efficacy and avoid the inconvenience and expense of continuous infusion over a long duration, administration of MTX in a unique sustained-release form has been investigated in this study.

MTX-loaded poly lactide co-glycolide (PLGA) microspheres were prepared by an emulsion solvent evaporation technique. A slow release for up to 30 days in vitro was triphasic and was dependent on copolymer composition and molecular weight of the polymer. Its antitumor efficacy in Sarcoma-180 tumor-bearing mice showed increased mean residence time (MRT) to 18 days(*103*). Methotrexate-loaded poly(ϵ-caprolactone) (PCL) implants were produced by the melt-molding technique. MTX PCL implants showed a slow release up to 105 days and 120 days in vitro and in vivo. MTX diffused from the implants revealed an antiproliferative effect on tumor cells. Finally, MTX

controlled and sustained release from the polymeric implants and efficiently reduced 42.7% of the solid tumor in mice paw. MTX PCL implants represented a contribution to improve the efficacy and safety of chemotherapy treatments, promoting long-term local drug accumulation in the targeted site (*104*). MTX-loaded poly(lactic acid) (PLA) microsphere prepared from different molecular weight PLAs using emulsification-solvent evaporation method showed a slow release for up to 2 to 3 week in vitro(*105*).

MTX was chosen as a model drug in this study because it is a water insoluble drug and can be used to prove that water insoluble drugs can be used in TACE, whereby prolonged exposure of the drug to the cancer cells is necessary for optimal efficacy.

Drug release from erodible polymer system

Erodible polymer systems are one of the dispersed systems that have been used in drug targeting and local drug delivery. Several drug release models that have been applied to this system are discussed below:

Release from a bulk erodible spherical pellet

Biodegradable polymers in a spherical matrix system can undergo bulk erosion and surface erosion. During bulk erosion, the polymer erosion hydrolyzes and forms low molecular weight oligomers, these oligomers below a specific threshold molecular weight dissolve in the aqueous medium. During this process, the permeability of the drug changes. The drug release from a bulk eroding spherical particle is given by(*106*):

$$Ln\left(\frac{x}{1-x}\right) = kt + m$$

where, X is the fraction of drug released, k and m are empirical constants, and t is time. The value of k is dependent on drug loading as well as size and shape of the delivery system.

Release from a surface erodible slab and spherical pellet

In an erodible polymeric matrix, the drug release is controlled by surface erosion of the polymer rather than bulk erosion. In this type of system, polymer erosion occurs the same rate as of the drug release. The drug release from a surface eroding particle is given by (*107*):

$$\frac{M_t}{M_0} = 1 - (1 - \frac{K_e\, t}{C_0\, r})^n$$

where n=3 for a sphere and n=l for a slab. M_t/M_0 is the faction of drug released, K_e is an erosion rate constant, r is represents the radius of a sphere or the half-thickness of a slab, and C_0 is the initial concentration of drug. When n = 1, an alternate form of above expression is:

$$\frac{M_t}{M_0} = \frac{K_e\, t}{C_0\, r}$$

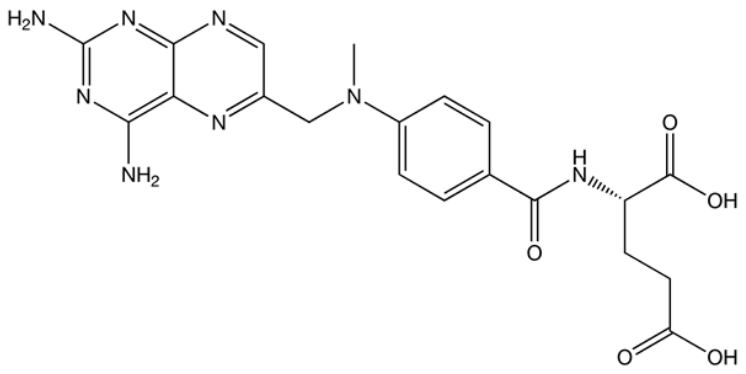

Figure I-19: Structure of methotrexate (MTX).

CHAPTER II

OBJECTIVES

The limitations for current bead systems, including non-biodegradable and biodegradable beads, used for transarterial chemoembolization (TACE) include low drug loading (up to 10% drug content) and only water soluble drugs can be loaded. Another limitation for current TACE biodegradable beads is that they only have a narrow range of bead sizes. In this study, one goal is to develop a new biodegradable bead or pellet which will have a wider size range, achieve high drug loading, have high drug loading efficiency, and load water soluble and water insoluble drugs. The specific objectives of this research are:

Primary objective #1: To identify and optimize extrusion/spheronization conditions to produce beads of oxidized cellulose (OC).

1) To evaluate whether OCs, having 17% carboxylic acid content (w/w), in regards to their suitablity for bead production by extrusion/spheronization.

2) To optimize the extrusion/spheronization method for preparation of OC beads using a fractional factorial experimental design. Water level, spheronization speed and spheronization time will be used as main factors for optimizing the process.

Primary objective #2: Investigate the use of OC base beads as drug carriers for methotrexate for use in TACE.

1) To prepare different sizes of drug-loaded OC-base beads containing methotrexate (MTX). Drug loading and drug loading efficiency will be determined.

2) To evaluate the physical and mechanical properties of MTX-loaded beads.

3) To investigate in-vitro drug release profiles from microspheres/beads designed for TACE using the T-apparatus for evaluating drug release.

CHAPTER III

PREPARATION AND CHARACTERIZATION OF OXDIZED CELLULOSE PELLETS/BEADS

Introduction

To produce pellets by wet extrusion/spheronization, the formulation must contain a pelletization excipient and meet specific rheological requirements for the process. During extrusion the wetted mass must show: i) suitable flow characteristics, which allow mass transport during the process; ii) self-lubricating properties without sticking to each other and; iii) sufficient rigidity to keep the shape of the extrudate. For the spheronization process the moistened extrudates must show: i) sufficient firmness; ii) enough brittleness to break into smaller pieces (cylinders) at the beginning of the spheronization process; iii) plasticity to convert the cylinders into pellets and; iv) sufficiently non-adhesive to retain spherical(*108*). Due to these required properties, the range of materials suitable to act as pelletization aids in the extrusion/ spheronization process is limited.

Microcrystalline cellulose (MCC) was the first excipient used for pelletization to produce pellets successfully with a relatively low amount of materials in the formulation. After its discovery for pharmaceutical pelletization by Reynolds (*27*) and Conine and Hadley (*26*), numerous investigations followed in which MCC showed its special role as a pelletization aid. During wet extrusion, MCC binds water, and therefore, the wet mass becomes rigid enough to be extruded. At the same time in the spheronization process, the

extrudates are sufficiently brittle to break into small cylinders and also plastic enough to convert into spherical pellets.

Research in recent years has investigated alternative pelletization excipients other than MCC. Lindner and Kleinebudde evaluated the use of powdered cellulose as a pelletization excipient (*109*). It was reported that pellets formulated with powdered cellulose were difficult to prepare since powdered cellulose required more water for extrusion, but its water holding ability was lower than MCC. Due to water movement during extrusion, the celullose inside the extruder was compressed, resulting in a dry mass which blocked the extruder (*110, 111*). Dukic´ et al. reported the application of a specific grade of modified starch for extrusion–spheronization purposes (*112*). It was a crystalline, high-amylose starch generated by gelatinization of amylose-rich starches, followed by enzymatic debranching of amylopectin molecules (*76*). Preparation of high-quality pellets was possible using this starch grade (*112*), but the incorporation of a binder (e.g. low molecular weight HPMC) was required to maintain the integrity of the pellets during spheronization. The use of chitosan for the production of pellets via extrusion–spheronization has also been reported by several authors (*65, 78, 113*). Chitosan requires the addition of either a granulation liquid having a specific pH, a second polymer (e.g. sodium alginate or HPMC) or a binder (HPMC). In 2005, Bornhöft et al. introduced carrageenan as a pelletisation aid for extrusion–spheronization (*64*). The iota, lamba and kappa-carrageenan subtypes were screened for pelletization behavior, and kappa-carrageenan was found to be a very promising substitute for MCC in pelletization. Kappa-carrageenan is a biopolymer extracted from red seaweed (*114*), and as such, commercial kappa-carrageenan products may have some variability in their

physicochemical behaviors. The major disadvantage of pellets formulated with kappa - carrageenan is their lower mechanical stability and the possibility of ionic interactions(*115, 116*). Tho et al. evaluated different pectins as possible pelletization excipients (*63, 79-81, 117, 118*). Most pectins are not suitable as pelletization excipients when processed with pure water as a wet massing liquid due to the high degree of swelling and the stickiness of the extrudates (*79*). A low-methoxylated (4%) pectin derivative which was low in soluble pectinic acid was successfully pelletized in combination with lactose and 1% riboflavin as a model drug using water for pelletization(*80*). Pectinic acid had a high drug loading capacity and produced disintegrating pellets that are well suited for fast delivery of drugs with low water solubility.

Oxidized cellulose (OC) hasn't be previously used as an extrusion/spheronization excipient. In this chapter, the possibility of using OC used as extrusion/spheronization excipient is evaluated and the preparation of OC beads is presented. The starting material, OC, contained 17% carboxylic acid content. OC powder was mixed with water to produce a wet mass and then extruded to make an extrudate. The extrudate was transferred into a spheronizer to be converted into spherical particles. Drying and sieving were then performed to obtain the desired size ranges of spherical particles.

Experimental

Materials

The starting materials for the preparation of oxidized cellulose (OC) were cotton linter sheet (Grade R 270; Southern Cellulose Products, Inc., Chattanooga, TN), phosphoric acid (85% w/w, food grade; Monsanto Pharmaceutical Ingredients, St. Louis, MO), nitric acid (69.9% w/w. A.C.S. grade; Fisher Scientific, Fair Lawn, NJ) and sodium nitrite (A.C.S. grade; Fisher Scientific, Fair Lawn, NJ). Calcium acetate, 0.1N NaOH and phenolphthalein were all from Fisher Scientific (Fair Lawn, NJ).

Preparation of Oxidized Cellulose (OC)

Oxidized celluloses (OCs) containing 17% carboxylic acid contents were prepared according to the method of Kumar and Yang (*119*) from cotton linter by treatment with a mixture of phosphoric acid(85%) and nitric acid(70%) in the presence of sodium nitrite at room temperature with 48 hours. The cotton linter-to-mix acids ratio was 1:14 (w/v). The ratio of phosphoric acid to nitric acid was 2:1(v/v). The OC preparation experiments were conducted on a 100 g (cotton linter weight) scale in a fume hood. The resulting products were first washed to a constant pH of 4~5 with distilled water and then with acetone and finally air dried.

Differential Scanning Calorimetry (DSC)

A differential scanning calorimeter (DSC-7, Perkin-Elmer, Boston, MA) equipped with a cooling unit and controlled by a Perkin-Elmer TAC-7 controller was used to

record the DSC thermograms of the samples. Weighed quantities of samples and water were mixed with a steel spatula in 3-mL glass vials for 2 min. A water content study and an equilibration study were carried out. After mixing the polymer and water, the individual wetted samples were allowed to equilibrate in separate tightly capped vials at room temperature for 60, 90, 120, and 210 min for the equilibration study and for 210 min for the water content study. After the holding time, vials were reweighed to check for any moisture loss, and approximately 10 mg of the wetted sample was accurately weighed in a pre-weighed aluminum DSC pan, and a lid was added to the same sample pan. The pans were not hermetically sealed to prevent pressure build up and allow moisture to escape easily from the pan during the heating cycle. The samples were placed into the 25 ºC sample compartment of the DSC under a nitrogen gas flow of 20 mL/min. and chilled immediately to -25 ºC at 10 ºC /min. and held at that temperature for 5 min. Samples were then scanned from -50 to 25 ºC at 5 ºC /min to determine the melting endotherm of water, followed by a heating from 25 to 120 ºC at 10 ºC /min to volatilize the water.

Degree of Crystallinity (DC)

Powder X-ray diffraction (PXRD) measurements were conducted over a 5º to 45º 2θ range using a Siemens diffractometer (Model D5000, Siemens Energy and Automation, Inc., Madison, WI), with monochromatic CuKα (α_1= 1.5460 Å, α_2= 1.5444 Å) X-ray radiation. The step width was 0.020º 2θ/min with a time constant of 0.5 sec. The Diffrac® Plus Eva software, version 2.0 (Siemens Energy and Automatization, Inc., Madison, WI) was used for calculation of peak areas. The DC was calculated by

separating the crystalline and amorphous scattering using peak and baseline options from the software toolbox according to the relationship:

$$X_{cr} = \frac{I_{cr}}{I_{cr}+I_a} \times 100\% \qquad \text{Eqn III-1}$$

Where, I_{cr} is the sum of the areas of all X-ray diffraction peaks and I_a is the area of the diffuse halo due to the amorphous region.

Preparation of Oxidized Cellulose Pellets/Beads

Oxidized celluloses containing 17% carboxylic acid content were used as starting materials. An appropriate amount of water was added to the dry OC to obtain a wet mass. The ratio of OC powder to water ranged between 45% to 60%. Table III-1 gives the results for three water levels in this range. The extruded mass was prepared by passing it through an oscillating granulator (Erweka AR400, Erweka, Heusenstamm, Germany) equipped with a 700 μm screen. The rod-shaped extrudate was spheronized into beads using a spheronizer (Spheronizer 120, Caleva, UK) at different rotation speeds and dwell times. The beads were dried at room temperature.

Optimization of Preparation of Oxidized Cellulose Pellets/Beads

Independent parameter value for the factor analysis with various water levels condition experiments for preparing OC 17 pellets/beads extrusion-spheronization were obtained (Table III-1). It can be seen that the lower and higher % water levels produce unacceptable spheronization. So, in the factor analysis a range of % water was set at ± 5%

around the acceptable value of 53%. The recommended spheronizer speed from the manufacturer was 1000 rpm and the maximum speed is 1800 rpm, so the upper and lower bounds for spheronizer speed were ± 400 rpm with 1400 rpm as mid-point value. Only a few spherical particles were obtained with spheronizer times shorter than 90 seconds and broken beads were obtained with spheronizer times longer than 300 seconds. So 90 seconds and 300 seconds were used to lower and upper bounds and the mid-point was 195 seconds.

A central composite design, using level of water added, spheronizer speed and spheronizer dwell time as independent variables and beads shape and yield of beads as dependent variables was employed. $\alpha = 1$ was used in this central composite design. The independent variables are listed in Table III-2. The sphericity and yield of beads between #20 and #35 mesh screens of each batch was used as the response variable with statistical modeling. JMP software (version 8.0, SAS, Cary, NC) was used for the statistical analysis. Based on the best-fitting model, contour plots were used to select the level of each factor that would optimize the yield and shape of beads. The following general experimental procedure was used to prepare OC beads.

Oxidized celluloses containing 17% carboxylic acid content (OC17) was used as the starting material. An appropriate amount of water was added to the dry powder to obtain a wet mass. The extruded mass was obtained by passing through an oscillating granulator (Erweka AR400, Erweka, Heusenstamm, Germany) equipped with a 700 μm screen. The rod-shaped extrudate was spheronized into pellets/beads using a spheronizer (Spheronizer 120, Caleva, UK). The pellets/beads were dried at room temperature.

Table III-1: Screening of water content for preparing OC17 pellets/beads.

Samples	**Water level 45%**	**Water level 53%**	**Water level 60%**
OC17	Few spherical particles	Spherical particles	Aggregation

Table III-2: Processing parameters and levels evaluated in the optimization study.

Main Factors	**Levels Used**
Water level (%)	48, 53, 58
Spheronizer Speed (rpm)	1000, 1400, 1800
Spheronizer Dwell Time (sec)	90, 195, 300

Response Factors: a. Yield
b. Bead shape

Carboxylic Acid Content of Oxidized Cellulose

The carboxylic acid content of OC was determined by the method described in the United Sates Pharmacopoeia 30/National Formulary 25 (*120*). Briefly, about 0.5 g of OC was accurately weighed and added to 50 ml of a 2% (w/w) calcium acetate solution. The mixture was shaken to ensure complete wetting of the sample. The mixture was allowed to stand at room temperature for 30 minutes. Two drops of a phenolphthalein test solution (1% w/v, USP) were then added, and the mixture was titrated with standard 0.1 N NaOH solution until the solution turned pale pink in color. A blank titration using 50 ml of the same 2% (w/w) calcium acetate solution was performed in the same manner. The carboxylic acid content (w/w) in the same was calculated, on the dry weight basis, using Equation III - 2:

$$\text{Carboxylic acid content (\%)} = \frac{\text{MWCOOH x N x V}}{\text{Weight of dry sample}} X\ 100 \qquad \text{Eqn III - 2}$$

where, N and V are normality and volume of the NaOH solution consumed in the titration, respectively. MW_{COOH} is the molecular weight of the free carboxylic acid group.

Fourier-Transform Infrared (FT-IR) Spectroscopy

Each sample (~ 2 mg) was ground and mixed with dry KBr (~ 400 mg, dried at 105 ^{o}C for 2 hours before use) with an agate mortar and pestle. The ground sample was scraped from the sides of the mortar with a microspatula. The triturated sample was then compressed into a flat-faced disk using a 0.5 inch diameter punch and die with a pair of wenches. IR spectra were obtained on a Nicolet 210 FT-IR spectrophotometer (Nicolet

Instrument Corp, Madison, WI), equipped with Omnic software (Nicolet Instrument Corp, Madison, WI). Spectra were obtained over the range of 650 cm^{-1} to 4000 cm^{-1}.

Moisture Sorption Isotherms of OC

The moisture sorption isotherms of the samples were obtained using a SGA-100 Symmetric Vapor Sorption Analyzer (EdgeTech, Milford, MA). About 10 mg of sample was put into the VTI sample pan and accurately weighted. The VTI instrument was calibrated using a 20.0 mg weight before each measurement. The samples were dried at 60 ^{o}C prior to use, and the heating rate was 5 ºC /min. The relative humidity (RH%) was increased slowly with a criterion of 0.01% weight change within 5 minutes. The sample sorption isotherms were determined at 25.0 ºC. The RH steps were 10%, 20%, 30%, 40%, 50%, 60%, 70%, 80%, 90% and 95%.

True density, bulk density and tap density

A helium micropycnometer (Model MPY-2, Quantachrome Corporation, Boyton Beach, FL) was employed to measure true density. Samples were dried in a vacuum desiccator (Precision Scientific Co., Chicago, IL) at 60 ºC at a reduced pressure of 60 mmHg for 24 h. The true density (ρ_{true}) was calculated by dividing the mass of the sample by its volume obtained from the equation:

$$V_p = V_c - V_r (P_1/P_2 - 1) \qquad \text{Eqn III - 3}$$

where, V_p is the sample volume, V_c is the cell volume, V_r is the reference volume, and P_1 and P_2 are the pressure inside and outside the cell, respectively.

Bulk density (ρ_{bulk}) was determined in a 100 ml graduated cylinder and calculated by: ρ = mass/volume. Tap density (ρ_{tap}) was determined after 1200 taps using a Vankel tap density analyzer (Model 50-1000, Vankel Industries, Cary, NC).

Beads shape

Bead shape was characterized by optical microscopy (Olympus BX-60, Center Valley, PA, USA). Digital photos were taken using a built-in camera. Approximately 50 beads were randomly chosen and their aspect ratio (ratio of longest feret to orthogonal feret) was calculated and used to express the sphericity of beads.

Results and Discussion

Preparation of Oxidized Cellulose

Oxidized cellulose containing 17% carboxylic acid content was used in this study. Each OC batch was prepared from cotton linters by treatment with a 1:2:0.042(mole ratio) mixture of phosphoric acid, nitric acid and sodium nitrite (Figure III-1) at room temperature for 24 hr as reported by Kumar and Yang (*121*). By controlling the reaction time, oxidized celluloses containing different carboxylic acid contents were prepared. OC17 readily dissolved in mild to strongly basic aqueous solutions. OC17 is practically insoluble in common organic solvents.

The FT-IR spectrum of OC17 and its characteristic peaks, along with peak positions, is presented in Figure III-2. The O-H stretching vibration from the free carboxylic acid group typically appears in the region of ~2400 cm^{-1} - ~3400 cm^{-1} and that the peak due to hydroxyl groups (H-bond) in alcohols in the region of 3200 - 3500 cm^{-1}. The characteristic C=O stretching vibration due to the free carboxylic acid groups in OC17 spectra was identified at 1744 cm^{-1}.

Thermal analysis of polymer–water systems

The interaction between water and polymer and water's distribution within a polymer-water system are critical for evaluation of the polymer's application in wet massing techniques. Formation of hydrogen bonds between water and polymer can plasticize the polymer matrix, thus, the interaction of water with the polymer is critical to pellet/bead fomation, processing, and performance. Three different types of water in hydrated polymers have been classified, free water (Type I), freezing bound water (Type II), and non-freezing bound water (Type III) (*122*). Free water is unbound water and the enthalpy and peak shape for its melting endotherm by differential scanning calorimetry (DSC) are similar to those of pure water (*123*). Bound water is associated with the hydrophilic groups of a polymer, depends on the chemical and higher order structure of the polymer and freezing bound water is categorized as having a weak interaction with the polymer and a melting temperature lower than that of bulk water (*124*). The freezing or melting of bound water that is strongly associated with the polymer that is not observed by DSC analysis it is called non-freezing bound water.

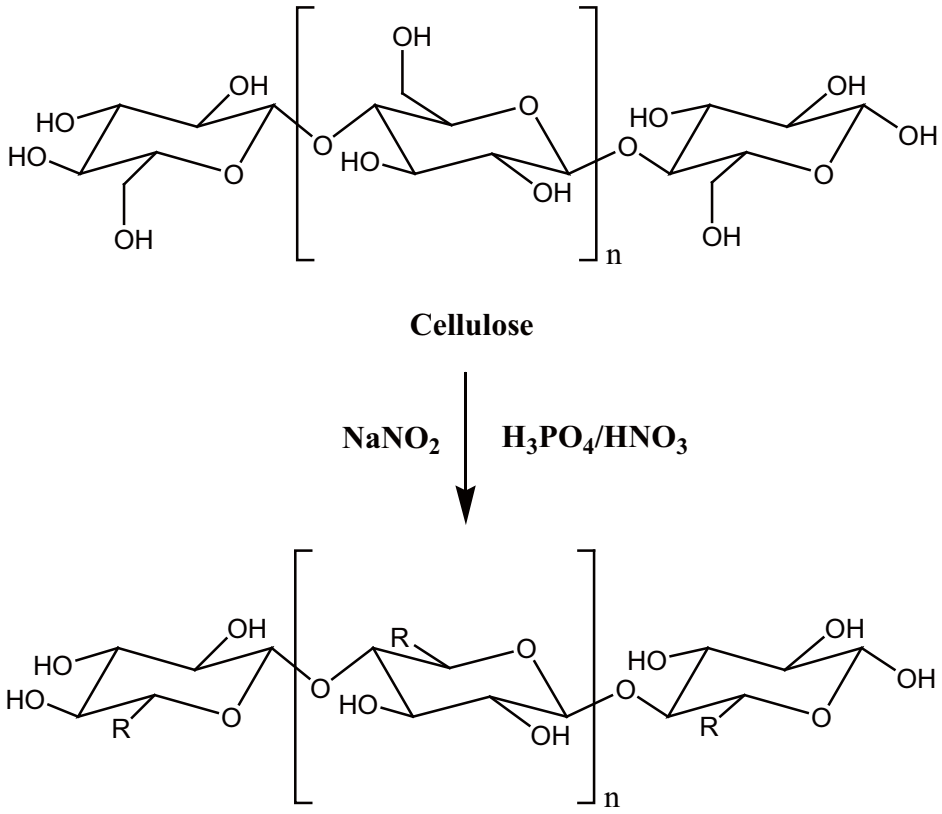

Figure III-1. Preparation of oxidized cellulose.

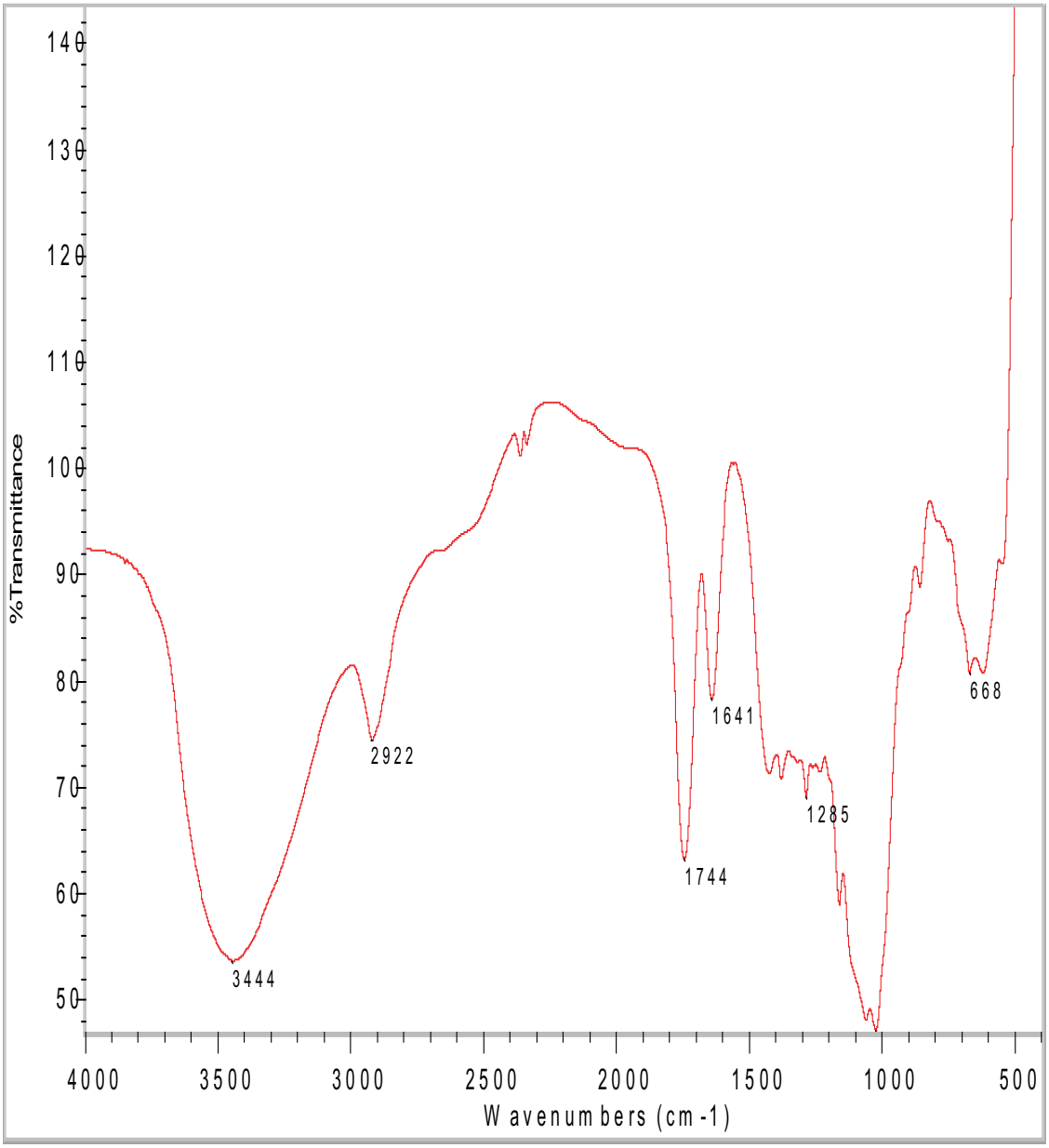

Figure III-2. FT-IR spectrum of oxidized cellulose.

Microcrystalline cellulose (MCC) is widely used as a pelletization aid because it possesses physical properties, including moisture retention and moisture distribution ability. MCC, OC17, chitosan, pectinic acid, starch 1500, cellulose acetates, carboxymethyl cellulose (CMC) and modified chitosan (MODCHIT) were used in this study to compare the interaction and distribution of water among these hydrophilic polymers (Figures III-3 - III-10). Typical DSC thermograms for these polymers at each water content level are shown in Figures III-11 - III-18. The melting peaks were analyzed for enthalpy. The actual water content (Wc) was determined as follows:

$$Wc\ (\%) = \frac{(Wi - Ws)}{Ws} \times 100 \qquad \text{Eqn III - 4}$$

where Wi is the initial mass of the sample studied and Ws is that of the dried sample. The dry sample weight was determined from the weight after heating to 120 ºC, where the thermogram indicated that the water had evaporated completely. The extrapolated melting peak onset temperature and the enthalpy of melting of freezing water were determined using the Pyris^{TM} thermal analysis software (Boston, MA). The quantity of nonfreezing bound water was then calculated from the difference between the weight of water in the pan and the amount of freezing water calculated from the observed enthalpy of fusion. The molecular weight of each polymer repeating unit (PRU) was determined from the chemical structure so that the number of molecules of nonfreezing water bound per PRU could be calculated as discussed later.

The melting peaks were analyzed for enthalpy, bound water content and bound water molecules per polymer repeat unit. The results are presented in Table III-3. The hydrated polymer samples containing low water content did have a melting endotherm near 0 ºC indicating that there was essentially no free water at this low water content.

Water molecules not present at the water–polymer interface will show melting characteristics similar to that of pure water and can be referred to as free water. In this study, one broad peak appeared which was due to both the free water and the freezing bound water. The enthalpy associated with the endothermic peak around 0ºC was less than should be observed if all of the pure water added to the sample was crystallized, indicating that some of the water in the sample did not freeze. With the assumption that non-freezing bound water accounts for this difference, the non-freezing bound water content was determined from the difference between the measured water content and the freezing water content as follows:

$$W_{nf} = W_c - W_f \qquad \text{Eqn III - 5}$$

where W_{nf} is the mass of the non-freezing bound water, W_c is the mass of measured water content, and W_f is the mass of freezing water (sum of free water and freezing bound water). The percentage non-freezing bound water content was calculated by:

$$C_b = (W_{nf}/W_s) \times 100 \qquad \text{Eqn III - 6}$$

where C_b is the percentage of nonfreezing bound water and W_s is the mass of the dry polymer sample. The number of molecules of nonfreezing bound water attached per polymer repeat unit (PRU) was calculated using:

$$M_n = (M_p \times C_b) / (18 \times 100) \qquad \text{Eqn III - 7}$$

where M_n is the number of nonfreezing bound water molecules per PRU, M_p is the average molecular weight of the polymer repeating unit, and 18 is the molecular weight of water.

It was observed that when the degree of crystallinity of the polymer samples increased, the amount of non-freezing bound water decreased. This suggests that only the amorphous regions in the polymer can be regarded as the adsorption sites for water molecules (*125*). Therefore, it is important to measure the crystallinity of the polymer to calculate the nonfreezing bound water molecules per PRU. The number of non-freezing bound water molecules attached per PRU in the amorphous region of polymer, M_{na}, was calculated with:

$$M_{na} = (M_n \times 100) / (100 - X_{cr}) \quad \text{Eqn III - 8}$$

where X_{cr} is the percent polymer crystallinity.

The values of C_b, M_n, and M_{na} increased as the water content increased for each polymer (Table III-3). As water content increases, polymer–polymer hydrogen bonds are broken, and this results in an increase in primary binding sites available for interaction with water. Disruption of polymer-water bonds increases the molecular mobility of polymer strands and thus water acts as a plasticizer (*126*). Finally, at high water content, even more primary binding sites can become available, since water is then also to bind to other water molecules, adding to those not bound to the primary sites (*123, 127*). This accounts for the increase in the number of non-freezing bound water molecules per PRU in the amorphous region as the water content increased. Analysis of variance showed that

there is a statistically significant difference in the number of non-freezing bound water molecules between PRU MCC, MODCHIT, CMC, Starch 1500 and cellulose acetates in their amorphous region (M_{na}) ($p<0.05$). The M_{na} values are not statistically different between the values for MCC, OC17, chitosan and pectinic acid ($p>0.05$), suggesting that the mechanism involved in the binding of water molecules to the hydrophilic groups of these polymers might be similar. Figure III-19 shows a linear relationship between the free water detected as a melting endotherm and the percentage polymer content which was suggested by Ford and Mitchell (*128*). The ratio corresponding to the minimum amount of water required to hydrate the polymer can be obtained by extrapolation to zero enthalpy. Any water above that amount would represent freezing water. The minimum amount of water required to hydrate the polymer was listed at Table III-4. The M_{na} values at 60, 90, 120, and 210 min are not significantly different, thus, a 60 min equilibration is adequate to achieve equilibrium binding of water molecules to the OC17 polymer repeating units.

Guggenheim-Anderson-de Boer (GAB) Analysis

The experimentally measured moisture sorption–desorption isotherms for MCC, MODCHIT, CMC, Starch1500, OC17, chitosan and pectinic acid are illustrated in Figure III-20, respectively, and show type II isotherms, commonly reported for water-insoluble hydrophilic polymers (*127*). The presence and distribution of moisture in various forms has been determined by establishing quantitative correlations between equilibrium moisture content and the ambient relative humidity. The GAB equation has been proposed for and applied most extensively to pharmaceutical powders.

The GAB equation is the Brunauer–Emmett–Teller (BET) equation extended by Van der Berg according to the modifications developed by Guggenheim, Anderson, and De Boer: (*129*)

$$W = \frac{W_m \times C_G \times K \times \left(P/P_0\right)}{\left[\left(1 - K \times \left(P/P_0\right)\right)\left(1 - K \times \left(P/P_0\right) + C_G \times K \times \left(P/P_0\right)\right)\right]} \quad \text{Eqn III - 8}$$

where, W is the mass of water (g) sorbed per gram of solid (g), W_m is the mass of water (g) in the form of a monolayer, C_G and K are parameters related to the heat of sorption of the monolayer and intermediate layer, respectively, and P/P_0 is the relative water vapor pressure.

In contrast to the BET equation, the GAB equation involves the additional parameter K and takes into account a layer or layers of sorbed water molecules, which may be taken up with a change in enthalpy intermediate to that of the water monolayer at the interface and the bulk water taken up in a non-specific manner. The parameters K and C_G can be determined as:

$$K = B_1 \times exp\left[\frac{H_L - H_m}{RT}\right] \quad \text{Eqn III - 9}$$

and

$$C_G = D \times \exp\left[\frac{H_1 - H_m}{RT}\right] \quad \text{Eqn III - 10}$$

where, B_1 and D are constants, H_L is the heat of condensation of water, H_m is the heat of

sorption of water in the intermediate layers, H_1 is the heat of sorption of water in the first sorbed monolayer, R is the gas constant, and T is absolute temperature.

The GAB equation can be rearranged to a polynomial expression:

$$\frac{\left({}^{P}/_{P_0}\right)}{W} = \frac{K}{W_m} \times \left({}^{1}/_{C_G} - 1\right) \times \left({}^{P}/_{P_0}\right)^2 + \frac{C_G - 2}{W_m \times C_G} \times \left({}^{P}/_{P_0}\right) + \frac{1}{W_m \times C_G \times K}$$

Eqn III - 11

where, W is the mass of water (g) sorbed per gram of solid (g), W_m is the mass of water (g) in the form of a monolayer, C_G and K are parameters related to the heat of sorption of the monolayer and intermediate layer, respectively, and P/P_0 is the relative water vapor pressure. The function, $(P/P_0)/W$ was calculated from the moisture sorption data obtained for MCC, OC17, chitosan, pectinic acid, starch 1500, cellulose acetate, CMC and MODCHIT and plotted vs. time (Figure III-21 – III-28).

The GAB equation was fit to the moisture sorption data obtained from MCC, OC17, chitosan, pectinic acid, starch 1500, cellulose acetate, CMC and MODCHIT using non-linear least-square regression analysis using Maple software (version 14, Maplesoft, Ontario), and the results are presented in Table III-6. The values of the monomolecular water parameter, W_m, from the GAB equation indicate there is monolayer coverage by water. But accounting for the idea that only the amorphous regions of the polymer take up water (*130*), the W_m value needs to be corrected by dividing the W_m by the fraction of non-crystalline region; this parameter is referred to as W_m^{Corr} . The W_m^{Corr} values obtained for MCC, OC17, chitosan, pectinic acid, starch 1500, cellulose acetates, CMC and MODCHIT are also presented in Table III-6. W_m^{Corr} values indicate that there is no statistical difference between MCC, OC17, chitosan and pectinic acid in monolayer

coverage, MCC, chitosan and pectinic acid were used as extrusion/spheronization excipient. Starch 1500, cellulose acetates, CMC and MODCHIT which can not be used as extrusion/spheronization excipient have significant different W_m^{Corr} value from MCC.

These results suggest that the chemical affinity of the amorphous region of MCC, OC17, chitosan and pectinic acid are similar at low water content. The bound water probably interacts with polar hydroxyl groups in MCC, OC17, pectinic acid and the polar hydroxyl and amine groups in chitosan. Since oxygen is more electronegative than nitrogen, the polarity difference causes the hydrogen bonding of water molecules with hydroxyl groups to be stronger than with amine groups. Reuda et al. (*131*). studied the interaction of water with starch and chitosan films (86% degree of deacetylation) by exposing the films to different relative humidities and then conducting infrared spectroscopy. It was concluded that, in the case of starch, a simple, symmetric water deformation band appears at 1647 cm^{-1} that indicates an interaction of water molecules with hydroxyl groups, whereas, in the case of chitosan, the water deformation band splits into two bands, one at 1647 and the other one at 1582 cm^{-1} which are related to water bound to hydroxyl and amine groups, respectively. The nature of the band splitting observed for chitosan indicated a stronger interaction of water molecules with the hydroxyl groups than with the amine groups. Based on the results of Tual's study, however; amine groups do not participate in the sorption mechanism at low partial pressure by moisture sorption isotherm analysis in chitosan(*132*). As a result, chitosan hydroxyl groups likely interact with water molecules first in the amorphous region at low water content. These observations account for the

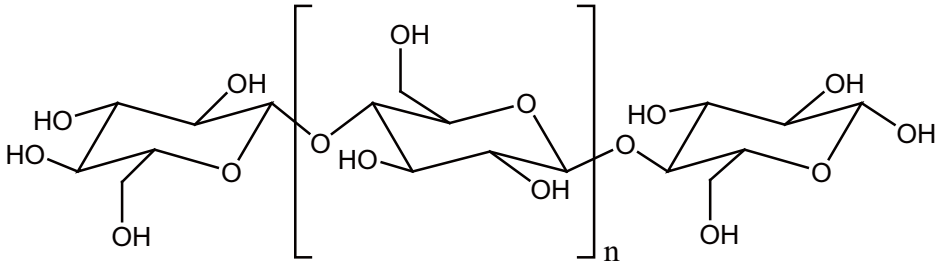

Cellulose

Figure III-3: Structure of cellulose.

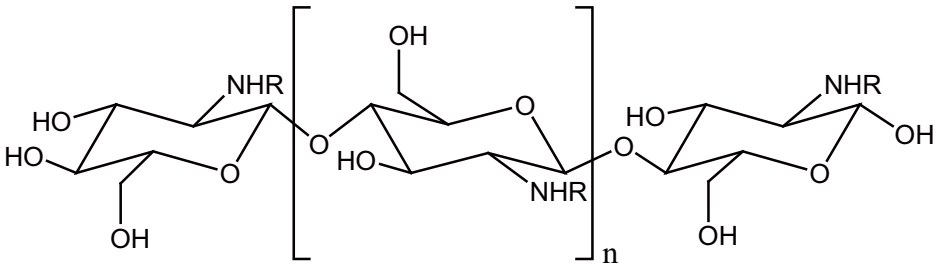

R=-H or $COCH_3$

Chitosan

Figure III-4: Structure of chitosan.

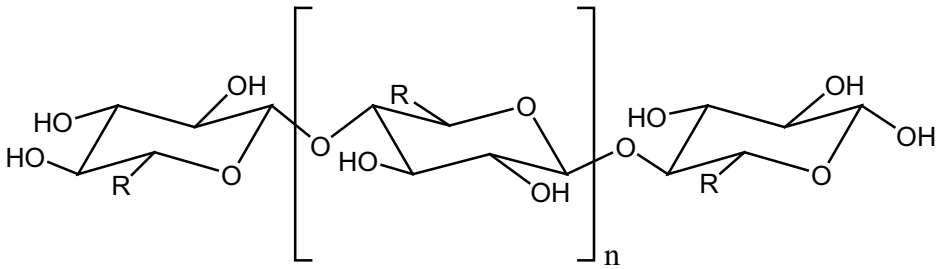

R= -CH_2OH or -COOH

Figure III-5: Structure of oxidized cellulose.

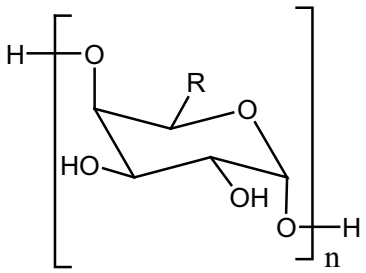

R= - COOH or $COOCH_3$

Figure III-6: Structure of pectinic acid.

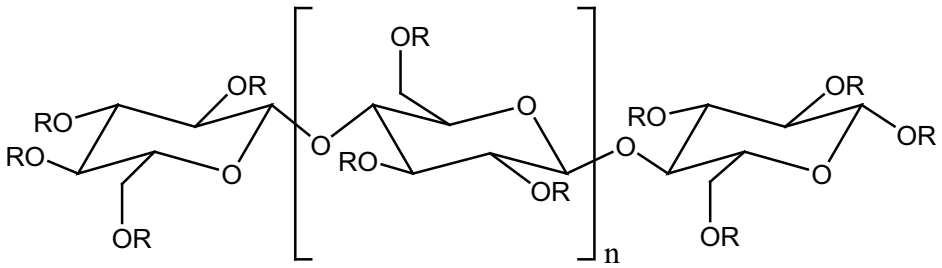

R= -H or CH_3CO

Figure III-7: Structure of cellulose acetate.

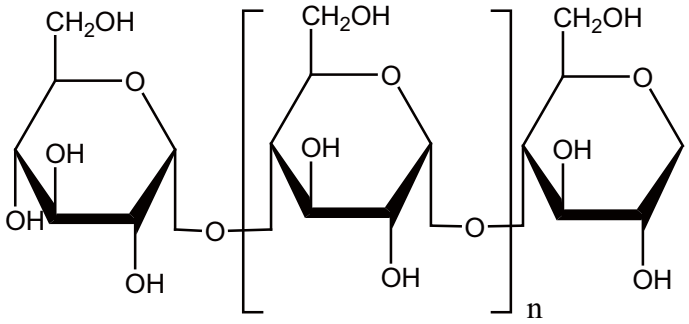

Amylose

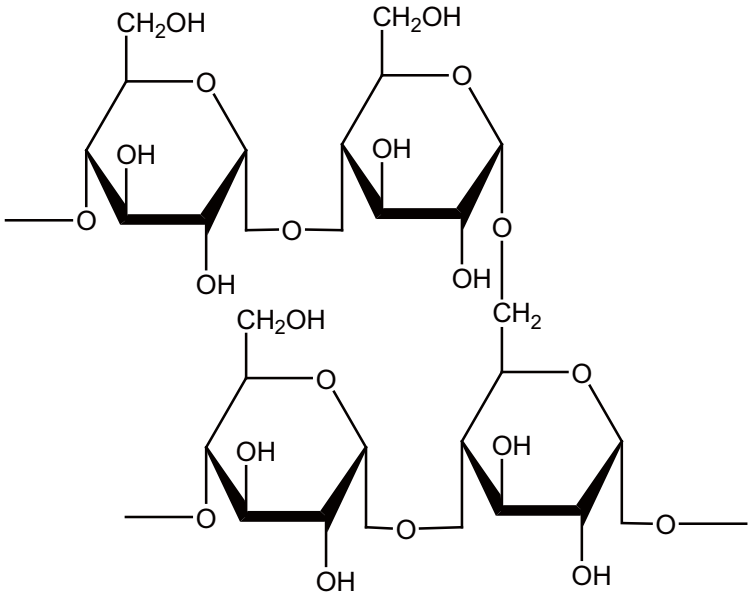

Amylopectin

Figure III-8: Structure of starch.

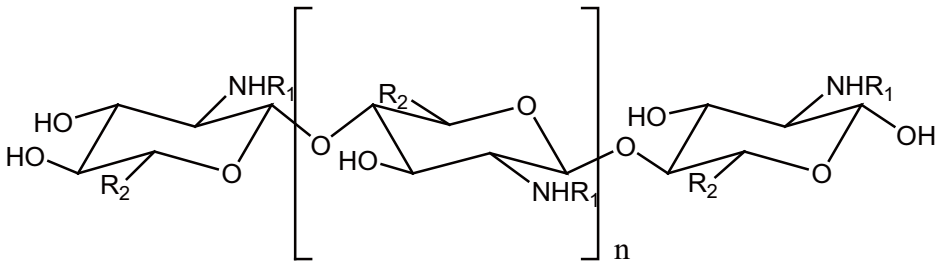

R_1= -H or $COCH_3$; R_2= -CH_2OH or CHO

Figure III-9: Structure of modified chitosan (MODCHIT).

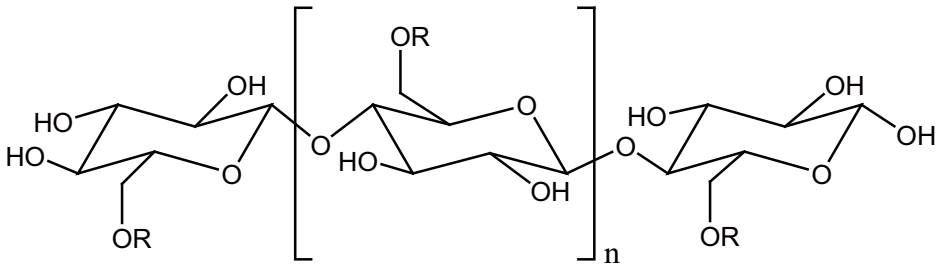

R = -H or $CH_2COO^-Na^+$

Figure III-10: Structure of carboxymethyl cellulose.

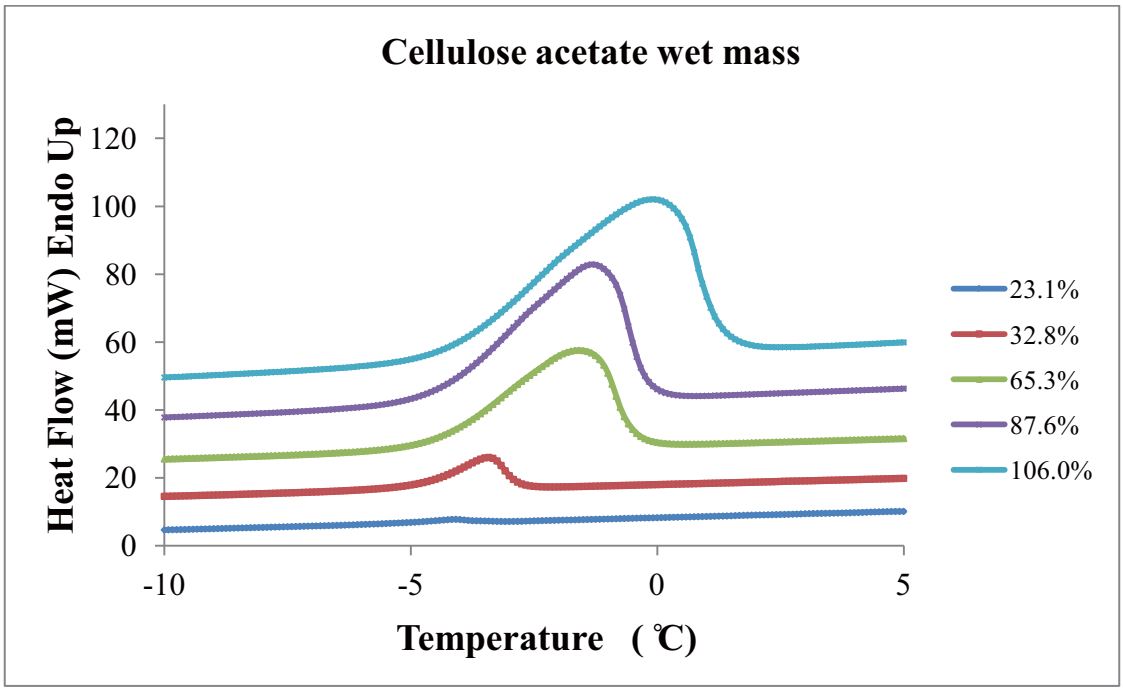

Figure III-11: Representative melting endotherms of water in cellulose acetate at each water content.

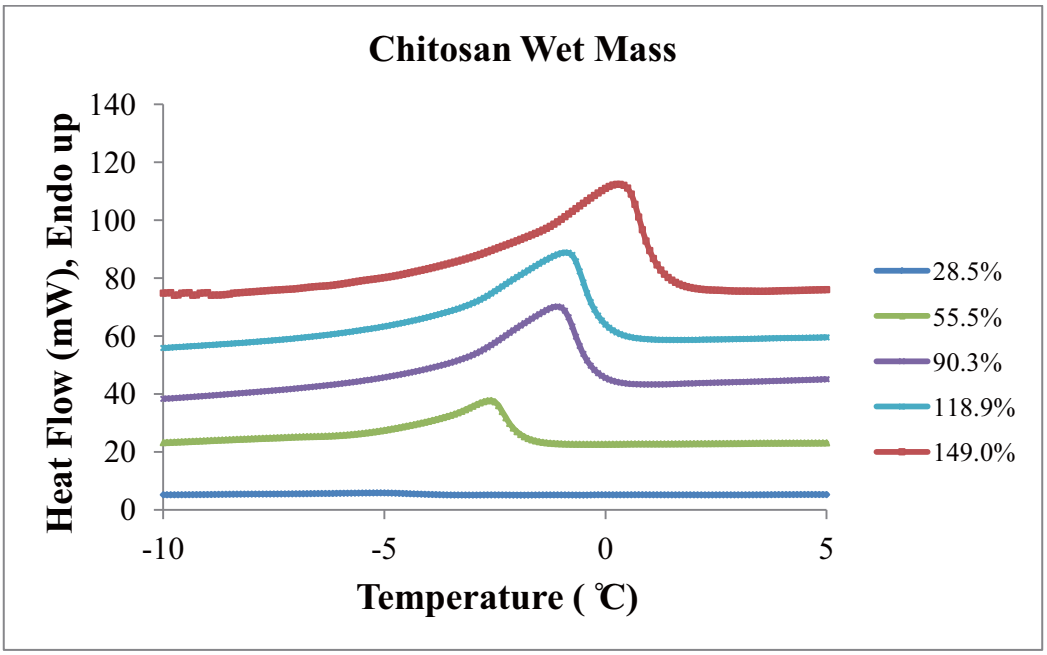

Figure III-12: Representative melting endotherms of water in chitosan at each water content.

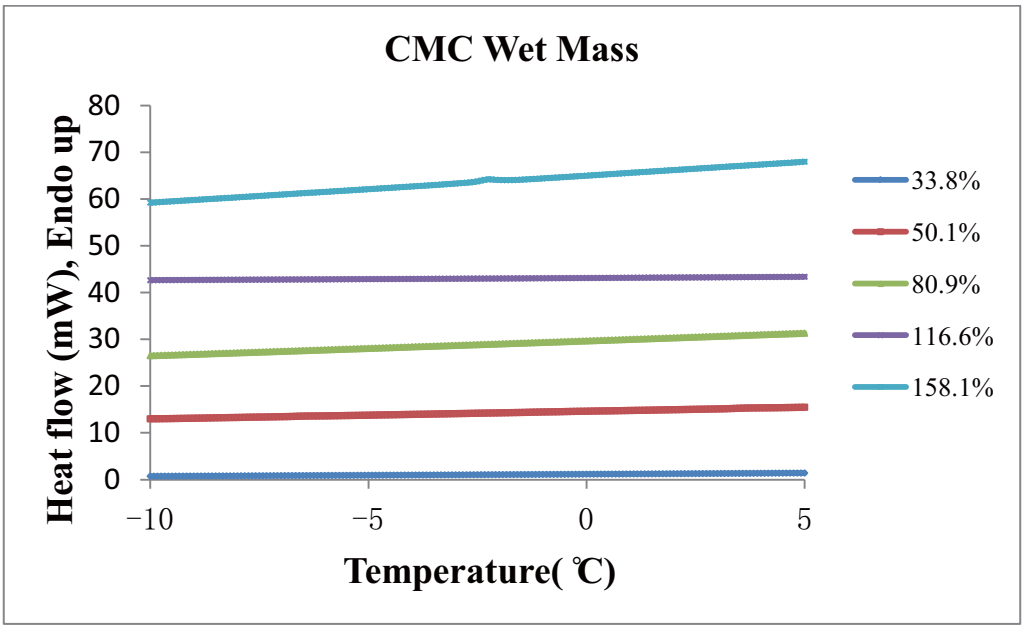

Figure III-13: Representative melting endotherms of water in carboxymethyl cellulose (CMC) at each water content.

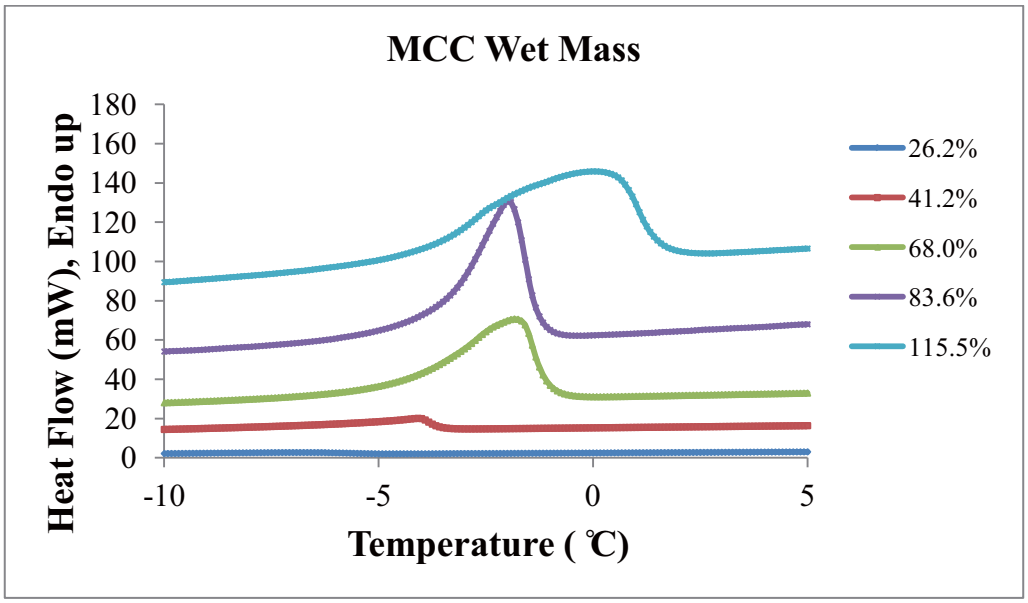

Figure III-14: Representative melting endotherms of water in microcrystalline cellulose (MCC) at each water content.

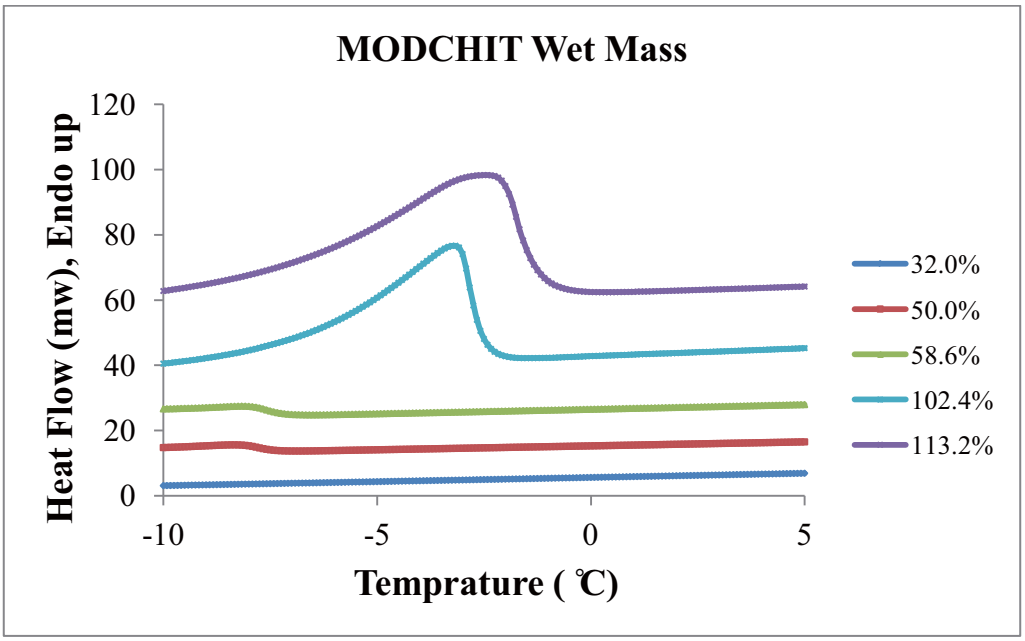

Figure III-15: Representative melting endotherms of water in modified chitosan (MODCHIT) at each water content.

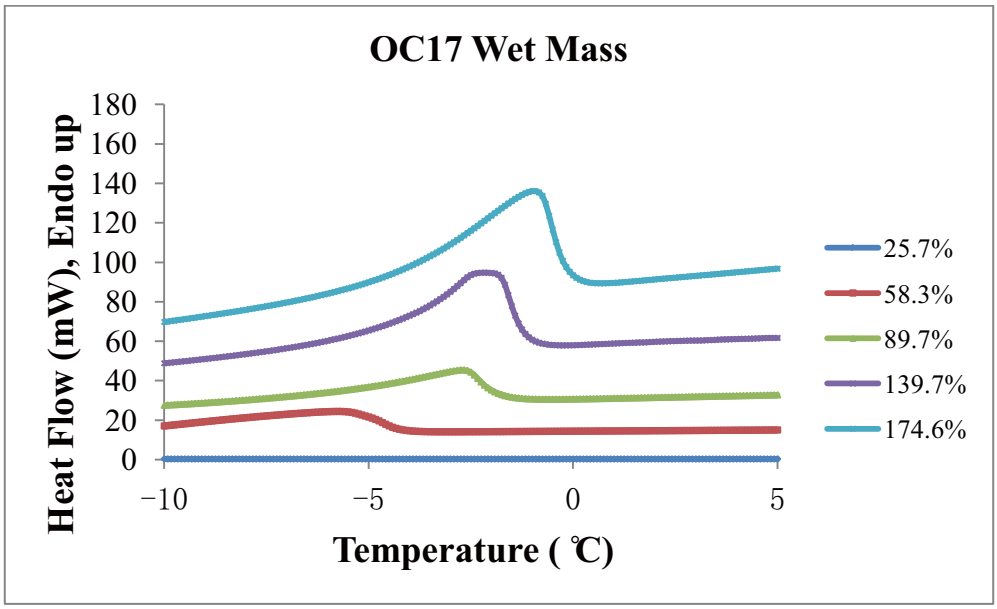

Figure III-16: Representative melting endotherms of water in oxidized cellulose (OC17) at each water content.

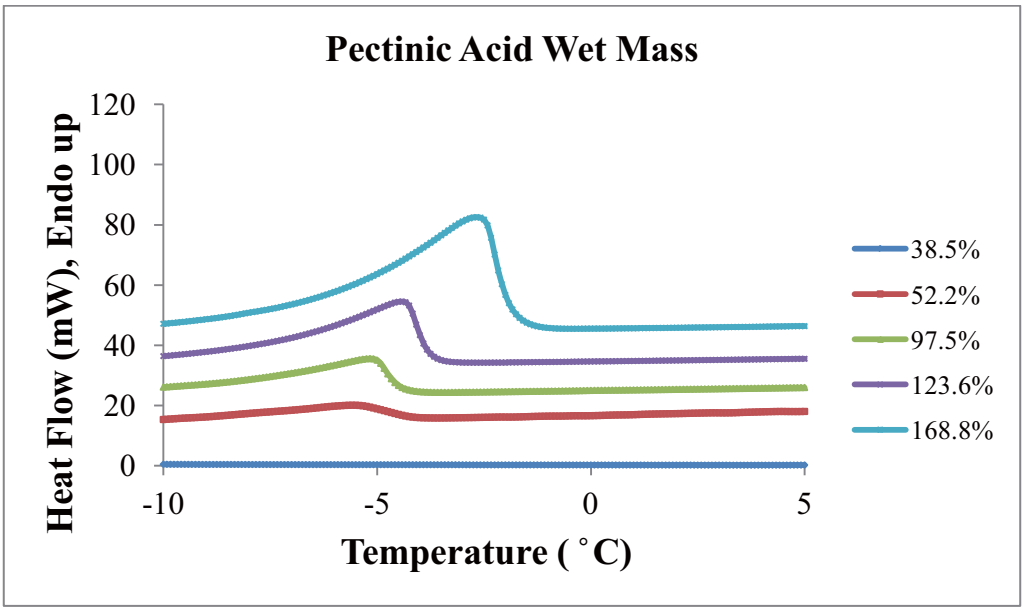

Figure III-17: Representative melting endotherms of water in pectinic acid at each water content.

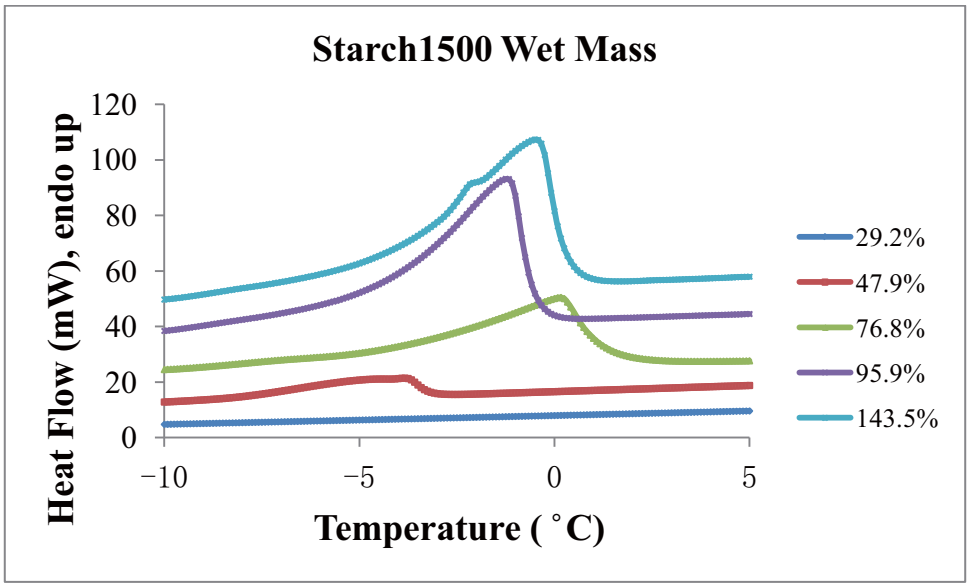

Figure III-18: Representative melting endotherms of water in Starch1500 at each water content.

Table III-3: Measured and calculated non-freezing bound water content in various polymers.

Material	W_c (% w/w dry mass)	C_b (% w/w dry mass)	PRU M_n	PRU M_{na}
MCC	115.5	23.05	2.07	6.91
	83.6	21.84	1.96	6.55
	68.0	21.38	1.92	6.41
	41.2	20.87	1.87	6.25
	26.2	19.98	1.79	5.99
OC17	174.6	49.80	4.73	6.76
	139.7	47.81	4.54	6.49
	89.7	47.65	4.53	6.47
	58.3	45.82	4.35	6.22
	25.7	25.67	2.44	3.48
Chitosan	149.0	38.51	3.44	6.89
	118.9	35.97	3.22	6.43
	90.3	33.74	3.02	6.04
	55.5	32.37	2.90	5.79
	28.5	28.52	2.55	5.10
Pectinic acid	168.8	57.68	5.62	7.21
	123.6	55.95	5.46	6.99
	97.5	53.19	5.19	6.65
	52.2	49.82	4.86	6.23
	38.5	38.53	3.76	4.82

W_c: actual water content; C_b: non-freezing bound water content; PRU M_n: bound water molecules per polymer repeat unit; PRU M_{na}: of bound water molecules per polymer repeat unit in the amorphous region.

Table III-3: (continued).

Material	W_c(%w/w dry mass)	C_b (% w/w dry mass)	PRU M_n	PRU M_{na}
Cellulose acetates	106.0	28.44	4.15	5.19
	87.6	25.71	3.75	4.69
	65.3	24.84	3.63	4.53
	32.8	23.44	3.42	4.28
	23.1	22.14	3.23	4.04
CMC	158.1	157.83	17.59	24.09
	116.6	116.56	12.99	17.79
	80.9	80.94	9.02	12.36
	50.1	50.14	5.59	7.65
	33.8	33.76	3.76	5.15
MODCHIT	113.2	57.10	5.23	10.47
	102.4	53.62	4.91	9.83
	58.6	51.33	4.71	9.41
	50.0	46.49	4.26	8.52
	32.0	31.98	2.93	5.86
Starch 1500	143.5	47.04	4.23	10.58
	95.9	42.75	3.85	9.62
	76.8	38.47	3.46	8.66
	47.9	35.34	3.18	7.95
	29.2	29.18	2.63	6.57

W_c: actual water content; C_b: bound water content; PRU M_n: bound water molecules per polymer repeat unit; PRU M_{na}: of bound water molecules per polymer repeat unit in the amorphous region.

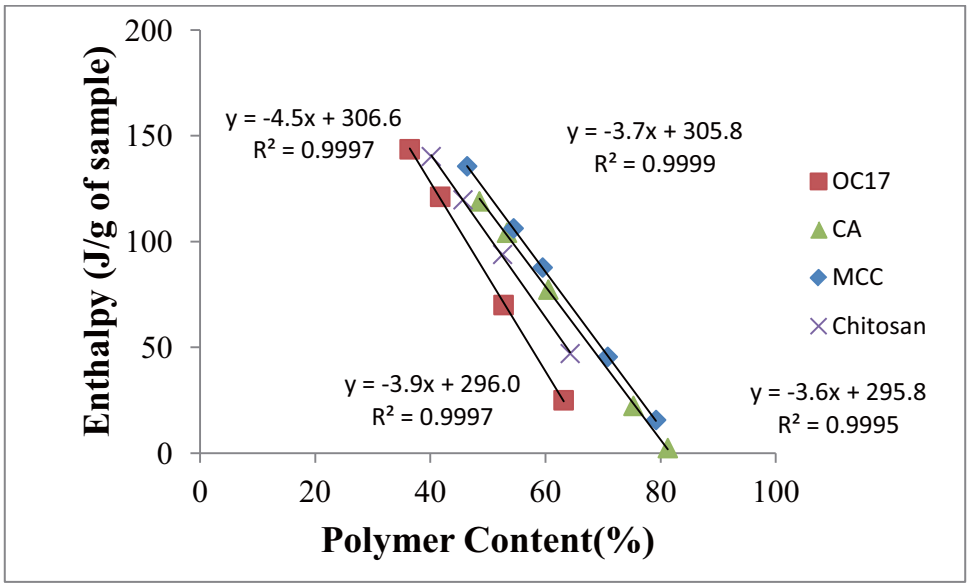

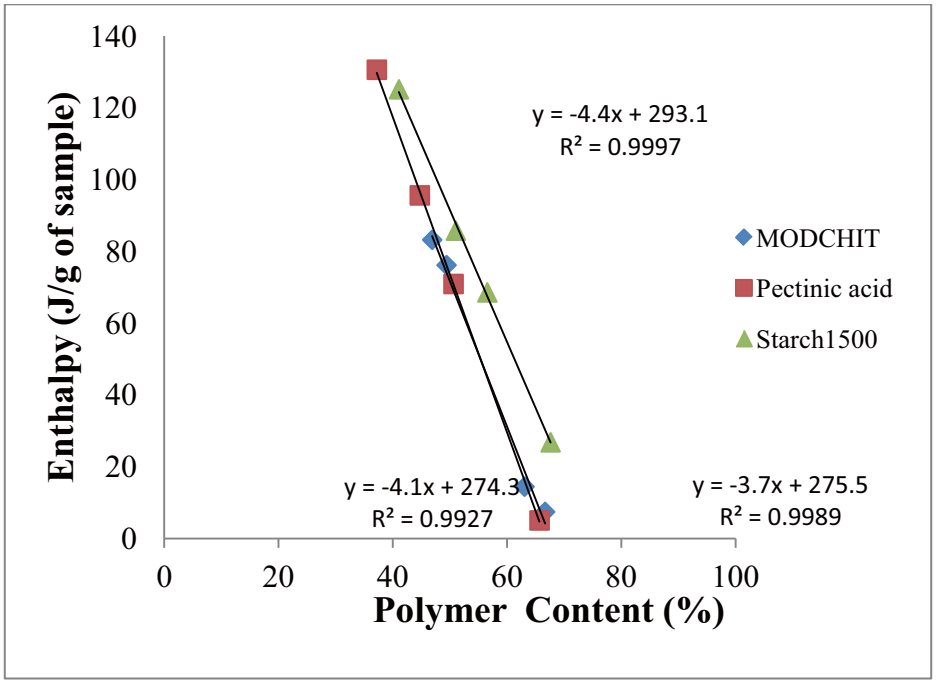

Figure III-19: Enthalpies of water melting (J/g) determined by DSC associated as a function of the percent polymer content for wet mass: enthalpy normalized based on total sample weight.

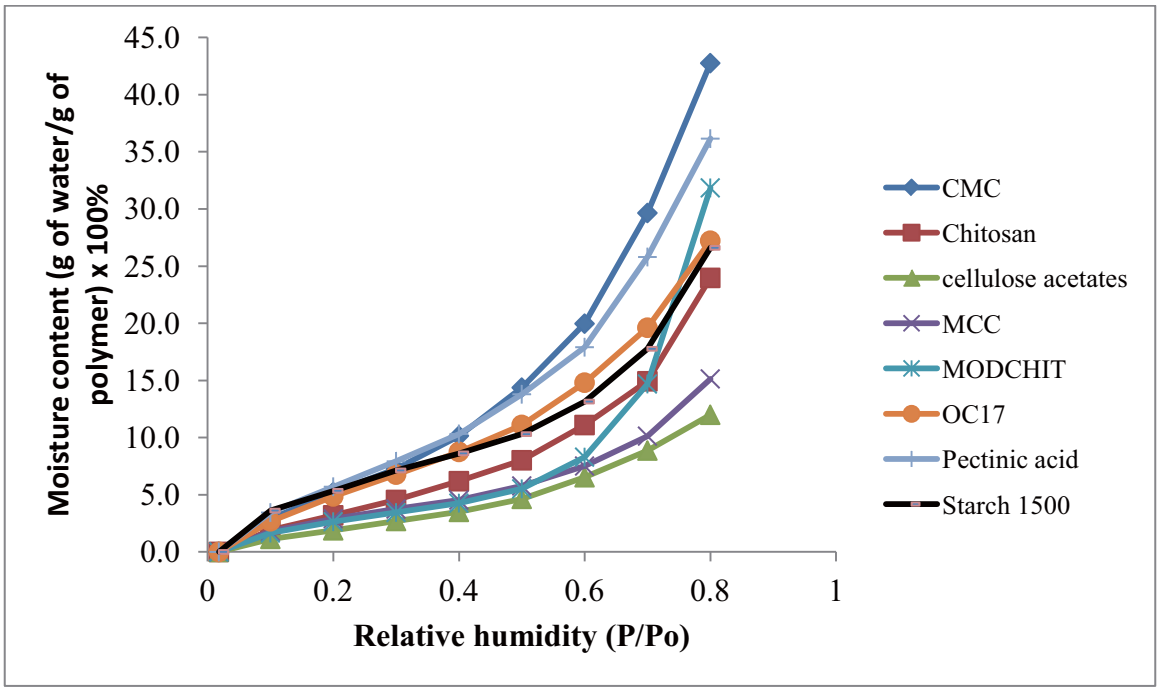

Figure III-20: Moisture sorption profiles determined by VTI for various polymers.

Table III-4: Minimum water content required to hydrate polymer (% w/w base on dry mass).

Sample	Minimum water content (%w/w)
MCC	19.9
OC17	45.7
Chitosan	30.5
Pectinic acid	49.9
MODCHIT	47.7
Starch 1500	33.5
CMC	158.0
Cellulose acetate	22.3

Table III-5. Equilibration time on the interaction between OC17 and water.

Time (min)	C_b (%w/w)	PRU M_n	PRU M_{na}
10	20.1	1.86	2.66
30	43.0	3.99	5.71
60	47.8	4.43	6.34
90	47.4	4.39	6.27
120	48.7	4.52	6.46
210	47.3	4.39	6.27

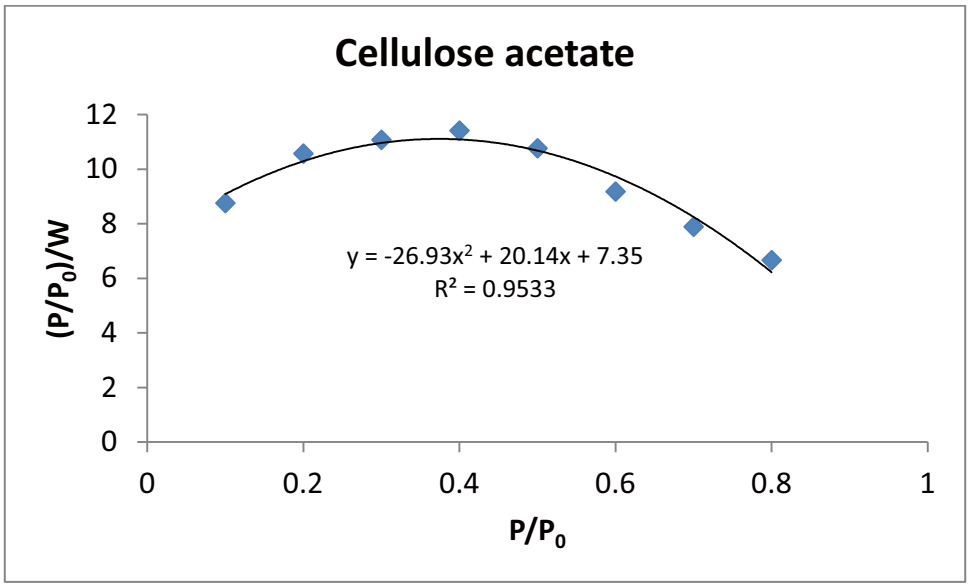

Figure III-21 : $(P/P_0)/W$ versus (P/P_0) for moisture sorption data of cellulose acetate. P/Po: relative humidity.

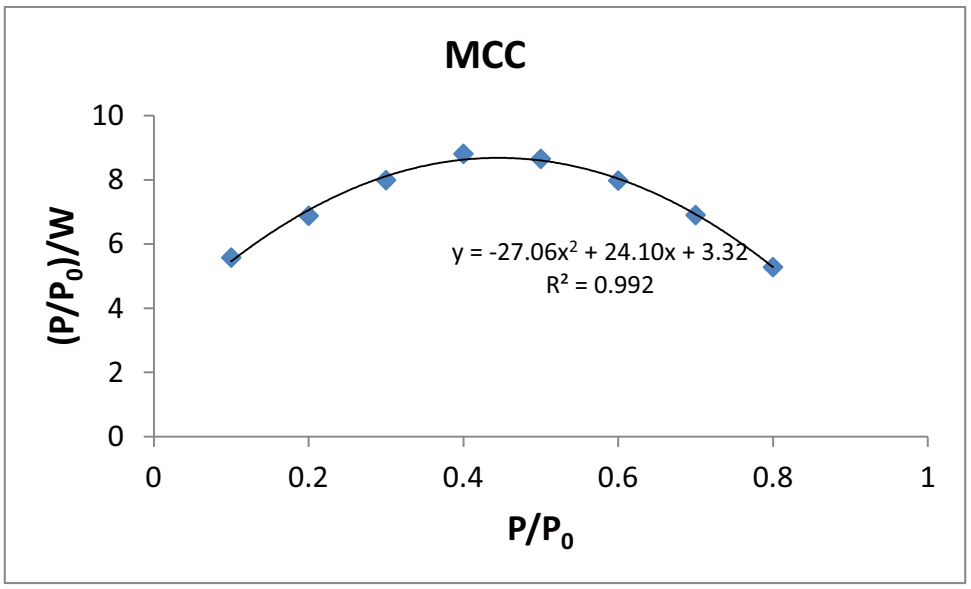

Figure III-22 : $(P/P_0)/W$ versus (P/P_0) for moisture sorption data of microcrystalline cellulose. P/Po: relative humidity.

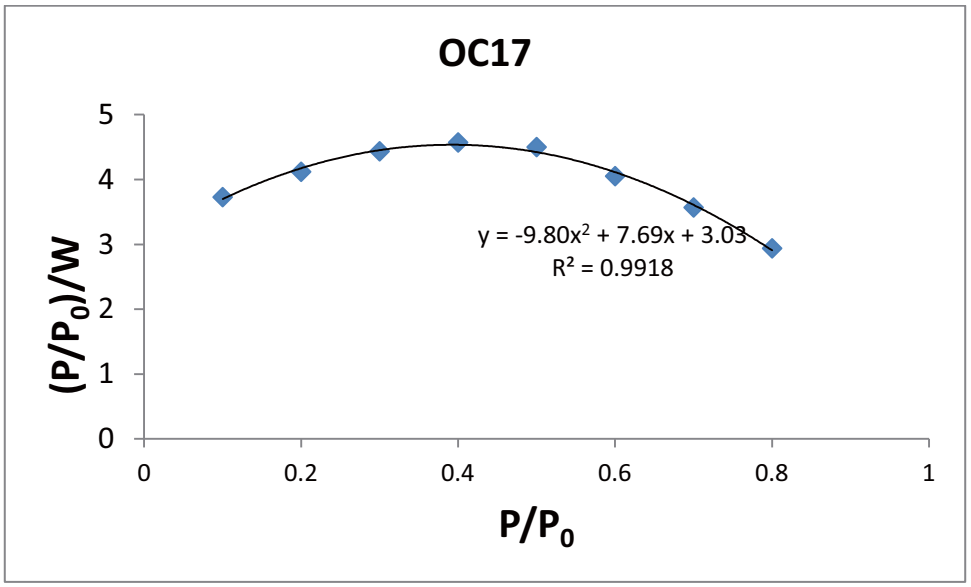

Figure III-23 : $(P/P_0)/W$ versus (P/P_0) for moisture sorption data of oxidized cellulose. P/Po: relative humidity.

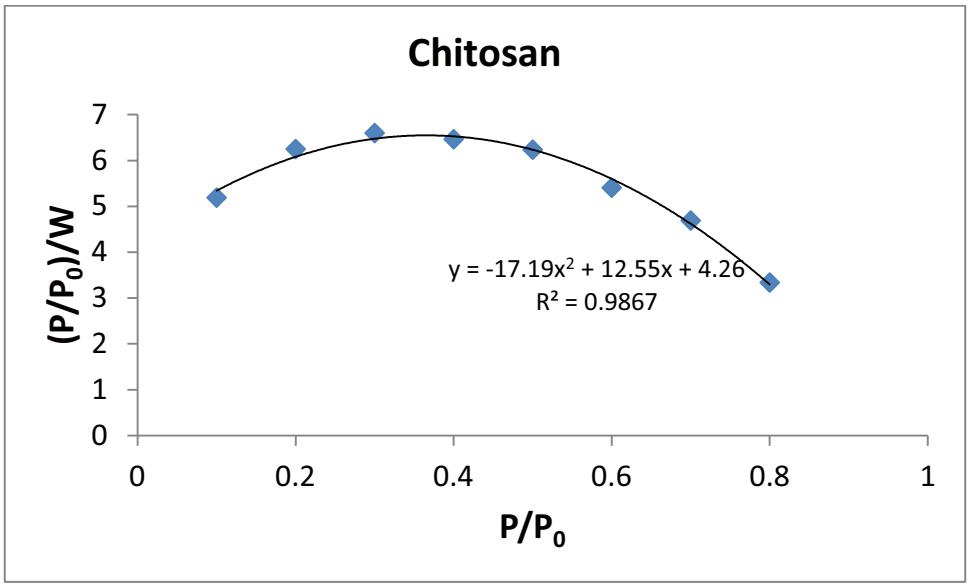

Figure III-24 : $(P/P_0)/W$ versus (P/P_0) for moisture sorption data of chitosan. P/Po: relative humidity.

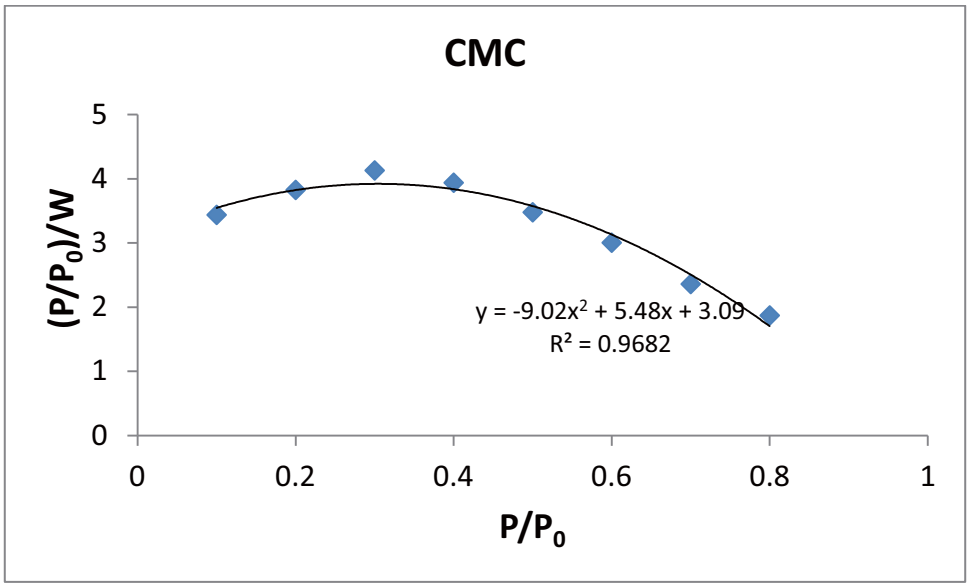

Figure III-25 : $(P/P_0)/W$ versus (P/P_0) for moisture sorption data of carboxymethyl cellulose. P/Po: relative humidity.

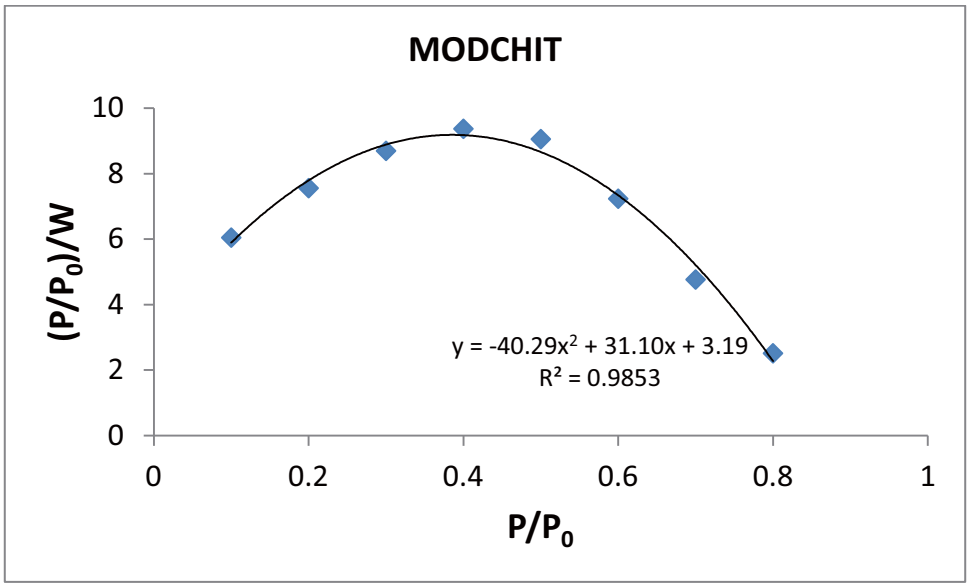

Figure III-26 : $(P/P_0)/W$ versus (P/P_0) for moisture sorption data of modified chitosan. P/Po: relative humidity.

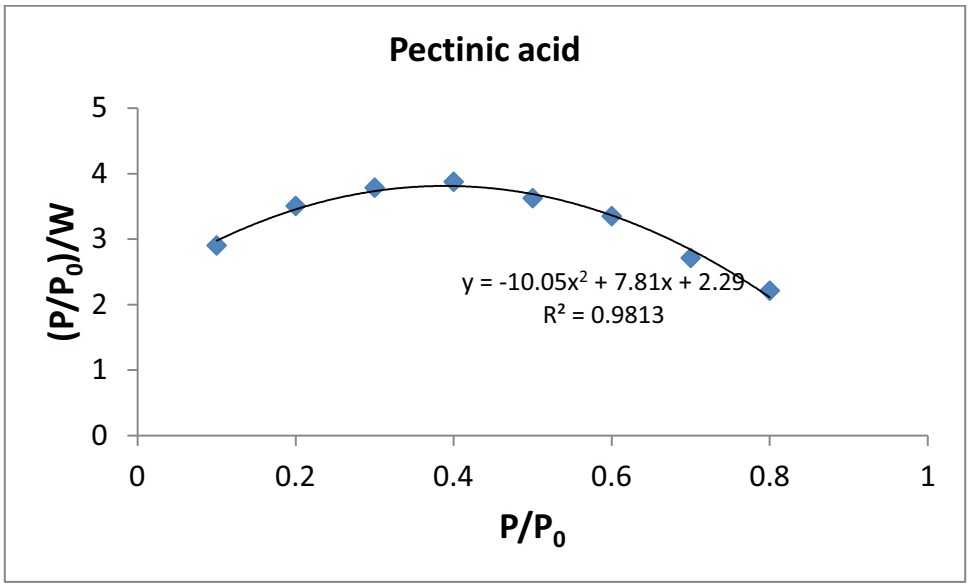

Figure III-27 : $(P/P_0)/W$ versus (P/P_0) for moisture sorption data of pectinic acid. P/Po: relative humidity.

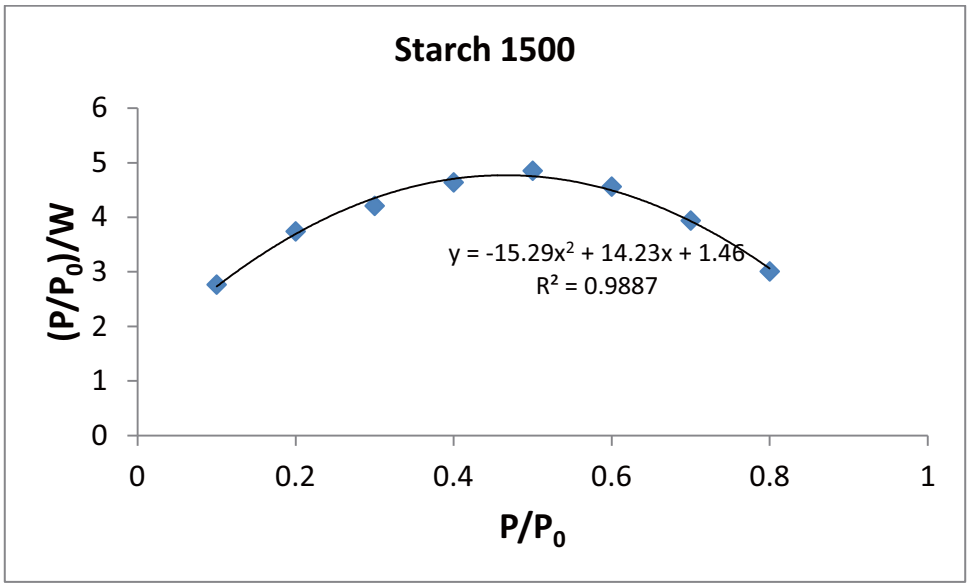

Figure III-28 : $(P/P_0)/W$ versus (P/P_0) for moisture sorption data of Starch 1500. P/Po: relative humidity.

Table III-6: GAB equation analysis.

Sample	W_m(g/g)	W_m^{Corr} (g/g)	r^2
MCC	0.034	0.113	0.9920
OC17	0.081	0.116	0.9918
Chitosan	0.053	0.106	0.9867
Pectinic acid	0.089	0.114	0.9813
Starch 1500	0.060	0.150	0.9887
Cellulose acetate	0.032	0.043	0.9533
CMC	0.100	0.220	0.9682
MODCHIT	0.027	0.053	0.9853

W_m: water weight in just monolayer; W_m^{corr}: W_m corrected for amorphous polymer content

lack of significant differences between MCC, OC17, chitosan and pectinic acid because interaction is mainly with the hydroxyl groups in the polymers.

Optimize Process of Oxidized Cellulose Pellets/Beads

Oxidized cellulose containing 17% carboxylic acid content was used for the study of pellet/bead preparation. OC fiber was ground by a ball mill. An appropriate amount of water was added (previously determined) to the dry powder to obtain a wet mass. The extruded mass was prepared by passing it through an oscillating granulator equipped with a 700 μm screen. The rod-shaped extrudate was spheronized, while still wet, into beads using a spheronizer at different rotation speeds and dwell times. The beads were dried at room temperature (Figure III -29).

The size distribution of beads manufactured by extrusion/spheronization technique depends on the equipment and processing conditions. The objective of the following studies of the work was to determine the necessary process conditions for preparing oxidized cellulose (OC) pellets. The yield is the percentage by weight of the defined sieve fraction between between #20 and #35 mesh related to the total weight of the batch. A simple and common parameter to describe micropellet shape from wet extrusion/spheronization is aspect ratio. The ideal value of the aspect ratio is 1. The closer the value gets to 1, the more spherical the pellet shape. Central composite design is an experimental design, useful in response surface methodology, for building a second order (quadratic) model. A full three-level factorial in three factors requires 27 trails. Instead of requiring 27 trails, central composite design can get by with only 15. Moreover, central composite design allows the inclusion of quadratic effects in order to provide a

more realistic model. The optimization of the preparation of beads was achieved using the central composite design (Table III-7) with the parameter ranges described earlier (Table III-2).

The coefficient values estimated for the bead shape and yield equations are listed in Tables III-8 and III-9. Table III-10 showed the results of aspect ratios for each run of central composite design. The coefficient values for the three dependent factors (water level (W), spheronizer time (ST) and spheronizer speed (SS)) in the bead model were -0.11, -0.07 and -0.16 respectively, and the p-values for all three factors were less than 0.1, suggesting that the bead shape was significantly affected by water level, spheronizer time and spheronizer speed. The terms W*ST, W*SS, SS*ST represent second order interactions between W and ST, W and SS and SS and ST, respectively. The estimated coefficient values for these interactions were -0.05, -0.075 and -0.05 and the p-values were less or equal to 0.10. For all higher order terms W^2, SS^2 and ST^2, the p-values were greater than 0.10, indicating these were non-significant factors. The coefficient estimates and the p-values obtained for the main effects in the yield equation show that the yield of beads is dependent primarily on the water level. The corresponding values for the W*ST, W*SS and SS*ST interaction terms suggest no significant interaction. All of the higher order terms, except for the water level, had a p-value of 0.0074, and the equations found by pooling the non-significant terms (p-values > 0.10) with the errors resulted in:

Bead shape = 1.51 -0.11 W -0.16 SS -0.07 ST -0.075 W*SS -0.05*W*ST -0.05 SS*ST

Yield = 61.62+ 14.49* W -14.12*W^2

where, W is water level, SS is the spheronizer speed, and ST is the spheronizer time. All of the individual terms in the above models were statistically significant (p-value ≤ 0.10). Note that the water level, spheronization speed and spheronization time were significant factors for bead shape. For yield, however, only water level was found to be a significant factor. In addition, interactions of water level with spheronization speed, water level with spheronization time and spheronization speed and spheronization time were also significant factors for beads shape. Based upon the above fitted equations, the predicted yield and bead shape surface map were constructed. Figures III-30 and III-31 illustrate the three-dimensional predicted surface map and profiler for the predicted yield and shape. The vertical dotted line for each factor shows its current value or current setting. The horizontal dotted line shows the current predicted value of yield or bead shape for the current values of factors. The black lines within the plots show how the predicted value changes when you change the current value of an individual factor. In fitting platforms, the 90% confidence interval for the predicted values is shown by a dotted blue curve surrounding the prediction trace. The maximum yield occurs in the region where water level was between 55 and 57%. At low spheronization speed, between 1000 and 1400 rpm, the yields stayed nearly same, then the yields decreased as spheronization speed was increased. For spheronization time, the yields decreased as spheronization time was increased. The better bead quality in terms of sphericity was obtained in the region with high water level, high spheronization speed and longer spheronization time. After taking into consideration both the yield and quality of beads, the combination of 55-57% water level, medium spheronization speed (1400 rpm) and high spheronization time (300 sec) was deemed the optimal condition for batches.

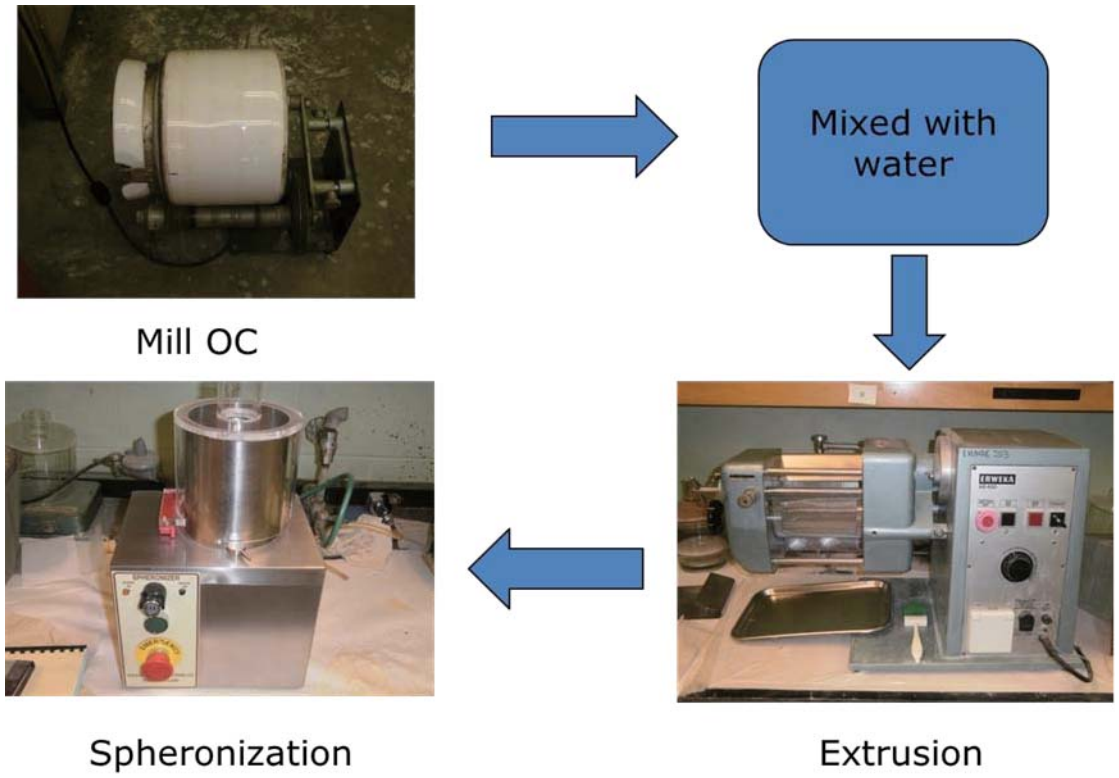

Figure III-29 : The process of preparation of oxidized cellulose pellets/beads.

Table III-7 Table of central composite fractional factorial experimental design (α = 1)

Run	Water added	Spheronizer Speed (rpm)	Spheronizer Time (sec)	Yield %	Bead shape (Aspect ratio)
1	0.48	1400	195	51.6	1.7
2	0.53	1000	195	60.1	1.8
3	0.58	1400	195	47.1	1.4
4	0.58	1800	90	66.1	1.4
5	0.53	1400	195	57.9	1.4
6	0.58	1000	90	65.5	1.8
7	0.58	1000	300	59.4	1.6
8	0.53	1800	195	52.2	1.4
9	0.48	1000	90	49.7	1.7
10	0.53	1400	195	57.9	1.5
11	0.53	1400	90	75	1.6
12	0.53	1400	300	71.5	1.5
13	0.48	1800	90	33.9	1.7
14	0.48	1800	300	18.8	1.5
15	0.48	1000	300	20.8	1.8
16	0.58	1800	300	41.6	1.2

Table III-8. Bead shape equation coefficient estimates.

Term	**Estimate**	**t-value**	***p*-value**
Intercept	1.51	43.09	0.00
Water level (W)	-0.11	-4.69	0.00
Spheronizer Speed (SS)	-0.16	-6.83	0.00
Spheronizer Time (ST)	-0.07	-2.99	0.02
W*SS	-0.08	-2.86	0.03
W*ST	-0.05	-1.91	0.10
SS*ST	-0.05	-1.91	0.10
W*W	0.01	0.15	0.89
SS*SS	0.06	1.25	0.26
ST*ST	0.01	0.15	0.89

Table III-9. Yield equation coefficient estimates.

Term	Estimate	t-value	p-value
Intercept	61.62	11.25	0.00
Water level (W)	14.49	3.96	0.01
Spheronizer Speed (SS)	-0.29	-0.08	0.94
Spheronizer Time (ST)	-3.81	-1.04	0.34
W*SS	5.08	1.24	0.26
W*ST	6.68	1.63	0.15
SS*ST	4.43	1.08	0.32
W*W	-14.13	-1.98	0.09
SS*SS	-7.36	-1.03	0.34
ST*ST	9.77	1.37	0.22

Table: III- 10 Results of aspect ratios for each run of central composite design.

Run #	1	2	3	4	5	6	7	8	9	10	11	12	13	14	15	16
Bead #	Aspect ratio	Aspect ratio	Aspect ratio	Aspect ratio	Aspect ratio	Aspect ratio	Aspect ratio	Aspect ratio	Aspect ratio	Aspect ratio	Aspect ratio	Aspect ratio	Aspect ratio	Aspect ratio	Aspect ratio	Aspect ratio
1	1.8	1.6	1.2	2.0	1.5	2.5	1.9	1.1	2.3	1.9	1.9	1.4	2.8	1.1	2.3	1.2
2	1.7	1.8	1.8	1.9	1.5	1.6	1.5	1.5	1.9	2.2	1.2	1.5	1.5	2.3	1.3	1.1
4	2.0	4.5	1.3	1.2	1.1	2.6	1.4	1.1	1.8	1.1	1.8	1.6	1.1	2.2	2.5	1.1
5	1.9	1.3	1.1	1.0	1.0	2.2	1.0	1.3	1.0	1.0	1.6	1.1	1.3	1.3	1.1	1.1
6	1.1	1.1	1.3	1.3	1.3	1.1	1.6	1.1	2.8	1.1	1.1	1.8	1.1	1.8	1.3	1.1
7	1.8	1.6	1.7	1.2	1.0	1.2	1.7	1.4	1.5	1.4	2.0	2.0	1.4	1.6	2.2	1.4
8	1.5	1.1	1.4	1.5	1.1	1.3	1.8	1.2	2.0	1.6	1.3	1.3	1.2	1.1	1.7	1.2
9	2.2	1.4	2.0	1.1	1.3	2.5	1.1	1.9	1.5	1.0	1.3	1.2	1.9	1.1	1.4	1.0
10	2.0	1.6	1.1	1.0	1.3	1.8	1.6	1.3	1.5	1.7	1.0	2.2	1.3	1.5	2.0	1.0
11	1.3	1.0	2.0	1.7	1.1	1.8	1.4	1.1	1.1	1.1	2.0	2.1	1.1	1.1	1.1	1.1
12	1.0	1.6	1.0	1.4	2.4	1.2	1.3	1.2	1.0	1.5	1.6	1.6	2.2	1.1	1.6	1.1
13	1.7	1.2	2.5	1.2	1.2	1.5	1.0	1.5	1.7	1.3	1.8	1.4	1.5	2.4	2.6	1.0
14	1.2	2.2	1.1	1.7	1.0	2.2	2.1	1.2	1.2	1.8	1.2	1.2	1.2	1.6	1.6	1.3
15	2.3	1.2	1.5	1.1	2.7	1.3	2.1	2.0	1.2	1.2	1.6	1.7	3.4	1.6	1.3	1.2
16	1.7	3.9	1.1	1.1	1.5	2.5	1.9	1.2	1.7	1.9	1.6	1.1	2.2	1.4	1.7	1.2
17	2.1	1.4	1.3	1.8	1.9	1.6	1.8	1.8	1.8	1.6	2.0	1.0	1.8	1.8	2.4	1.1
18	1.5	1.8	1.7	1.1	1.2	1.1	1.9	1.8	1.9	1.2	1.5	1.4	2.7	1.5	1.9	1.2
19	1.2	2.1	1.2	1.2	1.6	2.4	1.4	1.2	1.6	2.0	1.8	1.8	1.2	1.6	2.8	1.0
20	1.2	2.3	1.1	1.3	1.1	2.5	1.5	1.8	1.5	1.5	1.7	1.5	2.5	1.3	1.7	1.0
21	1.8	1.4	1.0	1.7	1.7	1.4	2.2	1.6	2.5	1.6	1.1	1.4	1.6	1.1	1.3	1.1
22	1.9	1.5	1.1	1.9	1.4	2.4	1.8	1.0	2.2	1.8	1.8	1.3	2.7	1.0	2.2	1.1
23	1.8	1.7	1.1	1.8	1.4	1.5	1.4	1.4	1.8	2.1	1.1	1.4	1.4	2.2	1.2	1.0
24	2.1	4.4	1.7	1.1	1.0	2.5	1.3	1.0	1.7	1.0	1.7	1.5	1.0	2.1	2.4	1.0
25	2.0	1.2	1.2	1.1	2.1	3.1	1.6	2.6	2.0	3.0	2.0	1.8	2.8	1.8	2.8	1.5
26	1.2	1.0	1.0	1.2	1.2	1.0	1.5	1.0	2.7	1.0	1.0	1.7	1.0	1.7	1.2	1.0

Table III-10 (continued)

Run #	1	2	3	4	5	6	7	8	9	10	11	12	13	14	15	16
Bead #	Aspect ratio	Aspect ratio	Aspect ratio	Aspect ratio	Aspect ratio	Aspect ratio	Aspect ratio	Aspect ratio	Aspect ratio	Aspect ratio	Aspect ratio	Aspect ratio	Aspect ratio	Aspect ratio	Aspect ratio	Aspect ratio
27	1.9	1.5	1.2	1.1	1.1	1.1	1.6	1.3	1.4	1.3	1.9	1.9	1.3	1.5	2.1	1.3
28	1.6	1.0	1.6	1.4	1.0	1.2	1.7	1.1	1.9	1.5	1.2	1.2	1.1	1.0	1.6	1.1
29	2.3	1.3	1.3	1.0	1.2	2.4	1.0	1.8	1.4	0.9	1.2	1.1	1.8	1.0	1.3	1.1
30	2.1	1.5	1.9	1.1	2.1	3.1	4.1	2.1	3.1	2.1	3.1	2.1	3.1	1.8	2.8	1.8
31	1.4	1.1	1.0	1.6	1.0	1.7	1.3	1.0	1.0	1.0	1.9	2.0	1.0	1.0	1.0	1.0
32	1.1	1.5	1.9	1.3	2.3	1.1	1.2	1.1	1.1	1.1	1.1	1.1	1.1	1.1	1.1	1.1
33	1.8	1.1	1.1	1.1	1.1	1.4	1.1	2.1	3.1	2.0	2.0	2.0	2.0	2.0	2.0	2.0
34	1.3	2.1	2.4	1.6	1.1	2.1	2.0	1.1	1.1	1.7	1.1	1.1	1.1	1.5	1.5	1.2
35	2.4	1.1	1.0	1.0	2.6	1.2	2.0	1.9	1.1	1.1	1.5	1.6	3.3	1.5	1.2	1.1
36	1.8	3.8	1.4	1.0	1.4	2.4	1.8	1.1	1.6	1.8	1.5	1.0	2.1	1.3	1.6	1.1
37	1.7	1.3	1.0	1.7	1.8	1.5	1.7	1.7	1.7	1.5	1.9	1.1	1.1	1.1	1.1	1.1
38	1.6	1.7	1.3	2.1	1.6	2.6	2.0	1.2	2.4	2.0	2.0	2.0	2.0	2.0	2.0	1.5
39	1.9	1.9	1.9	2.0	1.6	1.7	1.6	1.6	2.0	2.3	1.3	1.6	1.6	2.4	1.4	1.2
40	1.8	4.6	1.4	1.3	1.2	2.7	1.5	1.2	1.9	1.2	1.9	1.7	1.2	2.3	2.6	1.2
41	1.0	1.4	1.2	1.1	1.1	2.3	1.1	1.4	1.1	1.1	1.7	1.2	1.4	1.4	1.2	1.2
42	1.7	1.2	1.4	1.4	1.4	1.2	1.7	1.2	2.9	1.2	1.2	1.9	1.2	1.9	1.4	1.2
43	1.4	1.7	1.8	1.3	1.1	1.3	1.8	1.5	1.6	1.5	2.1	2.1	1.5	1.7	2.3	1.5
44	2.1	1.2	1.5	1.6	1.2	1.4	1.9	1.3	2.1	1.7	1.4	1.4	1.3	1.2	1.8	1.3
45	1.9	1.5	2.1	1.2	1.4	2.6	1.2	2.0	1.6	1.1	1.4	1.3	2.0	1.2	1.5	1.1
46	1.2	1.7	1.2	1.1	1.4	1.9	1.7	1.4	1.6	1.8	1.1	1.3	2.3	1.7	2.7	1.7
47	1.1	1.1	2.1	1.8	1.2	1.9	1.5	1.2	1.2	1.2	2.1	2.2	1.2	1.2	1.2	1.2
48	1.6	1.7	1.1	1.5	2.5	1.3	1.4	1.3	1.1	1.6	1.7	1.7	2.3	1.2	1.7	1.2
49	1.1	1.3	1.4	1.3	1.3	1.6	1.1	1.6	1.8	1.4	1.9	1.5	1.6	2.0	2.0	1.5
50	2.2	2.3	1.2	1.8	1.1	2.3	1.6	1.6	1.6	1.6	1.6	1.6	1.6	1.6	1.6	1.6
51	1.6	1.3	1.6	1.2	1.4	1.4	1.6	1.6	1.6	1.6	1.6	1.6	1.6	1.6	1.6	1.6

Table III-10 (continued)

Run #	1	2	3	4	5	6	7	8	9	10	11	12	13	14	15	16
Bead #	Aspect ratio	Aspect ratio	Aspect ratio	Aspect ratio	Aspect ratio	Aspect ratio	Aspect ratio	Aspect ratio	Aspect ratio	Aspect ratio	Aspect ratio	Aspect ratio	Aspect ratio	Aspect ratio	Aspect ratio	Aspect ratio
52	2.0	4.0	1.2	1.2	1.6	2.6	2.0	1.3	1.8	2.0	1.7	1.2	2.3	1.5	1.8	1.3
Avg	1.7	1.8	1.4	1.4	1.4	1.8	1.6	1.4	1.7	1.5	1.6	1.5	1.7	1.5	1.8	1.2

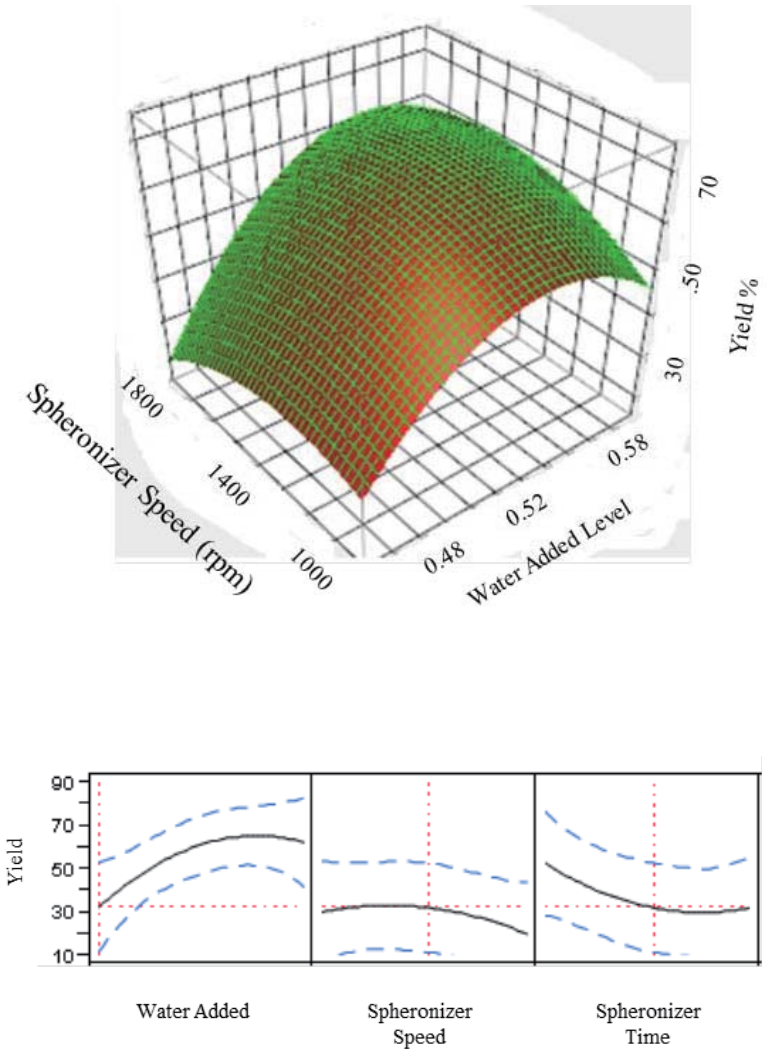

Figure III-30: The predicted surface plots and profiler for yield of OC beads.

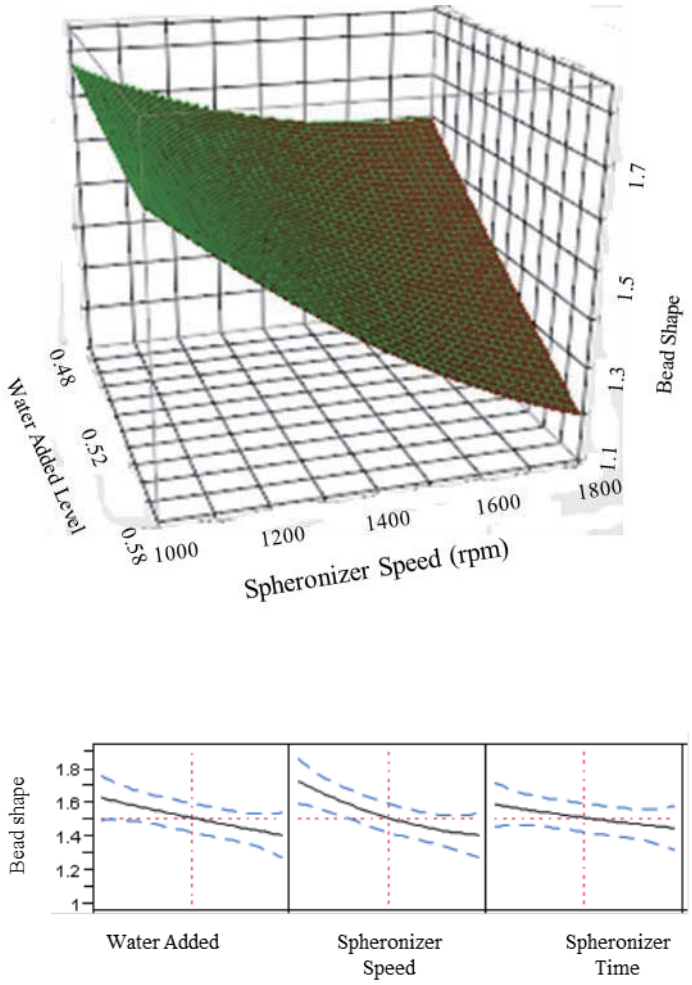

Figure III-31: The predicted surface plots and profiler for shape of OC beads.

CHAPTER IV

APPLICATION OF OXDIZED CELLULOSE BEADS in TACE

Introduction

Transarterial chemoembolization (TACE) has been practiced in patients for over 30 years. TACE results in a high intratumoral concentration of chemotherapy drugs and ischemic injury of tumor cells due to the fact that the chemotherapy agents are delivered directly into the artery and the arterial flow is temporarily decreased through embolization of the parent vessel (*3*). It is expected that drug eluting beads (DEB)-TACE decreases the systemic toxicity of the chemotherapeutic agent by limiting the exposure to only local tissues. In vivo data confirmed the slow sustained release of the drug. Doxorubicin-eluting beads provide a sustained delivery of drug for a period of 1 month and keep local tissue concentrations above a cytotoxic threshold in hepatocellular carcinoma (HCC)-bearing livers (*133*). Several bead/microsphere delivery systems varying in sizes from 40 μm to as high as 1200 μm, have been developed for TACE (Table IV-1). These beads were comprised of non-biodegradable polymer such as tris-acryl cross-linked with gelatin and poly(vinyl alcohol) (PVA) or biodegradable polymers such as chitosan and alginate. The limitations of current bead systems used for TACE are low drug loading and a limit to water-soluble drugs. The drug loading methods used in these bead systems were either ion-exchange or expanding-loading-shrinking. These methods typically achieve drug loading ≤ 10% drug loading. The other limitation for

Table IV-1: Currently available beads used for TACE.

Name	Material	Size ranger (µm)	Drug loading method	Drug	Source
DC beads	Modified PVA beads.	100-900	Ion-exchange	Positive charge drug and max 5% loaded	Biocompatibles, Farnham, UK.(*9*),(*10*),(*12*)
Tris-acryl gelatin beads	Tris-acryl gelatin	40-1200	Dipolar dipolar attraction	Water soluble drug and max 10% loaded	Biosphere Medical, Rockland,MA.(*7*)
Quadraspheres microspheres	poly(vinly alcohol-sodium acrylate) copolymer	50-200	Ion-exchange	Positive charge drug and max 5% loaded	BioSphere Medical, Roissy-en-France, France.(*14*)
Chitosan microsphere	Cross linked Chitosan	45-100	E-L-S	Water soluble drug and max 10% loaded	Kim et al. (*15*)
Chitosan coated alginate microspheres	alginate	100-400	W/O emulsion	Water soluble drug and max 6 5% loading efficiency	Misirli et al. (*16*)

the currently used biodegradable TACE beads are only available in a narrow size range. In instances where treatment is not complete or the tumor recurs, physicians would like to be able to access a tumor on multiple occasions in order to administer additional TACE treatments, as needed. It may not be possible to re-enter the feeding artery once this artery had been occluded by non-biodegradable beads, however.

Recently, considerable interest has been focused on the use of carboxyl-functionalized cellulose (6-carboxycellulose-commonly referred to as oxidized cellulose (OC)) as a drug carrier and a biomaterial. Oxidized cellulose with 3 to 25% carboxylic acid content is biodegradable and biocompatible (*134*). Currently, OC containing 16-24% free carboxylic acid groups is used in humans as a hemostatic agent and as a post surgical adhesion barrier (*82*). Studies show that OC also possesses antibacterial, (*135*) antitumor, (*136*) immunostmulant, (*137*) and wound healing properties (*138, 139*). Owing to the presence of carboxyl groups, it also serves as an immobilizing matrix for a variety of amine drugs, (*140-145*) for enzymes, (*146*) and for proteins. (*147*) Despite these properties, OC has seen a very little use in pharmaceutical formulation.

Methotrexate (MTX) is a common anticancer drug used for chemotherapy (Figure I-18). It is freely soluble in dilute solutions of alkaline hydroxides and carbonates; it is slightly soluble in dilute hydrochloric acid. The solubility changes from ~38 mg/mL in pH 7.4 buffer to ~ 2 mg/mL in pH 5.5 buffer (*101*). MTX has four pK_as due to the two amino groups and two carboxylic acid groups in the stucture. The basic pK_a values for the 2,4-diaminopteridine sections are less than 0.5 and 5.32. The acidic pK_a values for the p-aminobezoylglutamic acid are 4.83 and 3.76. Methotrexate decomposes upon melting at a temperature of 185-204 ^{o}C (*102*).

As a chemotherapeutic agent, MTX has been used in the treatment of several forms of cancer, and it is administered in high doses. The administration of large doses of MTX results in systemic toxicity. MTX is cell-cycle phase specific whereby prolonged exposure of the drug to the cancer cells is necessary for optimal efficacy. Sustained-release of this drug over a long period of time could improve MTX therapies and some sustained-release forms have been studied. MTX- loaded in OC18-chitosan cylinder (*121*), MTX-loaded poly lactide co-glycolide (PLGA) microspheres (*103*), methotrexate-loaded poly(ϵ-caprolactone)(PCL) implants (*104*) and MTX-loaded poly(lactic acid) (PLA) (*105*) systems have been studied, and slow release rates were shown in vitro. No degradation of MTX was reported during slow release. MTX was chosen as a model drug for this study due to its low water solublility to show that water insoluble drug can be used in TACE.

To overcome the limitations of current bead systems, the goal of thesis is to develop biodegradable beads which have wide size ranges, can achieve high drug loading and high drug loading efficiency, and can load water-soluble and water-insoluble drugs. In this study, the preparation and characterization of OC base beads is presented. The starting OC material contains 17% carboxylic acid content. Methotrexate (MTX) loaded OC17 beads were prepared by using an extrusion/spheronization method.

Experimental

Materials

Oxidized cellulose (OC) was prepared as described in chapter III. Acetonitrile was HPLC grade (Fisher Scientific, Fair Lawn, NJ). Potassium phosphate monobasic, sodium chloride, citric acid, dibasic sodium phosphate and streptomycin sulfate were all from Fisher Scientific (Fair Lawn, NJ). Methotrexate was received as a gift from the Monsanto Co. (Danton, OH). Carbopol@ 974P NF (carbomer) was from the BF Goodrich Co. (Cleveland OH). Omnipaque was obtained from GE Healthcare Inc. (Princeton, NJ).

Preparation of Oxidized Cellulose Beads

Oxidized celluloses (OCs) containing 17% carboxylic acid content were used as starting materials. An appropriate amount of water was added to the dry OC17 powder to obtain a wet mass. The ratio of OC powder to water ranged between 1: 0.8 to 1: 1.2 (w/w). The extruded mass was passed through an oscillating granulator (Erweka AR400, Erweka, Heusenstamm, Germany) equipped with different screen sizes (700 μm, 500 μm and 250 μm). The rod-shaped extrudate was spheronized into beads using a spheronizer (Spheronizer 120, Caleva, UK) at 1400 rpm for around 5 min. The beads were dried at room temperature

Preparation of Oxidized Cellulose/Carbomer Beads

Weight ratios of OC17 to Carbopol@ 974NF varied from 95:5 to 90:10. OC17 powder and Carbopol@ 974NF powder were added to a V-blender (Model LB429,

Patterson Kelley Co., East Stroudsburg, PA) with a blending time of ~ 45 minutes. An appropriate amount of water or a mixtures of water and ethanol (the ratio of water and ethanol ranged between 100:0 to 0:100) was added to the dry powder to obtain a wet mass. The ratio of OC17 powder to water or a water/ethanol mixture was from 1:0.8 to 1:1.2 (w/w). The extruded mass was passed through an oscillating granulator (Erweka AR400, Erweka, Heusenstamm, Germany) equipped with different sizes of screens (700 μm, 500 μm and 250 μm. The rod-shaped extrudate was spheronized into beads using a spheronizer (Spheronizer 120, Caleva, UK) at 1400 rpm for ~ 5 min.

Preparation of Oxidized Cellulose/MTX Beads

Ratios of OC17 to MTX were varied between 95:5 and 3:2. OC17 powder and MTX powder were added to a V-blender with a blending time is ~ 45 minutes. Appropriate amounts of water were added to the dry powder to obtain a wet mass. The ratio of OC/MTX powder to water ranged between 1:0.8 to 1:1.2 (w/w). The wet mass was passed through an oscillating granulator (Erweka AR400, Erweka, Heusenstamm, Germany) equipped with screen sizes of 700 μm, 500 μm or 250 μm. The rod-shaped extrudate was spheronized into beads using a spheronizer (Spheronizer 120, Caleva, UK) at 1400 rpm for ~ 5 min. The beads were dried at room temperature.

Preparation of Oxidized Cellulose/Carbomer/MTX Beads

The weight ratio of OC17 to Carbopol$^{@}$ 974NF was varied from 95:5 to 90:10. The ratio of OC17/Carbopol$^{@}$ 974 NF mixture to MTX was varied from 95:5 to 3:2. OC17, carbomer and MTX powder were added to a V-blender with a blending time of

approximately 45 minutes. An appropriate amount of water or mixture of water and ethanol (the ratio of water and ethanol was 70:30) was added to the dry powder to obtain a wet mass. The ratio of powder mixture to liquid ranged between 1:0.8 to 1:1.2 (w/w). The wet mass was passed through an oscillating granulator (Erweka AR400, Erweka, Heusenstamm, Germany) equipped with various screen sizes, 700 μm, 500 μm or 250 μm. The rod-shaped extrudate was spheronized into beads using a spheronizer (Spheronizer 120, Caleva, UK) at 1400 rpm for ~ 5 min. The beads were dried at room temperature.

Preparation of pH 7.4 Phosphate Buffered-Saline Solution

Potassium phosphate monobasic (0.6 g), sodium chloride (36.0 g), sodium phosphate dibasic (3.2 g), and streptomycin sulfate (0.4 g) were dissolved in distilled water. The volume was made to 4.0 L with water. The resulting solution was then passed through a 0.45 μm filter membrane (Xperteck Filters, Nylon 66, P. J. Cobert Associates, Inc., St. Louis, MO). The ionic strength of this solution was 0.165 M.

HPLC Analysis of Methotrexate (MTX)

The USP HPLC method was used to analyze MTX in release samples and to assess bead content.(*121, 148*) A Shimadzu HPLC system (Shimadzu Corporation, Columbia, Maryland), which consisted of a pump (Model LC-10AT), a system controller (Model SCL-10A), an auto injector (Model SIL-10A), an ultraviolet-visible spectrophotomeric detector (Model SPD-10AV) and a data processor/recorder (Model C-R5A) was used. Analyses were carried out on a Zorbax RX-C8 (5 μm; 4.6 mm x 250 mm, Mac-Mod Analytical, Inc., Chadds Ford, PA) reversed-phase analytical column. The

mobile phase contained a 9:1 (v/v) ratio of pH 6.0 citrate phosphate buffer solution and acetonitrile. The pH 6.0 buffer solution was prepared by mixing 370 mL of 0.1 M citric acid solution with 630 mL of 0.2 M dibasic sodium phosphate solution, and then adjusting the pH to 6.0 by adding either 0.1 M citric acid or 0.2 M phosphate buffer solution as needed. The mobile phase was filtered through a 0.45 μm nylon filter membrane (Chrom Tech. Inc., Apple Valley, MN), and then degassed using a Bransonic Ultrasonic cleaner (Model 5200, Bransonic Ultrasonic Corp., Danbury, CT) for 10 minutes before use. The mobile phase flow rate was 1 ml/min and the effluent was detected at 302 nm. Each sample for assay was filled into a 1.5 ml HPLC sample vial, covered with a screw cap and a rubber seal and placed in the autosampler. The injection volume was 10 μl.

MTX standards were stored at in room temperature up to 14 days. The concentrations of MTX standards were from 24 μg/ml to 394 μg/ml. MTX standards were measured by above method at 0, 1, 3, 7 and 14days. Calibration curves for each concentration are obtained to evaluate whether any degradation is happened for MTX.

Drug Loading Determination Method

MTX-loaded beads of varying ratios of MTX to OC17 or OC17/carbomer were ground to fine powders and portions (4~5 mg) were weighed and dispersed in 20 mL of pH 7.4 phosphate buffer. The dissolved sample was analyzed. The dispersion was shaken on a wrist action shaker (Model 75, Burrell Corp., Pittsburgh, PA) for 0.5 to 1 h. A 1 ml aliquot was withdrawn and appropriately diluted for HPLC assay. The diluted solution was filtered through a Gelman syringe filter unit (Nylon Acrodisc, 0.45 μm) and then

injected into an HPLC column for drug analysis. The percent drug loading in the sample and the drug entrapment efficiency were calculated by:

$$\text{Drug loading (\%)} = \frac{\text{MTX weight measured}}{\text{Sample weight}} * 100 \qquad \text{Eqn IV - 1}$$

$$\text{Entrapment efficiency (\%)} = \frac{\text{\% Drug loading}}{\text{\% Drug in initial mixture of fine powders}} * 100 \qquad \text{Eqn IV - 2}$$

True Density Determination

A helium displacement micropycnometer (Model MPY-2, Quantachrome Corp., Boynton Beach, FL) was employed for true density determination. Samples of polymer were dried in a vacuum desiccator (Model 68351, Precision Scientific Co., Chicago, IL) at 60^{o}C and at a reduced pressure of 40 mm Hg for 24 h before testing. Sample weights of ~ 1g (accurate measured) were used for analysis. The sample was out-gassed with helium for at least 40 minutes before each measurement. The control switch was turned to "cell out (P1)," followed by pressurizing the system to between 15 and 17 psi with helium, holding this pressure for one minute, and then the pressure was recorded. The control switch was then turned to the "cell in (P2)" position and the pressure value reading was recorded after one minute. The true density was calculated by dividing the mass of the material by its volume, obtained from:

$$V_p = V_c - V_r (P_1/P_2 - 1)$$

where, V_p is the sample volume, V_c is the cell volume, V_r is the reference volume, and P_1 and P_2 are as defined above.

Bulk/Tap Density Determination

Bulk density (ρ_{bulk}) was determined in a 100 mL graduated cylinder and calculated by: ρ_{bulk} = mass/volume. Tap density (ρ_{tap}) was determined after 1200 taps using a VanKel tap density analyzer (Model 50-1000, VanKel Industries, Cary, NC). More specificly, bulk density (ρ_{bulk}) was determined using a 100 ml graduated cylinder filled with 20 g of sample. The cylinder was tapped twice to remove the powder adhering to the walls, prior to recording the volume. Bulk density was calculated as: ρ_{bulk} = mass/volume. For tap density, the same graduated cylinder used to measure bulk was tapped 1,200 times using a VanKel tap density analyzer (Model 50-1000, VanKel Industries, Cary, NC). No further reduction in the tap volume was noted after 1,200 taps. The volume of the sample was then read and tap density calculated as ρ_{tap} = mass/volume. Density determinations were carried out in triplicate.

Bead Shape

The bead shape was characterized by optical microscopy (Olympus BX-60, Center Valley, PA, USA). Digital photos were taken using the built-in camera. Approximately 50 beads were randomly chosen and their aspect ratios (the ratio of longest feret to an orthogonal feret) was calculated and used to express the bead sphericity.

Swelling Test

The swelling value is expressed as the ratio of the expanded volume of the

OC17 or OC17/copolymer beads after being placed in PBS buffer compared to the initial beads volume. A sample of OC17 or OC17/carbomer (~ 1g) was manually dispersed in a 10 mL graduated cylinder filled with 10 mL of PBS buffer at room temperature. The cylinder was placed on a flat surface and the increase in bead volume was measured at a later time. The percentage swelling ratio was calculated by:

$$S = \frac{V_t - V_0}{V_0} X\ 100 \qquad \text{Eqn IV - 3}$$

where S is the swelling ratio (%); V_t is bead volume at time *t* and V_0 is the initial bead volume.

Physical Stability Test

OC17 or OC17/copolymer beads (~ 0.2g) were added to a 20 mL glass vial and 10 mL pH 7.4 PBS was added into vials. Then the samples were kept in an oven at 37 ^{o}C. The beads were examined for physical intergradations over an 8 weeks period.

Bead Compressibility

A flat, 5 mm diameter cylindrical probe was attached to Material Testing System Model LFplus (Lloyd Instruments, West Sussex, UK) equipped with a 50N load cell. A single bead of 700-900 μm size was placed on the sample pan beneath the probe. Bead was hydrated by water. Excess water was removed from the sample by wicking with tissue. The probe was positioned just above the sample. At 1st cycle, a force was applied to the probe at a rate of 10 mm/min until the bead showed a 15% compression strain.

Then force was released. At 2nd cycle, apply force to the bead until 15% compression strain at a rate of 10 mm/min. Five beads were tested. The percentage recovery was calculated by:

$$\text{Recovery (\%)} = \frac{\text{Force at 2nd cycle}}{\text{Force at 1st cycle}} * 100 \qquad \text{Eqn IV - 4}$$

Bead Suspendibility

Beads (~ 0.5 g) were mixed with 10 mL of a 1:1 (v/v) mixture of Omnipaque® 350 contrast medium and 10% PVP-saline solution. The homogeneity of this suspension was visually monitored. The mixture was considered homogeneous when the beads remained suspended in the dispersion medium for more than 1 min.

Bead Deliverability by Catheter

Bead deliverability was assessed by rating the ease of administration through a microcatheter. Different sized needles were employed to deliver different sized beads, with the acceptance criteria of pass/failure based on whether the lumen of the needle was occluded during delivery.

Release Study Using the T-apparatus

A dissolution test was carried out using a T-apparatus with pH 7.4 PBS solution (200 ml) at 37 ^{o}C (n=3); the rate of flow was set at ~ 50 ml/min(*149*). The apparatus was composed of a horizontal tube (internal diameter: 12 mm; length: 150 mm) connected to a cylindrical sealed tube (internal diameter: 8 mm; depth:

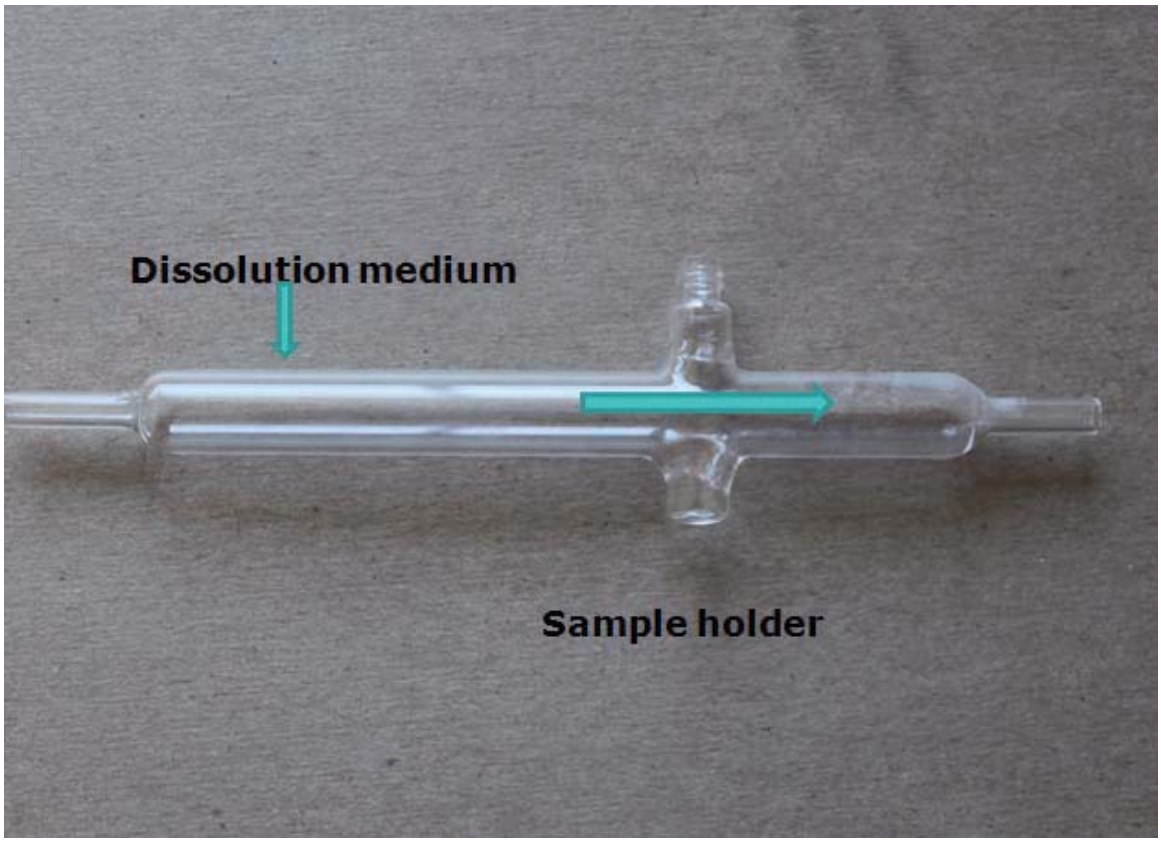

Figure IV-1: Diagram of T-cell of T-apparatus.

h=4 mm) (Fig. IV-1) (*150*). MTX loaded beads (~ 70 mg, 100 µm - 900µm) were used in the test. At appropriate times, 5 mL of medium was collected and immediately replaced with the same amount of the fresh medium. The amount of MTX released was measured by HPLC as described earlier.

Results and Discussion

Preparation of Oxidized Cellulose Beads

Oxidized cellulose beads containing 17% carboxylic acid content (OC17) were prepared by using extrusion/spheronization technology. The size range of beads produced by extrusion/spheronization ranged from 500 - 1500 µm. In order to produce 100 - 900 µm OC 17 beads, an oscillating granulator (Figure IV-2) was used. The granulator operates on the oscillating rotor principle by forcing materials through a sieve screen of a predetermined size. The sieve size determines the extrudate diameter. For producing different sizes of beads, 250, 500, 700 and 1000 µm screen sieves were used. The solid/liquid ratio during wetting and extrusion was the key parameter in developing a formulation for extrusion/spheronization. The water percentage required for producing different sized beads was determined and the results are given in Table IV-2. The percentage water content required for producing beads was decreased when the bead size decreased. During extrusion, the wet mass was compressed until water was squeezed out which then lubricates the particles flowing through the extruder. If the moisture is too low, the extrudate became more friable; with a higher moisture level, the extrudate becomes sticky and the extruded materials adhere to each other. When the sieve size was

decreased, greater force was needed to wet the mass and more water was squeezed out of the extruded mass.

Preparation of Oxidized Cellulose/Carbomer Beads

Carbopol® 974P is one member of the water-swellable carbomer family of polymers polymerized in ethyl acetate, a relatively non-toxic solvent, and is a polyacrylic acid. Carbopol® 974P swells up to 1000 times its original volume in water (*151*). When Carbopol® 974P is wetted, it becomes tacky, which introduces handling difficulties in the wet massing step with OC17during the extrusion–spheronization process (*152*). In near neutral or alkaline media, ionized carboxyls are formed and the negatively charged groups repel each other(*153*). Beads containing carbomer, MCC, and electrolytes were successfully manufactured by extrusion/spheronization (*152, 154*). These authors demonstrated that the electrolyte addition led to a decrease in the bioadhesive properties. In order to maintain the bioadhesive potentiality of the pellets, producing adhesive pellets containing Carbopol@ 974P by extrusion/spheronization without the addition of electrolytes was investigated. In this study, an ethanol-water mixture was used as the wetting liquid. The effect of ethanol was further investigated using different ratios of ethanol and water (100:0, 50:50 and 30:70). Figure IV-3 shows the optical photographs of OC17/carbomer beads obtained using different ratios of ethanol/water. With 100% ethanol, the resulting OC17/carbomer (95/5) beads were more irregular in shape. When the ratio of water and ethanol was 50:50 or 70:30, the shape of beads became more spherical.

Figure IV-2: Oscillating granulator used as an extruder.

Table IV-2. Water content required in wet mass for preparation of OC17 beads of different sizes.

Bead size	**Water content required (%)**
700-900 µm	52
500-700 µm	50
250 -500 µm	48
100- 250 µm	46

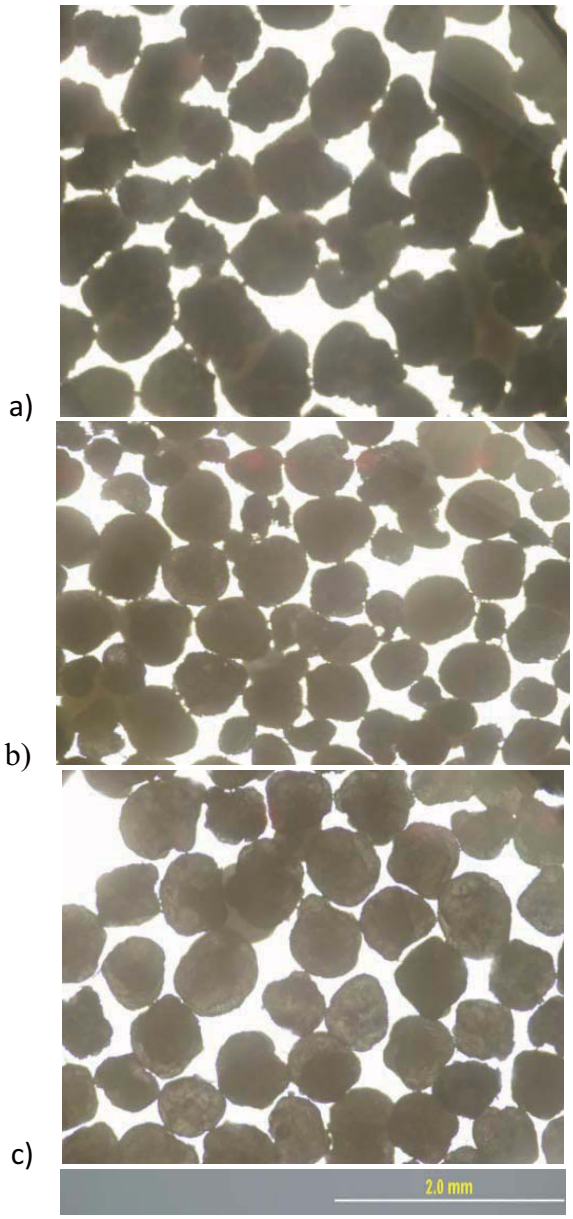

Figure IV-3: Optical micrographs of OC/carbomer (95/5) beads (700-900 μm) prepared using a) ethanol; b) ethanol:water (v/v) = 50:50; and c) ethanol:water (v/v) = 30:70 as granulating liquids.

Preparation of MTX Loaded OC17 Beads

OC17/MTX and OC17/carbomer/MTX beads were prepared by extrusion/spheronization. OC17 powder was physically mixed with appropriate amounts of MTX in a V-blender, corresponding to 95:5, 85:15, 4:1 and 3:2 dry weight ratios of OC17 and MTX. For OC17/carbomer/MTX formulations, the concentration of carbomer was kept at 5% and an ethanol/water mixture (30:70) was used as the wetting medium. Figures IV-4 – IV-7 show the micrographs of OC17/MTX beads with different concentrations of MTX, with size ranges from 100 to 900 μm. Figures IV-8 – IV-10 show OC17/carbomer MTX beads with different loading level of MTX with size ranges from 250 to 900 μm. Table IV-3 presents the wetting liquid concentrations which were used in the experimental design and which obtained the most spherical beads. All MTX-loaded beads appeared quite spherical in shape.

Determination of Drug Loading and Drug Loading Efficiency

Drug loading in the beads was determined by HPLC. The beads were ground into a powder and then extracted with pH 7.4 phosphate buffer. Table IV-3 lists the drug recovery from OC17/MTX powder containing different ratios of the OC 17 and MTX. Table IV-4 lists the drug recovery from OC17/carbomer/MTX powder containing different ratios of the OC 17/carbomer and MTX. The drug loading and drug loading efficiency were calculated according to Eqns IV-1 and IV-2. The results demonstrate that >99%

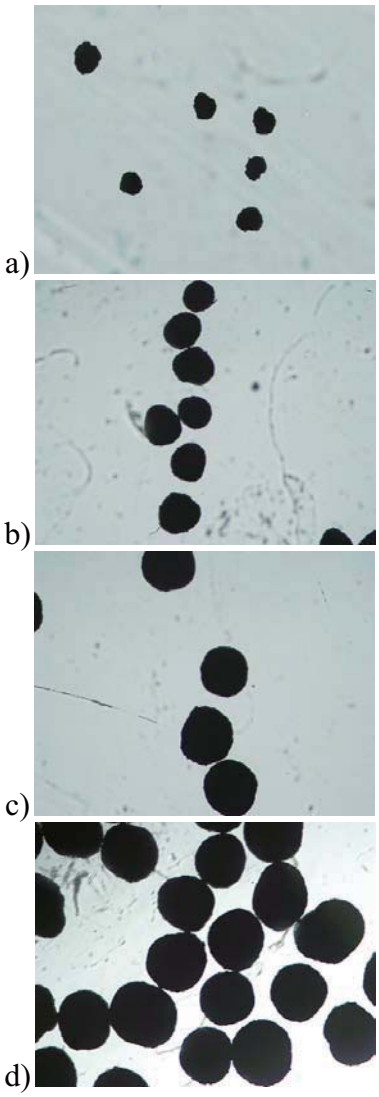

Figure IV-4: Optical micrographs of OC17/MTX (3:2) beads: a) 100-250 µm; b) 250-500 µm; c) 500-700 µm; d) 700-900 µm.

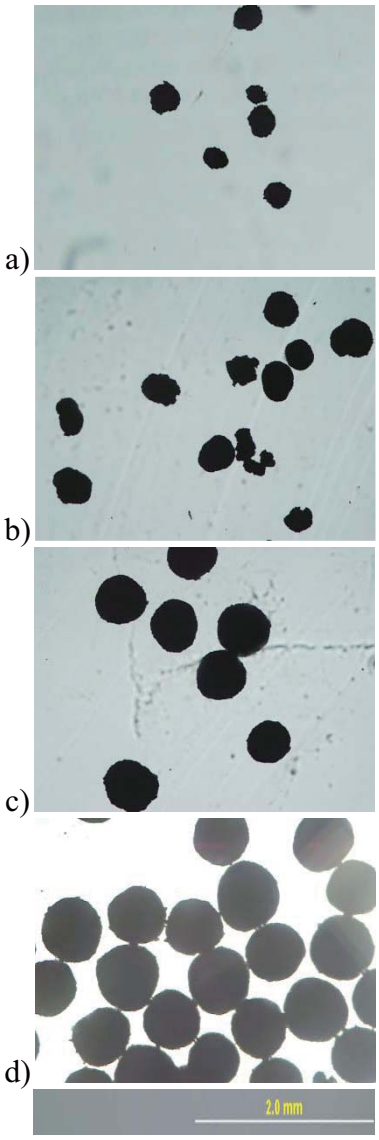

Figure IV-5: Optical micrographs of OC17/MTX (4:1) beads: a) 100-250 µm; b) 250-500 µm; c) 500-700 µm; d) 700-900 µm.

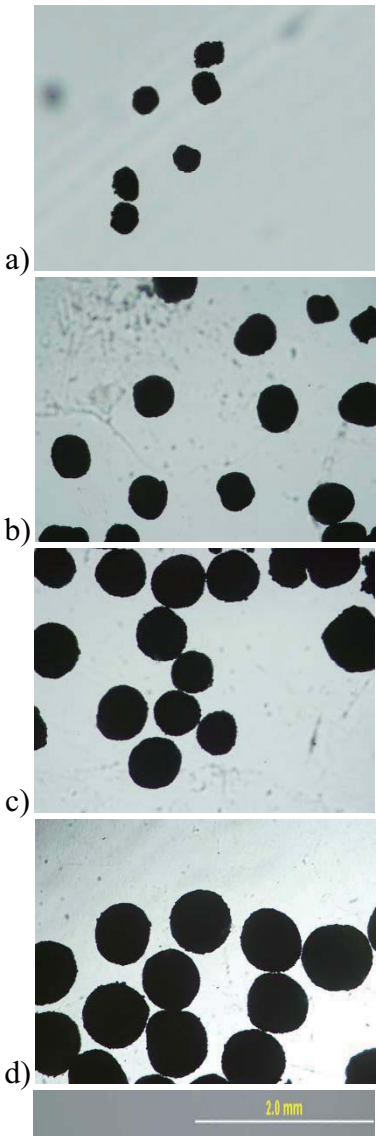

Figure IV-6: Optical micrographs of OC17/MTX (85:15) beads: a) 100-250 µm; b) 250-500 µm; c) 500-700 µm; d) 700-900 µm.

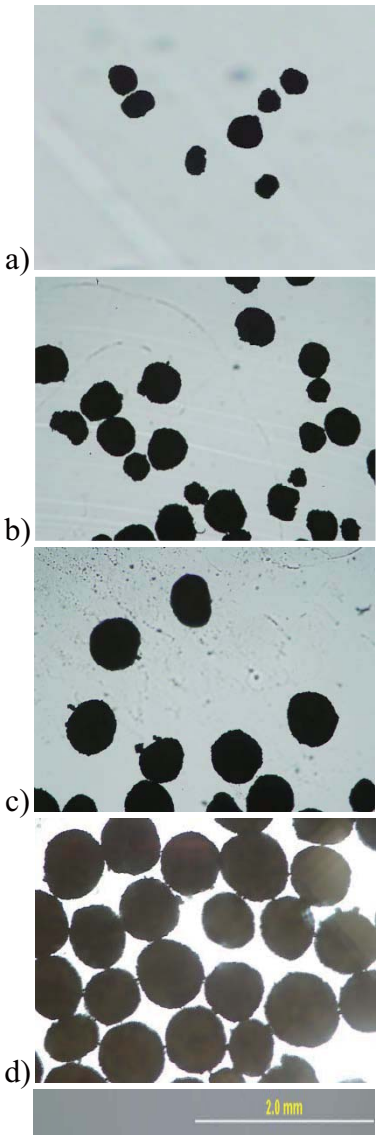

Figure IV-7: Optical micrographs of OC17/MTX (95:5) beads: a) 100-250 µm; b) 250-500 µm; c) 500-700 µm; d) 700-900 µm.

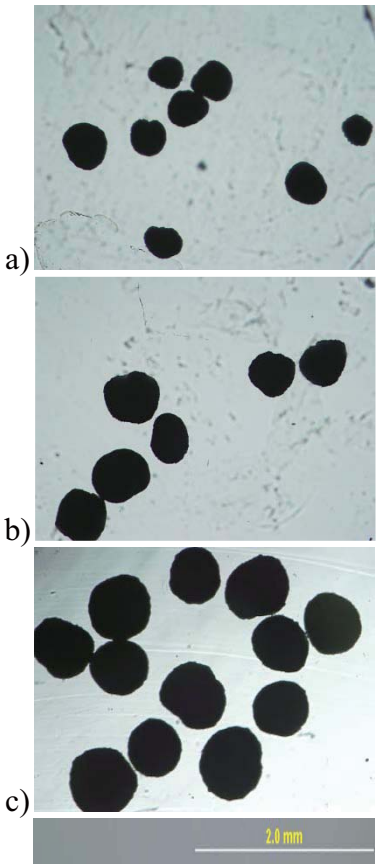

Figure IV-8: Optical micrographs of OC17/carbomer/MTX (55:5:40) beads: a) 250-500 µm; b) 500-700 µm; c) 700-900 µm.

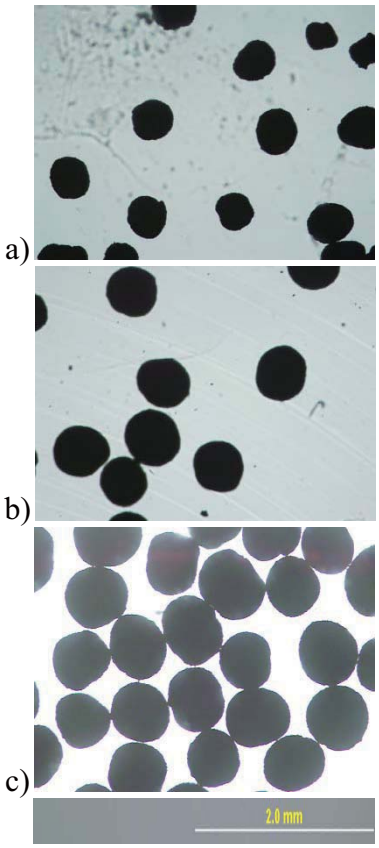

Figure IV-9: Optical micrographs of OC17/carbomer/MTX (70:5:25) beads: a) 250-500 µm; b) 500-700 µm; c) 700-900 µm

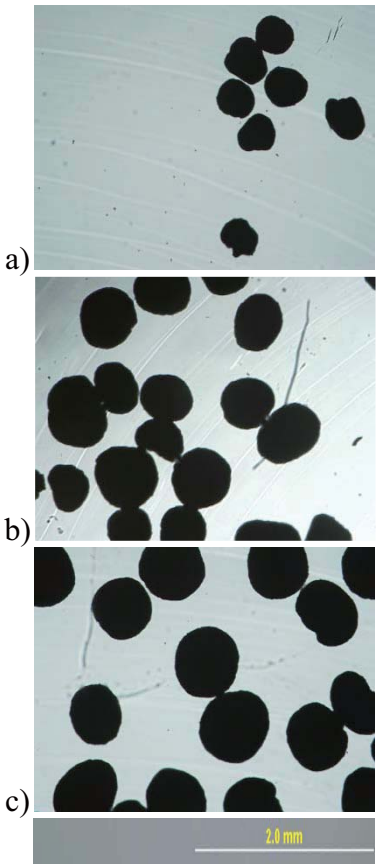

Figure IV-10: Optical micrographs of OC17/carbomer/MTX (90:5:5) beads: a) 250-500 µm; b) 500-700 µm; c) 700-900 µm.

Table IV-3: Drug loading and loading efficiency of OC17/MTX beads (700-850 μm). (n=3)

Sample	Drug content % (Theoretical)	Avg. drug content % (Experimental)	RSD(%)
OC17/MTX 95:5	5	5.05	0.13
OC17/MTX 85:15	15	15.24	0.98
OC17/MTX 4:1	20	20.72	0.63
OC17/MTX 3:2	40	40.43	1.45

RSD: relative stand deviation.

Table IV-4: Drug loading and loading efficiency for different sized OC17/MTX beads. (n=3)

Sample	Drug content % (Theoretical)	Avg. drug content % (Experimental)	RSD(%)
100-250 μm	15	15.25	0.51
250-500 μm	15	15.04	0.93
500-700 μm	15	15.14	0.30
700-900 μm	15	15.03	0.15

RSD: relative stand deviation.

Table IV-5: Drug loading and loading efficiency for OC17/carbomer/ MTX beads (700-850 μm) (n=3).

Sample	Drug content % (Theoretical)	Avg. drug content % (Experimental)	RSD(%)
OC17/carbomer/MTX 90:5:5	5	5.02	0.83
OC17/carbomer/MTX 70:5:25	15	15.63	0.91
OC17/carbomer/MTX 55:5:40	40	40.40	0.85

RSD: relative stand deviation.

Table IV-6: Drug loading and loading efficiency for different size of OC17/carbomer/MTX beads. (n=3)

Sample	Drug content % (Theoretical)	Avg. drug content % (Experimental)	RSD(%)
250-500 μm	15	15.15	1.80
500-700 μm	15	15.42	1.03
700-900 μm	15	15.16	1.50

RSD: relative stand deviation.

of the targeted of MTX amount was loaded into the beads, and the beads could hold up to 40% drug. Also, the bead size did not affect the drug loading efficiency. When drug content increased to 45%, lots of fines were obtained during spheronization. So the maximum drug content was kept at 40%.

Swelling Studies

Swelling values of the OC17 and OC17/carbomer beads in PBS (pH=7.4) buffer at 25 ^{o}C are shown in Figure IV-11. OC17 beads have a ~80% swelling ratio, and OC17 beads with 5 and 10% carbomer both have comparable swelling ratios of (~190%). When OC17 beads are placed in PBS pH=7.4 buffer at a pH higher than OC17's pK_a(3.5), the carboxylate moiety on the polymer backbone ionize, resulting in repulsion between the native charges, which adds to the swelling of the polymer. Carbomer homopolymers are acrylic acid polymers. In PBS buffer (pH=7.4), the carboxylate groups of carbomer are ionized and repel each other resulting in greater swelling. All beads reach equilibrium an swelling levels very quickly - within ~ 30 min. The swelling ratios don't increase significantly when carbomer content is increased from 5% to 10% in the formulation. Carbomer contents of 10% results in increased difficulty preparing beads, so the content of carbomer was kept at 5% in the formulation of OC17/carbomer beads.

Physical Stability Test

A physical stability test was conducted in PBS pH 7.4 buffer at 37 ^{o}C in a static environment. The physical stability test results are given in Tables IV-7, 8 and 9. The OC17/carbomer (95/5) beads are more stable than the OC17 beads (Table IV-7).

Carbopol® 974P is a cross-linked high molecular weight polymer (~ 1 x 10^4). When the beads are hydrated, the carbomer forms a hydrogel which is a tightly cross-linked network. Carbomer is highly ionized at pH 7.4 but is not water soluble. Ionization of the carboxyl groups in the carbomer at pH 7.4 resulted in uncoiling of the polymer chains and formation of a rigid gel(*155*). The rigid gel in the OC17/carbomer beads improves the bead physical stability.

OC17/MTX beads show a much shorter disintegration time than OC17 blank (Table IV-8) beads. The greater the MTX content in the OC17 beads, the shorter the disintegration time. The presence of MTX decreased the physical strength of the OC17 network, however, and the beads disintegrated faster. The physical stability of MTX-loaded OC17/carbomer beads is described in Table IV-9. MTX loaded up to 15% in OC17/carbomer beads showed faster disintegration times than OC17/carbomer blank beads, but when MTX loading was > 25%, the MTX loaded OC17/carbomer beads had almost the same disintegration time as OC17/carbomer blank beads. When MTX loading increased from 5 to 40%, the ratio of OC17 and carbomer decreased from 95:5 to 55:5. The higher gel integrity from carbomer was obtained from a lower ratio of OC17 and carbomer. The carbomer gel strength prevented the beads breaking as fast as those without carbomer. This may be the reason why a higher MTX content in OC17/carbomer beads showed longer disintegration time.

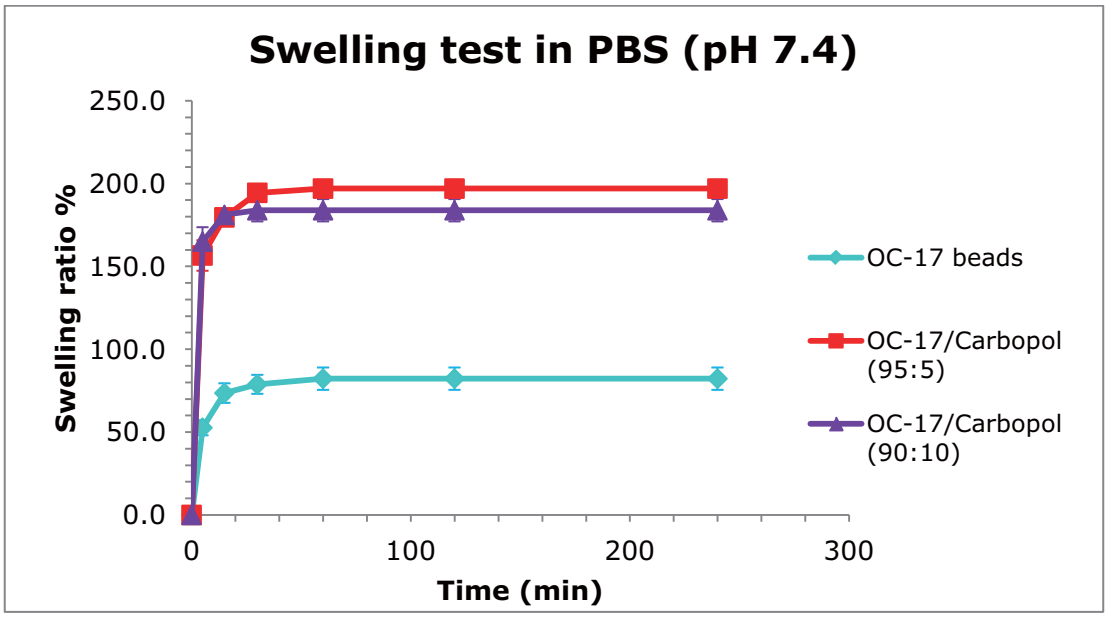

Figure IV-11: Swelling of OC base beads in pH 7.4 PBS at room temperature (n=3).

Table IV-7: Physical stability of OC placebo beads in pH 7.4 PBS at 37 °C.

Sample	**Bead disintegration time (weeks)**
OC17 beads	4
OC17/carbomer beads	> 6

Table IV-8: Physical stability of OC17/MTX beads in pH 7.4 PBS at 37 °C.

Beads (500-700 µm)	**Bead disintegration time (days)**
OC17:MTX (95:5)	10
OC17:MTX (85:15)	10
OC17:MTX (4:1)	7
OC17:MTX (3:2)	7

Table IV-9: Physical stability of OC17/carbomer/MTX beads in pH 7.4 PBS at 37 °C.

Beads (500-700 µm)	**Bead disintegration time (weeks)**
OC17:carbomer:MTX (90:5:5)	4
OC17:carbomer:MTX (80:5:15)	5
OC17:carbomer:MTX (70:5:25)	6
OC17:carbomer:MTX (55:5:40)	8

Suspension and Deliverability Studies

Beads are causing embolism introduced into the desired blood vessel via a catheter. They are mixed into suspension with suitable radiopaque contrast imaging agent as a delivery vehicle. A homogeneous mixture of beads in the vehicle can reduce aggregation and blockage of the catheter. A suspendability study was performed on the beads using a typical contrast agent, Omnipak®. Table IV-10 demonstrates that all products required a short time to disperse in the saline:contrast: PVP in which they were suspended before injection. The quality of the suspension is highly dependent on the viscosity of the solution and the ratio of mixing with saline and PVP. Typically, the embolic beads are designed to remain in suspension for at least 1 min. The time to disperse decreased as the bead size increased. Greater importance is the time for the beads to remain in suspension during delivery of beads through the catheter.

Deliverability is a key performance requirement for embolic beads. Table IV-11 gives the deliverability results. A suspension of 100-250 μm beads in saline-PVP-contrast medium could be delivered through a 23G or larger needle. Beads of 250-500 μm and 500-700 μm beads required a 21G or larger needle, while 700-900 μm beads required a 19G or larger needle. No bead aggregation or blockage was observed.

Compressibility of OC17 Base Beads

Contour@ SE (Boston Scientific Inc., USA) is a commercially available microspherical embolization product. Contour® SE microspheres are PVA-based and designed to combine the proven biocompatibility of PVA with a compressible, spherical shape for improved delivery. Contour® SE beads range in size from 100 to 1200 μm. The

compressibility of Contour® SE beads were compared to OC17 and OC17/carbomer beads. Beads in the size range of 900-1200 μm are not recommended for use in microcatheters by manufacturers, although some can be delivered successfully when used with the appropriate size catheter such as 4 Fr or 5 Fr (1.33 or 1.67 mm). Compressibility is particularly important for bead sizes in the range of 700-900 μm, as the products need to deform in order to pass through the lumen of the catheter, especially if the catheter is contorted in any way. Figure IV-12 shows the force (N) required to compress the bead products without drug in the size range 700-900 μm. The Contour® SE, OC17 and OC17/carbomer beads were shown to have compressibilities in the range 0.05-0.6 N. The force required to compress OC17 and OC17/carbomer was substantially lower than Contour SE, with a mean compression force of less than 0.1 N. This indicates that the OC17-containing product is far more easily compressed. Figure IV-13 shows the force required to compress beads containing MTX in the of 700-900 μm size range. The OC17 and OC17/carbomer beads seem to require an increasing compression force with increasing drug content. It is noted however, that even the highest dose of MTX did not increase the force significantly, and it is still within the same order of magnitude as that of unloaded beads. The beads loaded with drug maintained their compressible structure. Figure IV-14 shows the recovery of beads without drug after first compression. OC17 beads show the lowest recovery of ~50%. OC17/carbomer beads show ~80% recovery, close to that for Contour® SE. The carbomer in the beads results in a hydrogel structure, which exhibits a

Table IV-10: Time remaining in suspension after mixing with the contrast agent.

Sample name	Size (µm)	Solution	Time (sec)
OC-17	425-600	10% PVP saline: contrast agent=1:1	45
OC-17	425-600	20% PVP saline: contrast agent=1:1	>60
OC-17	600-850	20% PVP saline: contrast agent=1:1	55
OC-17	250-500	10% PVP saline: contrast agent=1:1	>60
OC-17/carbomer	250-500	10% PVP saline: contrast agent=1:1	>60

Table IV-11: Test for Deliverability of Beads.

Needle Size (G)	**Bead Size(μm) 700-850**	**Bead Size(μm) 500-700**	**Bead Size(μm) 250-500**	**Bead Size(μm) 100-250**
18 (~830μm)	Pass	Pass	Pass	Pass
19(~680μm)	Pass	Pass	Pass	Pass
20(~600μm)	Not pass	Pass	Pass	Pass
21(~510μm)	Not pass	Pass	Pass	Pass
22(~390μm)	Not pass	Not pass	Not pass	Pass
23(~310μm)	Not pass	Not pass	Not pass	Pass

Pass: No needle clogging. Not pass: Needle clogging.

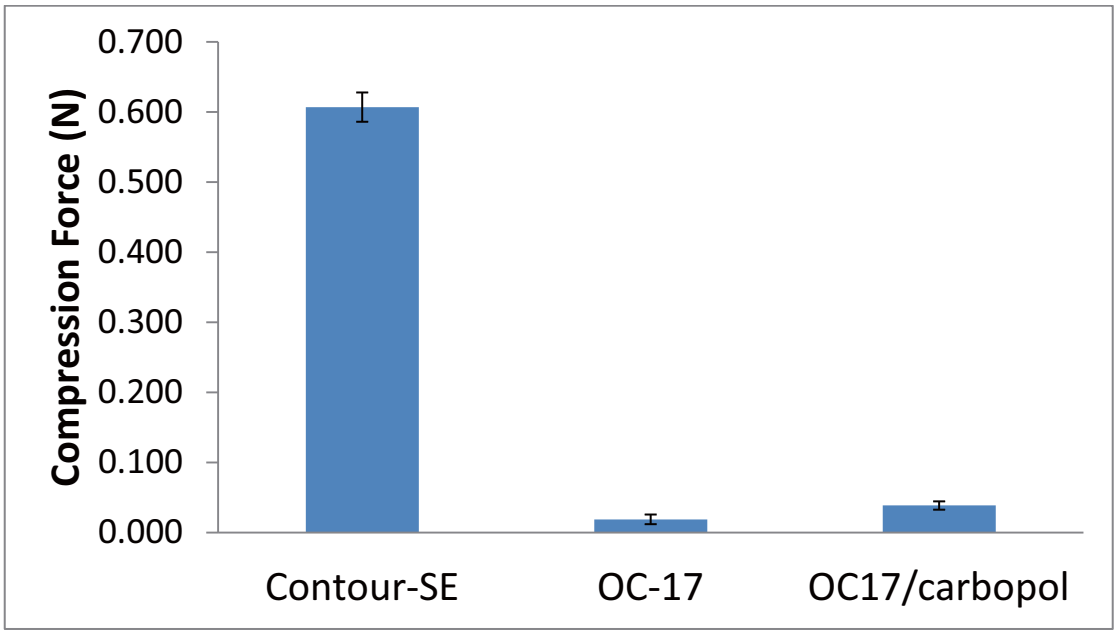

Figure IV-12: Compressibility test results for Contour-SE beads and OC17 beads (n=3).

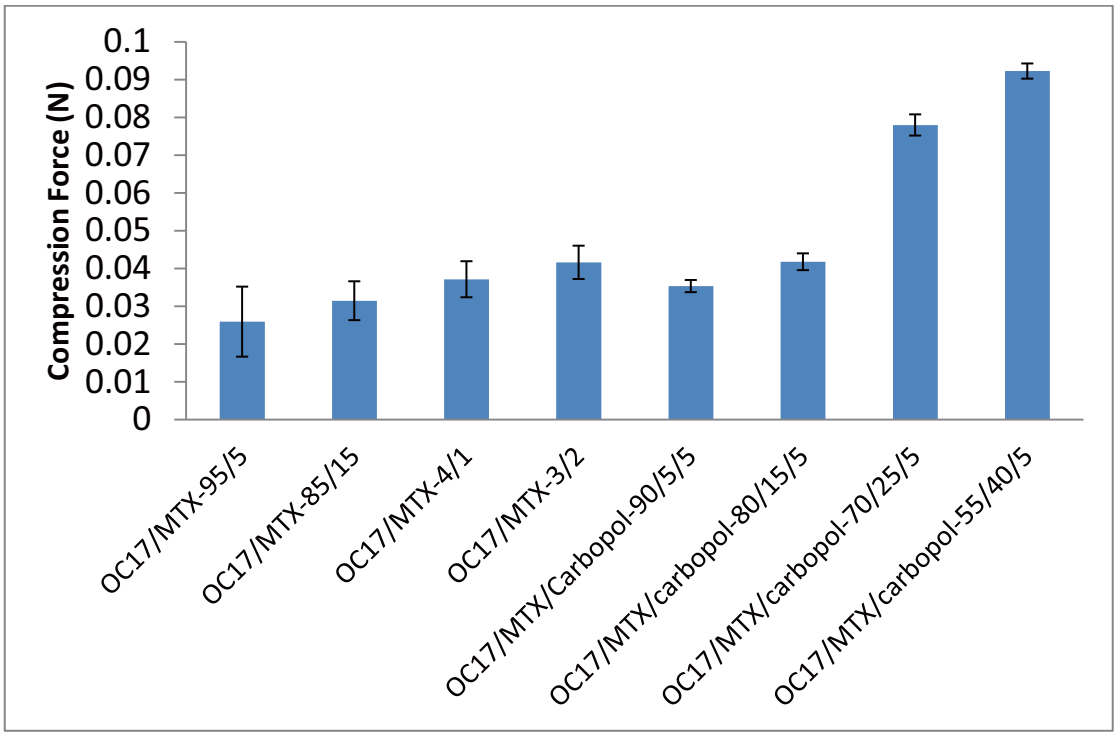

Figure IV-13: Compressibility test results for various MTX loaded beads (n=3).

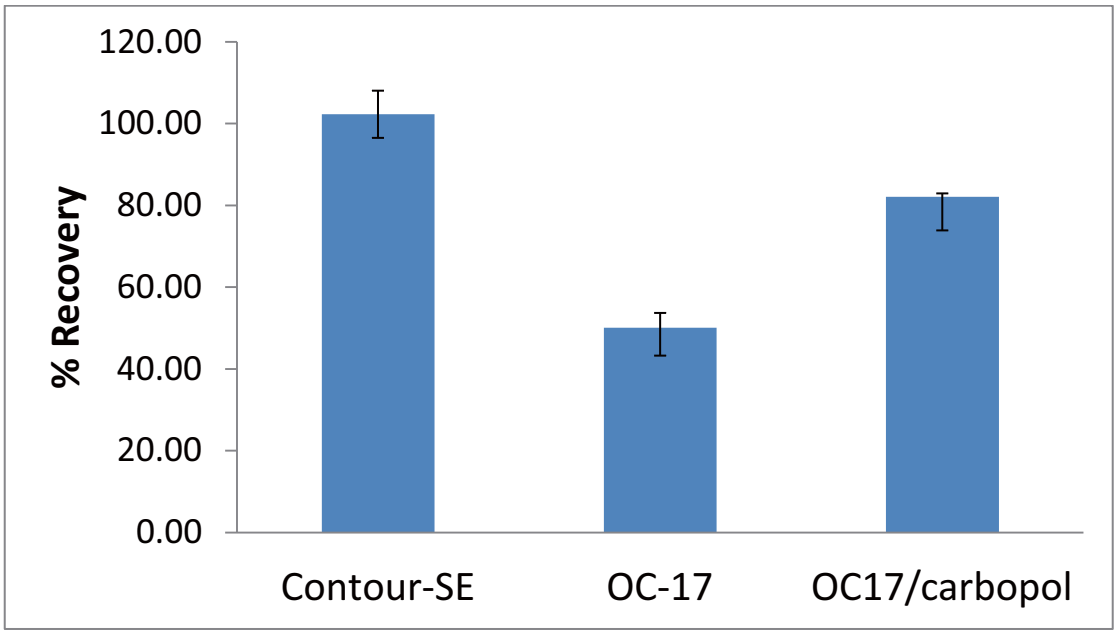

Figure IV-14: Percentage recovery of OC base beads following removal of the compression force (n=3).

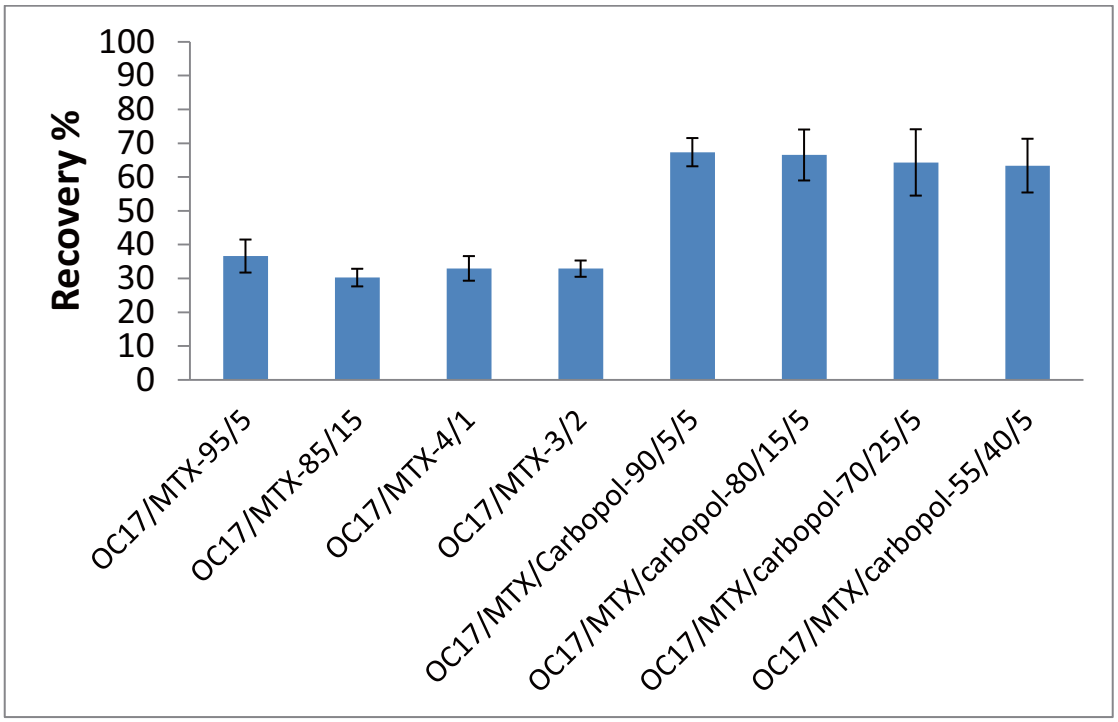

Figure IV-15: Percentage recovery of MTX loaded beads following removal of the compression force (n=3).

compressive response more elastic materials. Figure IV - 15 shows recovery of beads with drug after first compression. The percentage recovery for beads containing drug was reduced by ~10% compared to empty beads. The percentage of recovery doesn't change with increasing drug loading for OC17 and OC17/carbomer beads. The beads with low compression force can be easily deformed during delivery through the catheter. So the smaller catheter can be used to delivery larger size beads without breaking the beads. Higher recovery property of beads helps beads to retain their original shape after they have left the catheter.

In Vitro Release of MTX Beads

The USP Type II-apparatus dissolution is commonly used to test particle dissolution. The apparatus consists of rotating paddles and stirred using a paddle. It is difficult to simulate the release of drug from beads following administration via embolization. Since the drug release from the beads results from a complex processes, according chemical reactions inside the beads and diffusive-convective transport from the embolization site to the general circulation (Figure IV-16). A new experimental method for evaluation of the release profiles of drug-loaded beads designed for embolization was described by Amyot (*149*). The experimental device consists of a "T-shape" fluid path with a driven cavity mounted flush on a main tube (Figure IV-17). The loaded beads are placed at the bottom of the cavity, and the main flow of fluid through the device induces particular hydrodynamic disturbances in the driven cavity that influence the drug release from beads. One main feature of this device is that if produces two main hydrodynamic zones, each of them produces a specific form of mass transport: a mainly diffusive zone

at the bottom of the cavity and a mainly convective zone near the junction between the cavity and the main tube. The drug released from the beads then goes through three district zones: the bead bed, the mainly diffusive zone and the mainly convective zone.

Different drug release apparatuses for beads were reported recently (*11, 12, 150, 156*). Results from the T-apparatus disagreed with results obtaining using the USP dissolution method Type II-apparatus, where the elution rate was depend on the total surface area of the beads. The release rate with the T-apparatus was much slower than with the USP type II-apparatus dissolution method. The T-apparatus model consists of a closed loop system with a low flow rate and a low volume of elution medium to better mimic the in vivo conditions. Therefore, the amount of drug released is limited by both the drug solubility and the amount of the drug circulating the elution medium. Level A IVIVC for drug eluting beads has also been investigated (*11, 12*). Level A IVIVC represents a point-to-point relationship between an in vitro method and an in vivo input rate. Release using the T-apparatus was correlated to the areas under the curve (AUC) measured in patients treated with Dox loaded DC beads were studied. A strong linear point-by-point correlation between T-Apparatus and in vivo model was obtained over 24 h period. This suggested that release from the T-apparatus can be useful for predicting initial in vivo release behavior following a chemoembolization procedure.

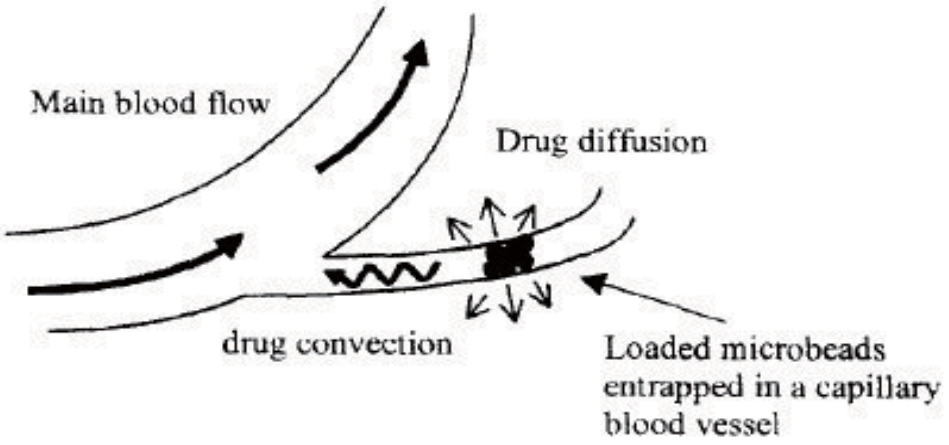

Figure IV-16: Schematic representation of an *in vivo* embolization procedure with drug loaded microbedas(*157*).

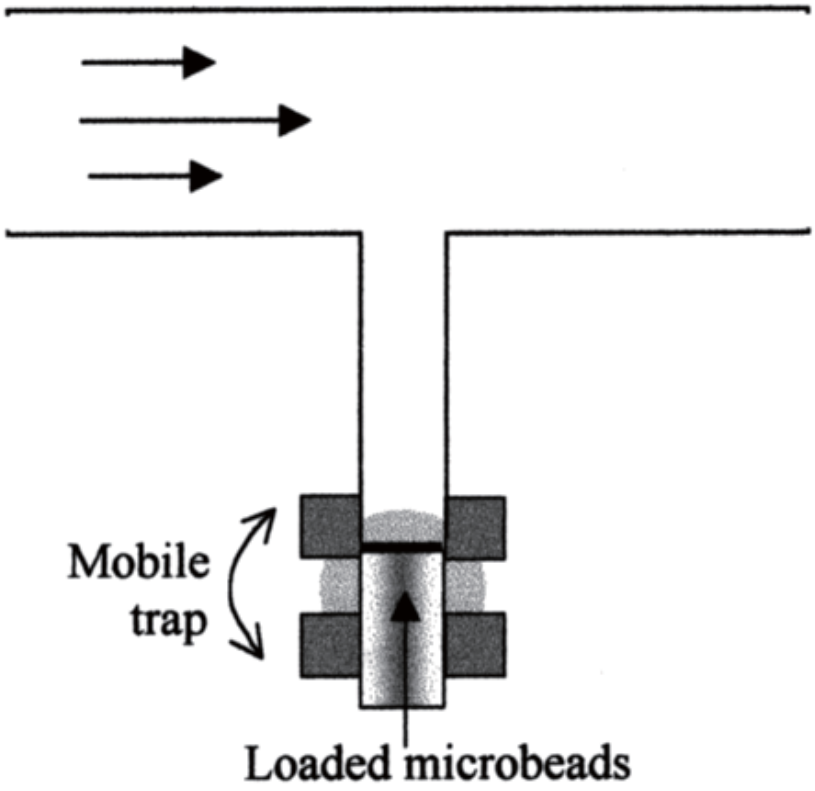

Figure IV-17: Schematic representation of test section of the experiment device.(*149*)

MTX in different sustained-release forms has been studied. MTX was slowly released in pH 7.4 PBS buffer at 37 °C up to 105 days, no degradation of MTX were reported (*103-105, 121*). MTX HPLC standards were stored in room temperature and avoiding light conditions up to 14 days. Figure IV-18 shows HPLC calibration curves prepared at these different time points. The numerical results are listed in Table IV-12.
A good linear calibration curve was obtained, and no degradation was found within 14 days.

In this study, the central portion of T-cell was composed of a horizontal tube (internal diameter: 12 mm; length :150 mm) connected to a cylindrical cavity (internal diameter: 10 mm; depth: 8 mm) (Figure IV-1). The sample is placed at the bottom of the cavity. The entire system consists of a closed loop and the total volume of dissolution medium is 300 ml. MTX release into PBS pH 7.4 buffer from OC17 and OC17/carbomer beads is shown in Figure IV-19 – IV-21, respectively. These plots demonstrate effect of drug content, bead size and carbomer on MTX release.

Figure IV-19 shows the percent MTX released as a function of time from OC17/MTX beads (700-850 μm) containing 5%, 15% and 40% MTX. All of the beads gave 100% release in 100 hours. The slightly slower drug release from the bead with 40% drug loading, compared to those with 5% and 15% MTX, could be attributed to a low pH microenvironment in the bead. MTX has a pH dependent solubility profile (*158*). The solubility changes from ~43 mg/ml in the pH 7.4 buffer to ~0.3 mg/ml at pH 5 buffer. The microenvironment in the bead during release would be expected to become more acidic with an increasing amount of MTX in the matrix, and then would consequently lower the solubility of MTX (*121*). The lower the solubility of MTX in OC17 beads

containing 40% MTX slows the drug release, but the faster disintegration of the OC17 beads containing 40% MTX accelerates the drug release. Consequently, OC17 beads containing 40% drug loading showed only slightly slower drug release than OC17 beads containing 5% and 15% MTX.

A comparison of the effect of bead size on MTX release from OC17/MTX (85:15) beads is shown in Figure IV-20. Nearly equal release rates were obtained from different size beads. The release rate is function of the surface area which contact with release media. In the T-cell, beads are placed in the bottom of cavity and packed closely together. Only one surface of the beads is exposed to the release media so that effect of the bead size minimized. Consequently, the release rate from the different size beads is nearly equal.

The MTX release profiles from OC17/carbomer beads are shown in Figure IV-21, the bead size was 700-850 μm. Release results showed that between 57% to 78% of the drug was released in 6 days, depending on the drug content. Decreasing MTX release rates were measured with increasing drug content. Compared to OC17/MTX beads, OC17/carbomer /MTX beads showed much slower release. As the near neutral dissolution medium enters the beads, the beads hydrate and the carboxylic acid groups on the carbomer would be expected to ionize. The hydration and then repulsion between these carboxylate ions causes the carbomer to swell and gel. The gel can then act as a rate-controlling barrier to drug release. The OC17/carbomer containing 40% MTX showed the slowest release compared to OC17/carbomer containing 5% and 25%. As mentioned previously, the more MTX is loaded in the beads, the slower the drug release because the solubility of MTX is decreased. The OC17/carbomer bead containing 40%

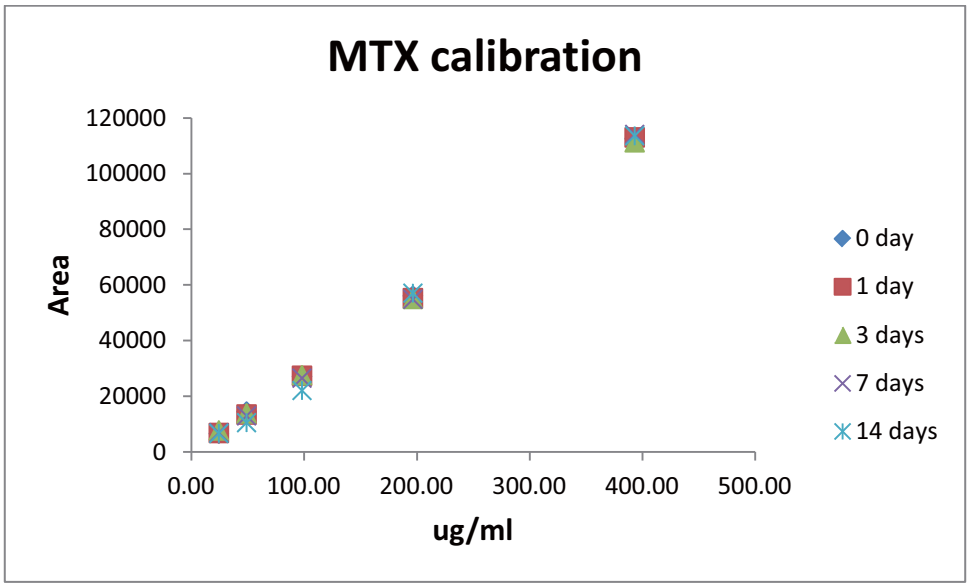

Figure IV-18: MTX HPLC standards stored at room temperature up to 14 days.

Table IV-12: Stability of MTX stored at room temperature (up to 14 days).

Conc. ug/ml	Area (0 day)	Area (1 day)	Area (3 days)	Area (7 days)	Area (14 days)
24.58	6614	6817	7736	6926	6661
49.16	14503	13463	13860	12974	10530
98.33	27118	27373	27565	26522	22078
196.66	56104	55258	54984	54858	57049
393.31	112558	113005	111265	114101	113578
Slope	286.81	288.34	281.67	292.00	297.53
r^2	0.9998	0.9999	0.9999	0.9995	0.9967

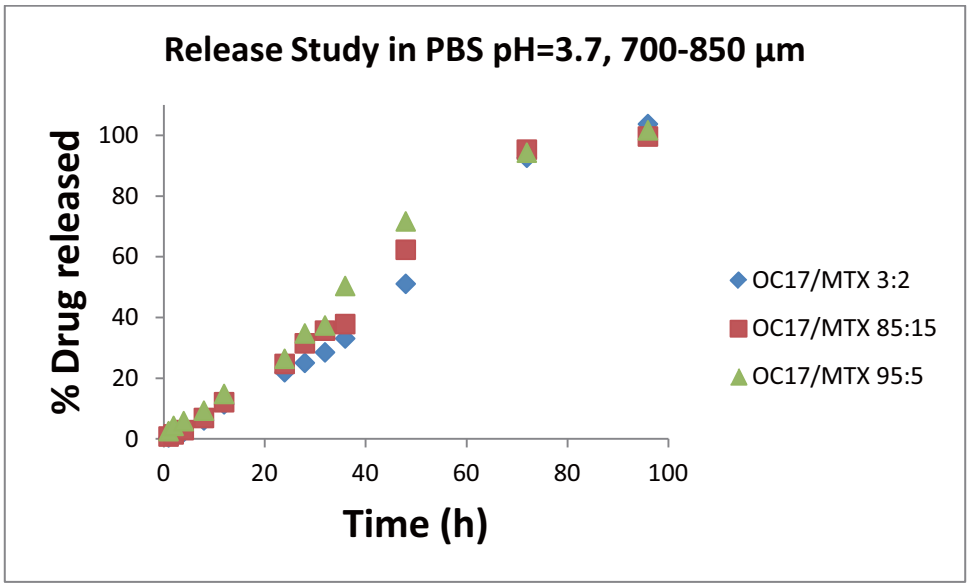

Figure IV-19: In vitro release study – T-Apparatus OC17/MTX beads (700-850 um) with different drug loadings in pH 7.4 PBS solution at 37 °C (n=3).

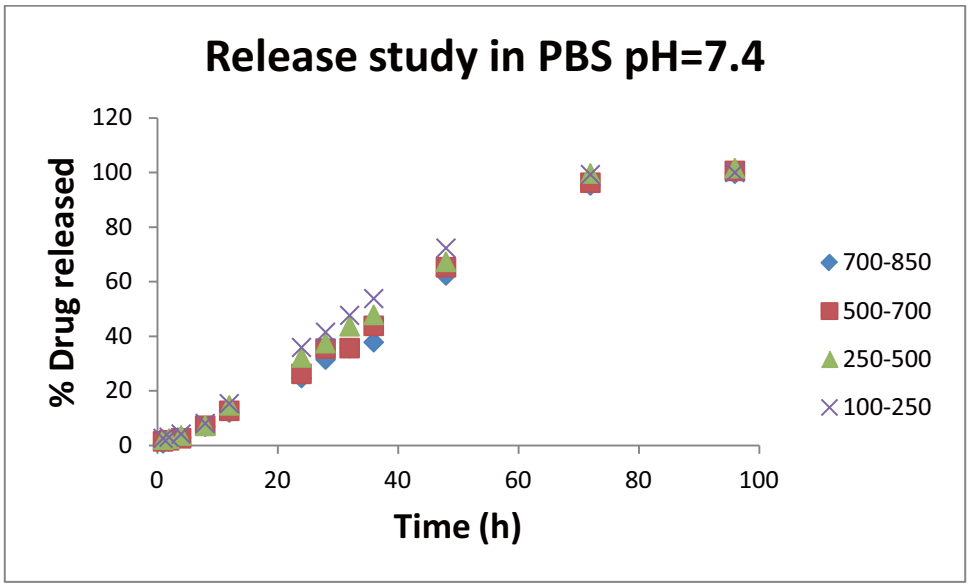

Figure IV-20: In vitro release study – T-Apparatus OC17/MTX(85:15) beads with different size in pH 7.4 PBS solution at 37 °C (n=3).

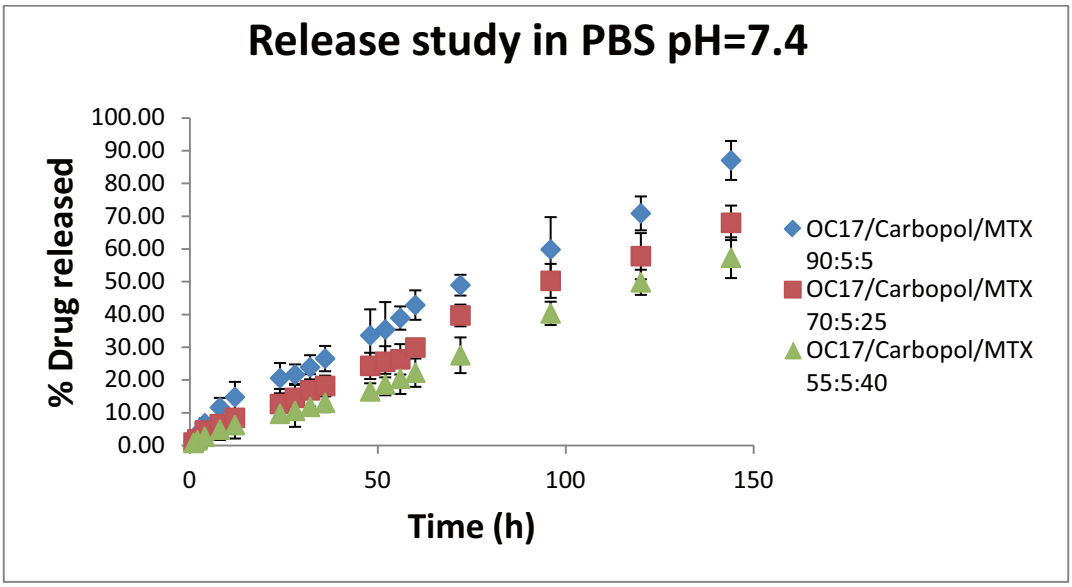

Figure IV-21: In vitro release study – T-Apparatus OC17/carbomer/MTX beads (700-850um) with different drug loadings in pH 7.4 PBS solution at 37 °C (n=3).

MTX has the longest disintegration time compare to OC17/carbomer containing 5% and 25% MTX.

When MTX loading was increased from 5% to 40%, the ratio of OC17 and carbomer decreased from 95:5 to 55:5. A better integrity of the gel was formed by the carbomer was obtained from when there was a lower ratio of OC17 and carbomer. So the OC17/carbomer beads containing 40% MTX have longer disintegration times. The slow disintegration further reduces the release.

Modeling MTX Release From T-apparatus

OC can slowly dissolve/degrade in pH 7.4 PBS solution (*121*). The mechanism of dissolution/degradation of OC in PBS pH 7.4 solution may be an ionization reaction of the carboxyl groups or hydrolysis of polymer chains (*159*). Several models for drug release from erodible polymer matrices are discussed in Chapter I, including surface erosion model for slabs and for spheres and a bulk erosion model. Since OC17 slowly dissolved in pH 7.4 PBS solution, the release data from OC17/MTX and OC17/MTX/carbomer beads were analyzed using these erodible polymer matrix models.

The functions, M_t/M_0, 1-(1-M_t/M_0)^(1/3) and ln(X/(1-X)) vs. time were calculated from the release data and plotted(Figure IV-22 – IV-27). M_t is the amount of drug released from beads in a time t. M_0 is the total amount of loaded drug. X is the faction of drug released. The surface erosion model for a slab produced the best fit to the release data from the OC17/MTX and OC17/MTX/carbomer beads (r^2= 0.9696 – 0.9938), and the bulk erosion model showed the poorest fitting (r^2= 0.8270 – 0.9834).

There are several polymer erosion mechanisms(*160*). In principle, dissolution of a

hydrophobic polymer was achieved by a chemical reaction that can take place either at a pendent group of the polymer or within the polymer backbone. When the chemical reaction is confined to the pendent group of a polymer, no backbone cleavage takes place and one of the reaction products is a water-soluble polymer. Side-group reaction might be the rapid process that leads to chain solubilization When backbone cleavage take place, the hydrolyzed polymer forms low molecular weight small polymers, but backbone cleavage might be the slow process. The poor fitting of the bulk erosion model could be due to ionization of carboxyl groups on the surface of the polymer matrix. While in unionized form OCs are water-insoluble, but following ionization of the carboxylic acid function of group, OCs become more water-soluble. These free carboxylic acid groups would generate an acidic microenvironment (*96*). Even though water may permeate into the polymer matrix, the percentage of polymer dissociation in the interior is low because of the more acidic microenvironment. Only solubilized polymer at the surface can participate in the erosion process. The linearity of drug release over the time provides strong evidence for a surface-erosion mechanism (*160*).

The surface erosion model for a slab shows better fit to the OC17/MTX and OC17/MTX/carbomer release data (r^2 = 0.9696 – 0.9938) than the surface erosion model for spheres (r^2 = 0.8538 – 0.9888). This may due to the geometry of the T-apparatus (Figure IV-1) where MTX-loaded beads are at the bottom of the cavity. Drug release is only from the surface of these beads, so the polymeric beads as a group may function more like a slab than as individual spheres.

In the surface-erosion model, drug release shows a clear dependence on polymer erosion rate (*160*). From results of a physical stability test on MTX-loaded beads in PBS

pH 7.4 buffer at 37 ^{o}C in a static environment, the bead disintegration times follow the order OC17/MTX (3:2) > OC17/MTX (95:5) > OC17/MTX/carbomer (95:5:5) > OC17/MTX/carbomer (70:25:5) > OC17/MTX/carbomer (55:40:5). The release rate order using the surface-erosion model for a slab was: OC17/MTX (95:5)> OC17/MTX (3:2) > OC17/MTX/carbomer (95:5:5) > OC17/MTX/carbomer (70:25:5) > OC17/MTX/carbomer (55:40:5). This release rate order was almost the same as the order for bead disintegration except for the OC17/MTX beads. Due to the shape of the T-apparatus, two different hydrodynamic areas exist in the cell (*149*). The first area is at the bottom of the cavity holding the beads and the fluid is fairly stationary. This area could be called a diffusion area, where transport occurs primarily by diffusion with little convection. The second area is a convective area at the top of the cavity due to rapid flow of release medium past this surface. In the T-apparatus system, hydrodynamic conditions are constant and mass transfer is by both convection and diffusion. The T-apparatus model consists of a closed loop system with a low flow rate and a low elution medium volume. Therefore, the amount of drug released is limited by both the solubility and the amount of the drug circulating in the elution medium. MTX has a pH dependent solubility profile. The solubility changes from ~ 38 mg/mL at pH 7.4 to ~ 2 mg/mL at pH 5.5 (*101*). The acidic microenvironment from the degrading OC in the matrix would lower the solubility of the MTX release from the matrix. This may be why OC17/MTX beads have a reverse release rate order compared to OC17/MTX/carbomer beads.

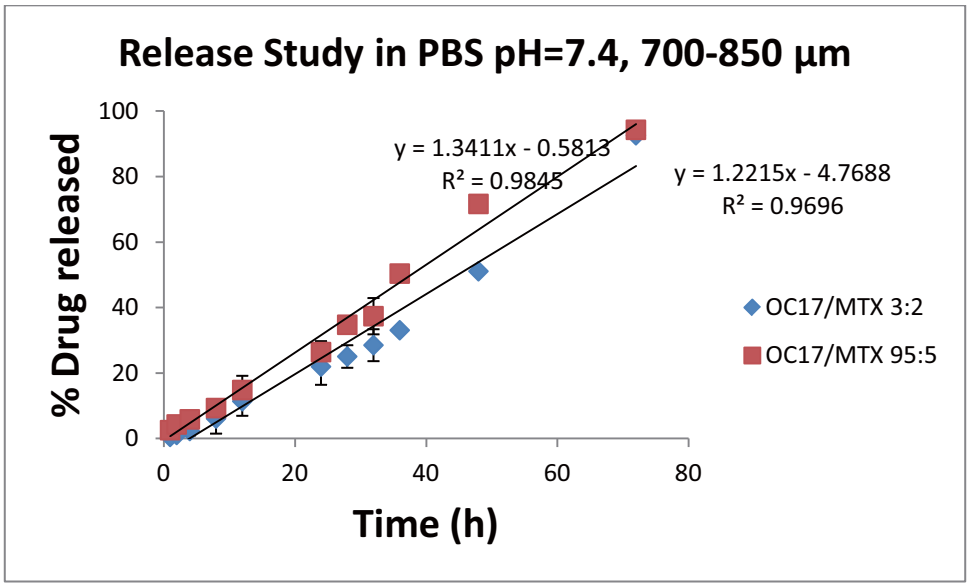

Figure IV-22: Surface erosion model (slab) fitting of the MTX release data of OC17/MTX beads.

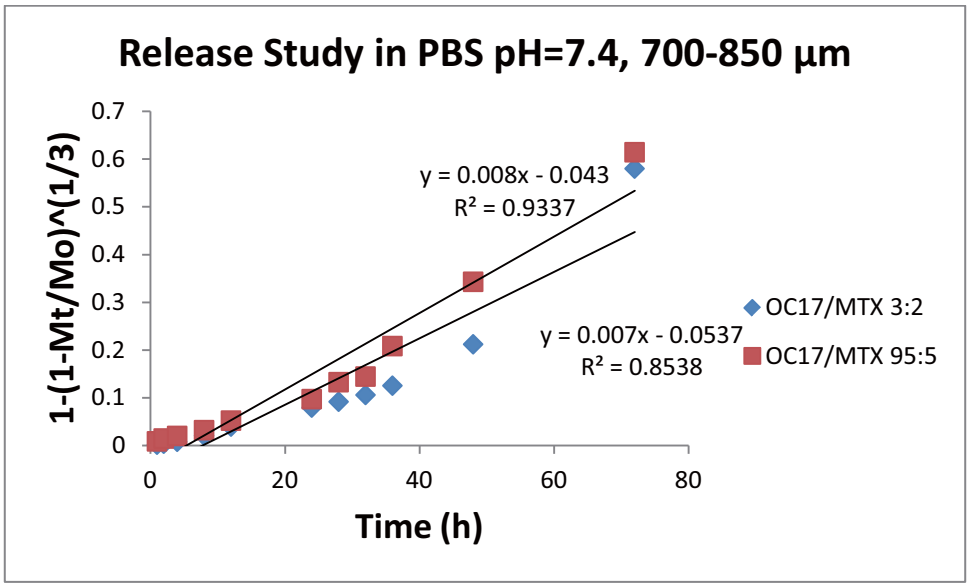

Figure IV-23: Surface erosion model (spheres) fitting of the MTX release data of OC17/MTX beads.

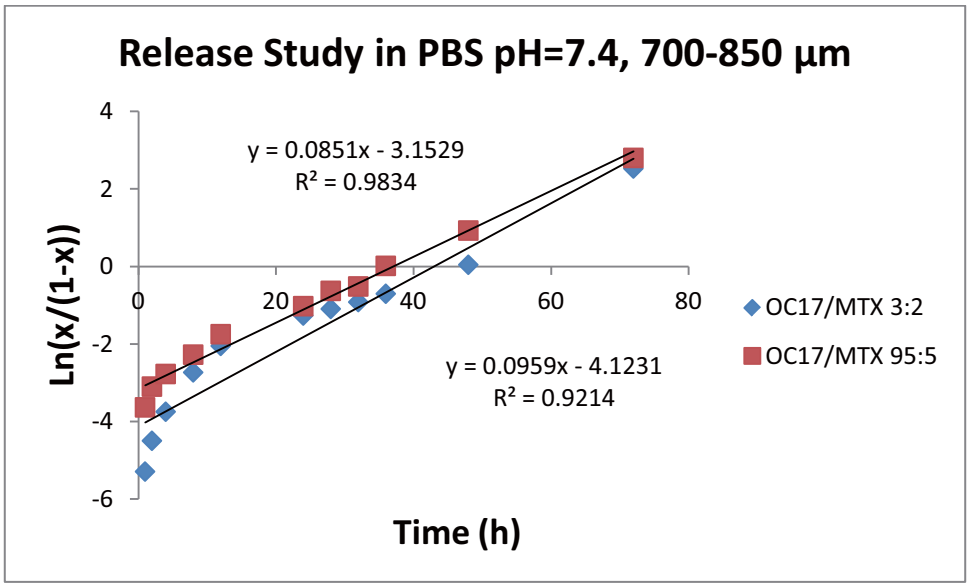

Figure IV-24: Bulk erosion model fitting of the MTX release data of OC17/MTX beads.

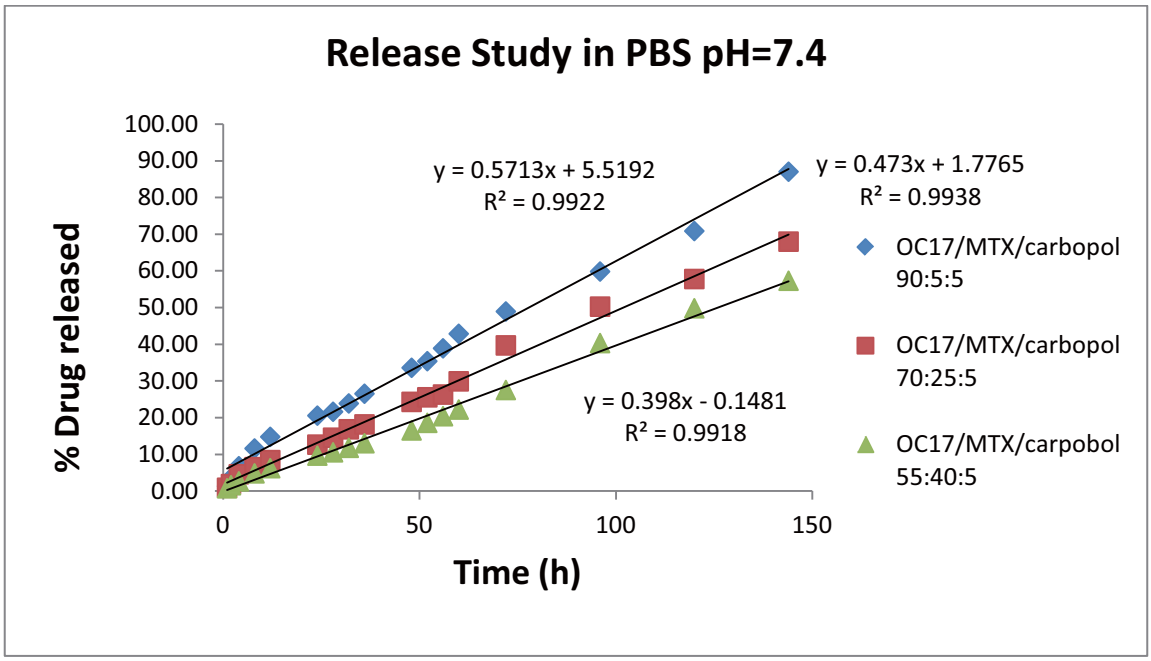

Figure IV-25: Surface erosion model (slab) fitting of the MTX release data of OC17/MTX/carbomer beads.

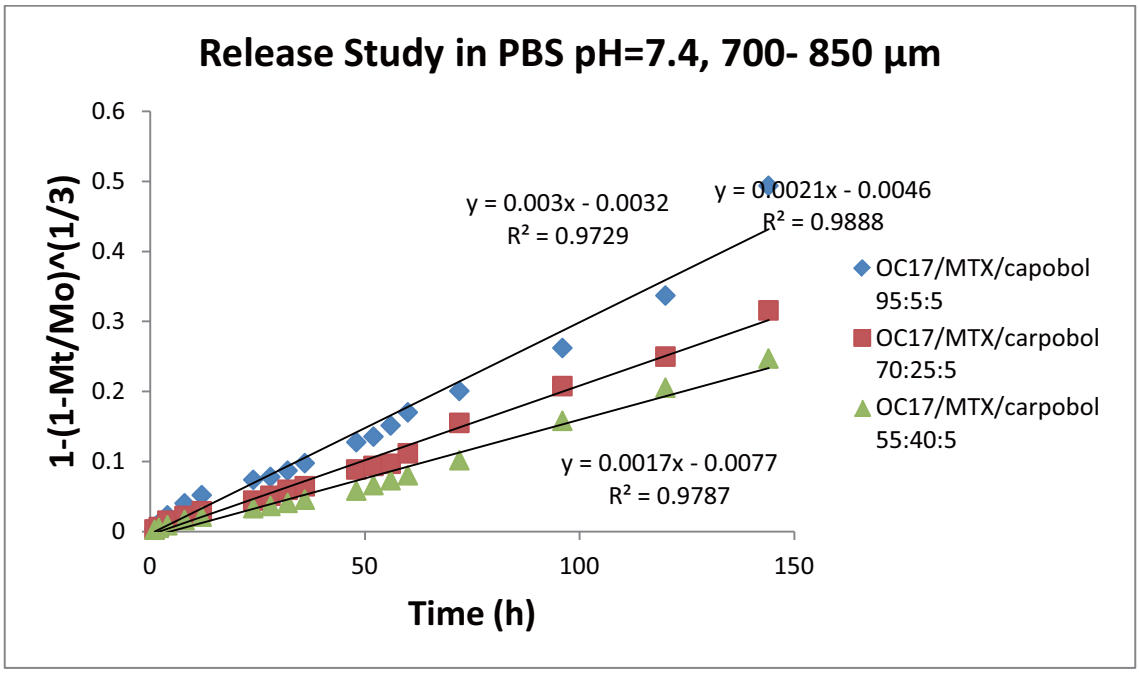

Figure IV-26: Surface erosion model (spheres) fitting of the MTX release data of OC17/MTX/carbomer beads.

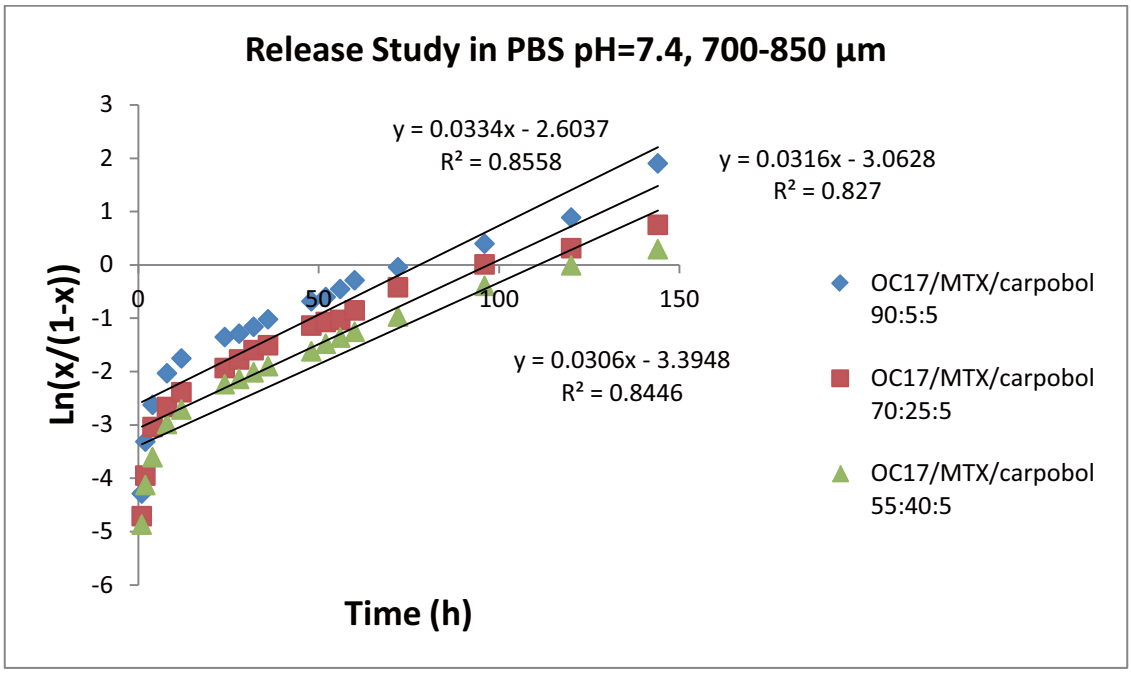

Figure IV-27: Bulk erosion model fitting of the MTX release data of OC17/MTX beads.

CHAPTER V

CONCLUSIONS

The overall goal of Transarterial chemoembolization (TACE) is to deliver a high dose of drug directly to a tumor and able to access a tumor on multiple occasions in order to administer additional DEB-TACE treatments as needed. This project demonstrated biodegradable material oxidized cellulose (OC17) could be used for TACE.

Extrusion/spheronization technology was chosen for drug loading method. It must be noted that not every polymer can be successfully extruded and spheronized. Oxidized cellulose (OC) was chosen in this study, which has similar structure as microcrystalline cellulose (MCC). OC was evaluated as new excipient for extrusion/spheronization in this study. Differential scanning calorimetry (DSC) and dynamic vapor sorption analysis were used to compare the interaction and distribution of water within MCC and OC. The amounts of nonfreezing and freezing water in hydrated samples were determined from melting endotherms obtained by DSC. There has no statistically different between MCC and OC at the desorbed amount of water per unit in amorphous area. The moisture sorption profiles were analyzed according to the Guggenheim-Anderson-de Boer (GAB) equation. The adsorbed monolayer was not statistically different for MCC and OC after accounting for the amorphous content of the polymers. These results suggest that OC has similar property as MCC and thus aid in the production of beads by extrusion and spheronization.

The optimization of OC17 bead/pellet preparation was studied in more detail. A composite central design was applied to optimize the levels of process variables for

producing oxidized cellulose (OC17) beads using the extrusion-spheronization technique. Among the factors studied, water level, spheronization speed, and spheronization time significantly affected bead formation. The combination of 55-57% water level, medium spheronization speed (1400 rpm) and high spheronization time (300 sec) was deemed the optimal condition for OC17 bead batches.

OC 17 beads containing methotrexate (MTX), an anti-cancer drug, were prepared. Up to 40% drug content beads can be prepared by extrusion/spheronization. Carbomer was also used in some beads with to alter the physical properties of the beads, such as compressibility and MTX release profile. The physical properties of OC 17-MTX beads showed that these beads could be delivered by a catheter. The physical properties of OC 17-MTX beads demonstrated they could be used for transarterial chemoembolization (TACE). T-apparatus which resembles closely the in vivo situation in embolization procedures was used for MTX release in this study. The release data showed slow release for MTX beads. Also, analysis of the MTX release profiles demonstrated that a surface erosion mechanism (slab) best described the release results.

In summary, oxidized cellulose (OC17) beads can be prepared by using extrusion/spheronization. OC beads can meet the future direction of drug eluted beads in TACE, (i.e., biodegradable, wide size range, high loading drug content and capable to load water soluble and insoluble drug).

CHAPTER VI

FUTURE STUDIES

This study proved that processing beads with oxidized cellulose by using extrusion/spheronization showed several advantages. Further studies need to be conducted to get more applications for this technology. First, one problem with current DEB technology is that there is a limit to small molecules that can be delivered. Extrusion/spheronization with oxidized cellulose approach should be conducted to deliver a peptide or other biomolecule and encapsulate them into a bead to be delivered intra-arterially. Compactability between oxidized cellulose and peptide or biomolecule, maximum drug loading, and peptide or biomolecule drug release from oxidized cellulose beads should be studied in the future studies. Second, DEB-TACE lacks the intraprocedural imaging feedback of in the target tumor, which is seen with fluoroscopy or CT. During DEB-TACE, the embolization process is monitored by detecting changes in antegrade flow of soluble iodinated contrast in which DEBs are diluted. The embolization is continued until a desired embolization endpoint is reached or reflux of contrast material into non-target vessels is observed, without specific feedback on DEB or drug location. Extrusion/spheronization with oxidized cellulose approach can be conducted to develop image-able spherical beads that can be visualized with magnetic resonance and X-ray-based imaging or both. Water soluble contrast material is better optional because it can dissolve in water which is used as extrusion media. Third, this thesis only studied release mechanism in vitro, in vivo experiments for oxidized cellulose beads should be studied to get more understanding of release mechanism. Finally, scale-

up studies should be conducted if oxidized cellulose beads want to be taken to the manufacturing industrial scale to see the reproducibility of these results.

REFERENCES

1. Yamada, R., Nakatsuka, H., Nakamura, K., Sato, M., Itami, M., Kobayashi, N., Minakuchi, K., Onoyama, T., Kanno, T., Monna, T., and Yamamoto, S. (1980) Hepatic artery embolization in 32 patients with unresectable hepatoma, *Osaka City Med. J. 26*, 81-96.

2. Yamada, R., Sato, M., Kawabata, M., Nakatsuka, H., Nakamura, K., and Takashima, S. (1983) Hepatic artery embolization in 120 patients with unresectable hepatoma, *Radiology 148*, 397-401.

3. Lewandowski, R. J., Geschwind, J., Liapi, E., and Salem, R. (2011) Transcatheter intraarterial therapies: rationale and overview, *Radiology 259*, 641-657.

4. Liapi, E., and Geschwind, J. F. (2011) Transcatheter arterial chemoembolization for liver cancer: Is it time to distinguish conventional from drug-eluting chemoembolization?, *Cardiovasc. Intervent. Radiol. 34*, 37-49.

5. Lewis, A. L., and Dreher, M. R. (2012) Locoregional drug delivery using image-guided intra-arterial drug eluting bead therapy, *J. Control. Release 161*, 338-350.

6. Brown, D. B., Gould, J., Gervais, D. A., Goldberg, S., Murthy, R., Millward, S. F., and Rilling, W. S. (2007) Transcatheter therapy for hepatic malignancy: standardization of terminology and reporting criteria, *J. Vasc. Interv. Radiol. 18*, 1469-1478.

7. Vallee, J. N., Lo, D., Guillevin, R., Reb, P., Adem, C., and Chiras, J. (2003) In vitro study of the compatibility of tris-acryl gelatin microspheres with various chemotherapeutic agents, *J. Vasc. Interv. Radiol. 14*, 621-628.

8. Laurent, A., Beaujeux, R., Wassef, M., Ru¨fenacht, D., Boschetti, E., and Merland, J. (1996) Trisacryl gelatin microspheres for therapeutic embolization, I: development and In vitro evaluation, *AJNR Am. J. Neuroradiol. 17*, 533-540.

9. Lewis, A. L., Gonzalez, M. V., Lloyd, A. W., Hall, B., Tang, Y., Willis, S. L., Leppard, S. W., Wolfenden, L. C., Palmer, R. R., and Stratford, P. W. (2006) DC bead: in vitro characterization of a drug-delivery device for transarterial chemoembolization, *J. Vasc. Interv. Radiol. 17*, 335-342.

10. Lewis, A. L., Gonzalez, M. V., Leppard, S. W., Brown, J. E., Stratford, P. W., Phillips, G. J., and Lloyd, A. W. (2007) Doxorubicin eluting beads - 1: Effects of drug loading on bead characteristics and drug distribution, *J. Mater. Sci. Mater. Med. 18*, 1691-1699.

11. Gonzalez, M. V., Tang, Y., Phillips, G., Lloyd, A., Hall, B., Stratford, P., and Lewis, A. (2008) Doxorubicin eluting beads—2: Methods for evaluating drug elution and in-vitro:in-vivo correlation, *J. Mater. Sci.: Mater. Med. 19*, 767-775.

12. Taylor, R. R., Tang, Y., Gonzalez, M. V., Stratford, P. W., and Lewis, A. L. (2007) Irinotecan drug eluting beads for use in chemoembolization: In vitro and in vivo evaluation of drug release properties, *Eur. J. Pharm. Sci. 30*, 7-14.

13. Tang, Y., Taylor, R. R., Gonzalez, M. V., Lewis, A. L., and Stratford, P. W. (2006) Evaluation of irinotecan drug-eluting beads: A new drug–device combination product for the chemoembolization of hepatic metastases, *J. Control. Release 116*, e55-e56.

14. Lee, K. H., Liapi, E. A., Cornell, C., Reb, P., Buijs, M., Vossen, J. A., Ventura, V. P., and Geschwind, J. F. (2010) Doxorubicin-loaded QuadraSphere microspheres: plasma pharmacokinetics and intratumoral drug concentration in an animal model of liver cancer, *Cardiovasc. Intervent. Radiol. 33*, 576-582.

15. Kim, J. S., Kwak, B. K., Shim, H. J., Lee, Y. C., Baik, H. W., Lee, M. J., Han, S. M., Son, S. H., Kim, Y. B., Tokura, S., and Lee, B. M. (2007) Preparation of doxorubicin-containing chitosan microspheres for transcatheter arterial chemoembolization of hepatocellular carcinoma, *J. Microencapsul. 24*, 408-419.

16. Misirli, Y., Ozturk, E., Kursaklioglu, H., and Denkbas, E. B. (2005) Preparation and characterization of Mitomycin-C loaded chitosan-coated alginate microspheres for chemoembolization, *J. Microencapsul. 22*, 167-178.

17. Ghebre-Sellassie, I., and Knoch, A. (2006) *Pelletization techniques. Encyclopedia of Pharmaceutical Technology*, Vol. 4, Marcel Dekker Inc., New York and Basel. pp 2651-2663.

18. Zhang, G. H., Schwartz, J. B., and Schnaare, R. L. (1990) Effect of spheronization technique on drug release from uncoated beads, *Drug Dev. Ind. Pharm. 16*, 1171-1184.

19. Zhang, G. H., Schwartz, J. B., Schnaare, R. L., Wigent, R. J., and Sugita, E. T. (1991) Bead coating: II. Effect of spheronisation technique on drug release from coated spheres., *Drug Dev. Ind. Pharm. 17*, 817-830.

20. Jones, D. (1994) Air suspension coating for multiparticulates, *Drug Dev. Ind. Pharm. 20*, 3175-3206.

21. Vuppala, M. K., Parikh, D. M., and Bhagat, H. R. (1997) Application of powder-layering technology and film coating for manufacture of sustained-release pellets using a rotary fluid bed processor, *Drug Dev. Ind. Pharm. 23*, 687-694.

22. Kleinebudde, P., and Knop, K. (2007) *Direct pelletisation of pharmaceutical pellets in fluid-bed processes, Handbook of Powder Technology: Granulation*, Vol. 11, Elsevier, London.

23. Kristensen, J., Schäfer, T., and Kleinebudde, P. (2002) Development of fast-disintegrating pellets in a rotary processor, *Drug Dev. Ind. Pharm. 28*, 1201-1212.

24. Liew, C. V., Chua, S. M., and Heng, P. W. S. (2007) Elucidation of spheroid formation with and without the extrusion step, *AAPS PharmSciTech 8*, E70-E81.

25. Liew, C., Wan, L., and Heng, P. (2000) Role of base plate rotational speed in controlling spheroid size distribution and minimizing oversize particle formation during spheroid production by rotary processing, *Drug Dev. Ind. Pharm. 26*, 953.

26. Conine, J. W., and Hadley, H. R. (1970) Preparation of small solid pharmaceutical spheres, *Drug. Cosmet. Ind.*, 38-41.

27. Reynolds, A. D. (1970) A new technique for the production of spherical particles, *Manuf. Chem. 41*, 40-43.

28. Lambert, S. E., Reilly, W. J., and Schwartz, J. B. (1995) Reprocessing of microcrystalline cellulose spheres with high drug concentrations, *Drug Dev. Ind. Pharm. 21*, 2121-2128.

29. Hileman, G. A., Goskonda, S. R., Spalitto, A. J., and Upadrashta, S. M. (1993) A factorial approach to high-dose product development by an extrusion spheronization process, *Drug Dev. Ind. Pharm. 19*, 483-491.

30. Trivedi, N. R., Rajan, M. G., Johnson, J. R., and Shukla, A. J. (2007) Pharmaceutical approaches to preparing pelletized dosage forms using the extrusion-spheronisation process, *Crit. Rev. Ther. Drug Carr. Syst. 24*, 1-40.

31. Hileman, G. A., Goskonda, S. R., Spalitto, A. J., and Upadrashta, S. M. (1993) Response surface optimization of high dose pellets by extrusion and spheronization, *Int. J. Pharm. 100*, 71-79.

32. Podczeck, F., and Knight, P. (2006) The evaluation of formulations for the preparation of pellets with high drug Loading by extrusion/spheronization, *Pharm. Dev. Technol. 11*, 263-274.

33. Erkoboni, D. F. (2003) *Extrusion/spheronization, Pharmaceutical Extrusion Technology.*, Marcel Dekker, New York. pp 277-322.

34. Ojile, J. E., Macfarlane, C. B., and Selkirk, A. B. (1982) Drug distribution during massing and its effect on dose uniformity in granules, *Int. J. Pharm. 10*, 99-107.

35. Vervaet, C., Baert, L., and Remon, J. P. (1995) Extrusion-spheronisation a literature review, *Int. J. Pharm. 116*, 131-146.

36. Lövgren, K., and Lundberg, P. J. (1989) Determination of sphericity of pellets prepared by extrusion spheronization and the impact of some process parameters, *Drug Dev. Ind. Pharm. 15*, 2375-2392.

37. Elbers, J. A. C., Bakkenes, H. W., and Fokkens, J. G. (1992) Effect of amount and composition of granulation liquid on mixing, extrusion and spheronization, *Drug. Dev. Ind. Pharm. 18*, 501-517.

38. Baert, L., Fanara, D., De Baets, P., and Remon, J. P. (1991) Instrumentation of a gravity feed extruder and the influence of the composition of binary and ternary mixtures on the extrusion forces, *J. Pharm. Pharmacol. 43*, 745-749.

39. Woodruff, C. W., and Nuessle, N. O. (1972) Effect of processing variables on particles obtained by extrusion—spheronization processing, *J. Pharm. Sci. 61*, 787-790.

40. Hellén, L., Yliruusi, J., Merkku, P., and Kristoffersson, E. (1993) Process variables of instant granulator and spheroniser: I. Physical properties of granules, extrudate and pellets, *Int. J. Pharm. 96*, 197-204.

41. Kleinebudde, P., and Lindner, H. (1993) Experiments with an instrumented twin-screw extruder using a single-step granulation/extrusion process, *Int. J. Pharm. 94*, 49-58.

42. Lindberg, N. O., C., T., P., H., and L., O. (1988) Extrusion of an effervescent granulation with a twin-screw extruder, Baker Perkins MPF 50 D. Influence in intragranular porosity and liquid saturation, *Drug. Dev. Ind. Pharm. 14*, 1791-1798.

43. Gamlen, M. J., and Eardley, C. (1986) Continuous extrusion using a raker perkins MP50 (multipurpose) extruder, *Drug. Dev. Ind. Pharm. 12*, 1701-1713.

44. Kleinebudde, P. (1995) Use of a power-consumption-controlled extruder in the development of pellet formulations, *J. Pharm. Sci. 84*, 1259-1264.

45. Lindberg, N.-O., Tufvesson, C., and Olbjer, L. (1987) Extrusion of an effervescent granulation with a twin screw extruder, Baker Perkins MPF 50 D, *Drug. Dev. Ind. Pharm. 13*, 1891-1913.

46. Lindberg, N.-O., Myrenas, M., Tufvesson, C., and Olbjer, L. (1988) Extrusion of An effervescent granulation with a twin screw extruder, Baker Perkins MPF 50D. Determination of mean residence time, *Drug. Dev. Ind. Pharm. 14*, 649-655.

47. Newton, J. M. (2006) *Extrusion and Extruders. Encyclopedia of Pharmaceutical Technology*, Vol. 3, Marcel Dekker Inc., New York and Basel. pp 1712-1728

48. Ku, C. C., Joshi, Y. M., Bergum, J. S., and Jain, N. B. (1993) Bead manufacture by extrusion/spheronization – a statistical design for process optimization, *Drug. Dev. Ind. Pharm. 19*, 1505-1519.

49. Hicks, D. S. a. F., H.L., (1989) *Extrusion and spheronizing equipment, In: Pharmaceutical Pelletisation Technology,*, Marcel Dekker Inc., New York and Basel. pp 71-100.

50. Rowe, R. C. (1985) Spheronisation: A novel pill-making process?, *Pharm. Int. 6*, 119-123.

51. Wilson, D. I., and Rough, S. L. (2007) *Extrusion-Spheronisation, In: Handbook of Powder Technology: Granulation*, Vol. 11, Elsevier, London.

52. Fielden, K. E., Newton, J. M., and Rowe, R. C. (1992) A comparison of the extrusion and spheronization behaviour of wet powder masses processed by a ram extruder and a cylinder extruder, *Int. J. Pharm. 81*, 225-233.

53. Fielden, K. E., Newton, J. M., and Rowe, R. C. (1989) The effect of lactose particle size on the extrusion properties of microcrystalline cellulose-lactose mixtures, *J. Pharm. Pharmacol. 41*, 217-221.

54. Kanbe, H., Hayashi, T., Onuki, Y., and Sonobe, T. (2007) Manufacture of fine spherical granules by an extrusion/spheronization method, *Int. J. Pharm. 337*, 56-62.

55. Baert, L., and Remon, J. P. (1993) Influence of amount of granulation liquid on the drug release rate from pellets made by extrusion spheronisation, *Int. J. Pharm. 95*, 135-141.

56. Hasznos, L., Langer, I., and Gyarmathy, M. (1992) Some factors influencing pellet characteristics made by an extrusion/spheronisation process Part I.: effects on size characteristics and moisture content decrease of pellets, *Drug. Dev. Ind. Pharm. 18*, 409-437.

57. Wan, L. S. C., Heng, P. W. S., and Liew, C. V. (1993) Spheronization conditions on spheroid shape and size, *Int. J. Pharm. 96*, 59-65.

58. Newton, J. M., Chapman, S. R., and Rowe, R. C. (1995) The influence of process variables on the preparation and properties of spherical granules by the process of extrusion and spheronisation, *Int. J. Pharm. 120*, 101-109.

59. Bataille, B., Ligarski, K., Jacob, N., Thohas, C., and Duru, C. (1993) Study of the influence of spheronization and drying conditions on the physico-mechanical properties of neutral spheroids containing Avicel PH 101 and lactose, *Drug Dev. Ind. Pharm. 19*, 653-671.

60. Dyer, A. M., Khan, K. A., and Aulton, M. E. (1994) Effect of the drying method on the mechanical and drug release properties of pellets prepared by extrusion-spheronization, *Drug Dev. Ind. Pharm. 20*, 3045-3068.

61. Berggren, J., and Alderborn, G. (2001) Effect of drying rate on porosity and tabletting behaviour of cellulose pellets, *Int. J. Pharm. 227*, 81-96.

62. Song, B., Rough, S. L., and Wilson, D. I. (2007) Effects of drying technique on extrusion–spheronisation granules and tablet properties, *Int. J. Pharm. 332*, 38-44.

63. Tho, I., Kleinebudde, P., and Sande, S. (2001) Extrusion/spheronization of pectin-based formulations. II. Effect of additive concentration in the granulation liquid, *AAPS PharmSciTech 2*, article 27.

64. Bornhöft, M., Thommes, M., and Kleinebudde, P. (2005) Preliminary assessment of carrageenan as excipient for extrusion/spheronisation, *Eur. J. Pharm. Biopharm. 59*, 127-131.

65. Charoenthai, N., Kleinebudde, P., and Puttipipatkhachorn, S. (2007) Use of chitosan-alginate as alternative pelletization aid to microcrystalline cellulose in extrusion/spheronization, *J. Pharm. Sci. 96*, 2469-2484.

66. Dukić-Ott, A., Remon, J. P., Foreman, P., and Vervaet, C. (2007) Immediate release of poorly soluble drugs from starch-based pellets prepared via extrusion/spheronisation, *Eur. J. Pharm. Biopharm. 67*, 715-724.

67. Fielden, K. E., Newton, J. M., O'Brien, P., and Rowe, R. C. (1988) Thermal studies on the interaction of water and microcrystalline cellulose, *J. Pharm. Pharmacol. 40*, 674-678.

68. Ek, R., and Newton, J. M. (1998) Microcrystalline cellulose as a sponge as an alternative concept to the crystallite-gel model for extrusion and spheronization, *Pharm. Res. 15*, 509-512.

69. Sonaglio, D., Bataille, B., Ortigosa, C., and Jacob, M. (1995) Factorial design in the feasibility of producing Microcel MC 101 pellets by extrusion/spheronization, *Int. J. Pharm. 115*, 53-60.

70. Podczeck, F., Knight, P. E., and Newton, J. M. (2008) The evaluation of modified microcrystalline cellulose for the preparation of pellets with high drug loading by extrusion/spheronization, *Int. J. Pharm. 350*, 145-154.

71. O'connor, R. E., and Schwartz, J. B. (1985) Spheronization II: Drug Release from Drug-Diluent Mixtures, *Drug. Dev. Ind. Pharm. 11*, 1837-1857.

72. O'Connor, R. E., and Schwartz, J. B. (1985) Spheronization II. Drug release from drugdiluent mixtures, *Drug Dev. Ind. Pharm. 11*, 1837-1857.

73. Zimm, K. R., Schwartz, J. B., and O'Connor, R. E. (1996) Drug release from a multiparticulate pellet system, *Pharm. Dev. Technol. 1*, 37-42.

74. Tester, R. F., Karkalas, J., and Qi, X. (2004) Starch—composition, fine structure and architecture, *J. Cereal Sci. 39*, 151-165.

75. Dukić, A., Mens, R., Adriaensens, P., Foreman, P., Gelan, J., Remon, J. P., and Vervaet, C. (2007) Development of starch-based pellets via extrusion/spheronisation, *Eur. J. Pharm. Biopharm. 66*, 83-94.

76. Chiu, C.-W., Henley, M., and Altieri, P. (1994) Process for making amylase resistant starch from high amylose starch, *US Patent*, 5,281,276.

77. Steckel, H., and Mindermann-Nogly, F. (2004) Production of chitosan pellets by extrusion/spheronization, *Eur. J. Pharm. Biopharm. 57*, 107-114.

78. Jess, K., and Steckel, H. (2007) The extrusion and spheronization of chitosan. (cover story), *Pharm. Technol. Eur. 19*, 21-30.

79. Tho, I., Kleinebudde, P., and Sande, S. (2001) Extrusion/spheronization of pectin-based formulations. I. Screening of important factors, *AAPS PharmSciTech 2*, article 26.

80. Tho, I., Sande, S. A., and Kleinebudde, P. (2002) Pectinic acid, a novel excipient for production of pellets by extrusion/spheronisation: preliminary studies, *Eur. J. Pharm. Biopharm 54*, 95-99.

81. Tho, I., Arne Sande, S., and Kleinebudde, P. (2003) Disintegrating pellets from a water-insoluble pectin derivative produced by extrusion/spheronisation, *Eur. J. Pharm. Biopharm. 56*, 371-380.

82. Stillwell, R. L., Marks, M. G., Sferstein, L., Wiseman, D. (1997) Oxidized cellulose: chemistry, processing, and medical application, *Drug Target Deliv. 7*, 291-306.

83. Kumar, V., and Banker, G. S. (1993) Chemically-modified cellulosic polymer, *Drug Dev. Ind. Pharm. 19*, 1-31.

84. Shorygin, P. P., and Khait, E. V. (1937) Nitration of cellulose with nitric acid and nitrogen peroxide, *Zh. Obsch. Khim. 7*, 188-192.

85. Yackel, E. C., and Kenyon, W. O. (1942) The oxidation of cellulose by nitrogen dioxide, *J. Am. Chem. Soc. 64*, 121-127.

86. Wanleg, H. (1956) Process for the preparation a rotation product., *US Patent*, 2,758,112.

87. Painter, T. J. (1977) Preparation and periodate oxidation of C-6-oxycellulose: conformational interpretation of hemiacetal stability, *Carbohydr. Res. 55*, 95-103.

88. Walimbe, A. M., Pandya, B. N., and Lalla, J. K. (1978) Preparation of oxidized cellulose, *BP. Res. Ind. 23*, 162-165.

89. Bertocchi, C., Konowicz, P., Signore, S., Zanetti, F., Flaibani, A., Paoletti, S., and Crescenzi, V. (1995) Synthesis and characterisation of polyglucuronan, *Carbohydr. Polym. 27*, 295-297.

90. Kumar, V., and Yang, T. (2002) HNO_3/H_3PO_4–$NaNO_2$ mediated oxidation of cellulose — preparation and characterization of bioabsorbable oxidized celluloses in high yields and with different levels of oxidation, *Carbohydr. Polym. 48*, 403-412.

91. Syamala Devi, K., Sinha, T.J.M., Vasudevan P. (1986) Biosoluble surgical material from 2,3-dialdehyde cellulose, *Biomaterials 7*, 193-196.

92. (2007) *USP30/NF25 (United States Pharmacopoeia 30/National Formulary 25).* Washington, DC.p1687

93. Asthton, W. H. (1968) Oxidized cellulose product and method for preparing the same, *US Patent*, 3,364,200.

94. Dimitrijevich, S. D., Tatarko, M., Gracy, R. W., Linsky, C. B., and Olsen, C. (1990) Biodegradation of oxidized regenerated cellulose, *Carbohydr. Res. 195*, 247-256.

95. Dimitrijevich, S. D., Tatarko, M., Gracy, R. W., Wise, G. E., Oakford, L. X., Linsky, C. B., and Kamp, L. (1990) In vivo degradation of oxidized, regenerated cellulose, *Carbohydr. Res. 198*, 331-341.

96. Yang, D. (2005) Preparation and characterization of oxidized cellulose esters and their use in drug delivery, The University of Iowa, Iowa City, USA

97. Haney, A. F., and Doty, F. (1992) Comparsion of the peritoneal cells elicited by oxidized regenrated cellulose (Interceed)$^{@}$ and expanded polytetrafluoroethlrnr (Gore-Tex surgical membrance) in a murine model, *Am. J. Obstet. Gynecol. 166*, 1137-1149.

98. Zhu, L., Kumar, V., and Banker, G. S. (2004) Examination of aqueous oxidized cellulose dispersions as a potential drug carrier. I. Preparation and characterization

of oxidized cellulose-phenylpropanolamine complexes, *AAPS PharmSciTech 5*, e69.

99. Dol'berg, E. B., Yasnitskii, B. G., Shuteeva, L. N., and Kovalev, I. P. (1973) Reaction of oxidized cellulose with medicinal compounds. II Reaction of oxidized cellulose with isonicotinic acid hydrazide., *Zh. Prikl. Khim. 46*, 2121-2123.

100. Kumar, V., Kang, J. C., and Hohl, R. J. (2001) Improved dissolution and cytotoxicity of camptothecin incorporated into oxidized-cellulose microspheres prepared by spray drying, *Pharm. Dev. Tech. 6*, 459-467.

101. Florey, K. (1976) *Analytical Profiles of Drug Substances,* Academic Press, New York. pp 283-306

102. *Merck Index, 9th edition*, Merk & Co. Inc., Rahway.pp 4288 & 5858.

103. Singh, U. V., and Udupa, N. (1997) In vitro characterization of methotrexate loaded poly(lactic-co-glycolic) acid microspheres and antitumor efficacy in Sarcoma-180 mice bearing tumor, *Pharm. Acta Helv. 72*, 165-173.

104. Pereira, A. D. F. (2013) Efficacy of methotrexate-loaded poly(ε-caprolactone) implants in ehrlich solid tumor-bearing mice, *Drug Deliv. 20*, 168-179.

105. Singh, U. V., and Nduopa, N. (1997) Preparation, characterization, and antitumor efficacy of biodegradable poly(lactic acid) methotrexate implantable films, *Drug Deliv. 4*, 101-106.

106. Fitzgerald, J. F., and Corrigan, O. I. (1993) Mechanism governing drug release from poly-alpha-hydroxy aliphatic esters., *ACS Sym. Ser. 520*, 311-326.

107. Hopfenberg, H. B. (1976) Controlled release from erodible slabs, cylinders, and spheres. , *Controlled Release Polymeric Formulation*, pp182-194.

108. Fielden, K. E., Newton, J. M., and Rowe, R. C. (1992) The influence of lactose particle size on spheronization of extrudate processed by a ram extruder, *Int. J. Pharm. 81*, 205-224.

109. Lindner, H., and Kleinebudde, P. (1994) Use of powdered cellulose for the production of pellets by extrusion/spheronisation, *J. Pharm. Pharmacol. 46*, 2-7.

110. Fechner, P. M., Wartewig, S., Füting, M., Heilmann, A., Neubert, R. H. H., and Kleinebudde, P. (2003) Comparison of microcrystalline cellulose and powdered cellulose before and after extrusion/spheronization by FT-Raman spectroscopy and ESEM, *AAPS Pharm. Sci. 5* 5-6.

111. El Saleh, F., Jumaa, M., Hassan, I., and Kleinebudde, P. (2000) Influence of cellulose type on the properties of extruded pellets. Part II: production and properties of pellets, *STP Pharm. Sci. 10*, 379-385.

112. Dukic, A., Mens, R., Adriaensens, P., Foreman, P., Gelan, J., Remon, J. P., and Vervaet, C. (2007) Development of starch-based pellets via extrusion/spheronisation, *Eur. J. Pharm. Biopharm. 66*, 83-94.

113. Agrawal, A. M., Howard, M. A., and Neau, S. H. (2004) Extruded and spheronized beads containing no microcrystalline cellulose: influence of formulation and process variables, *Pharm. Dev. Tech. 9*, 197-206.

114. (2007) *USP30/NF25 (United States Pharmacopoeia 30/National Formulary 25)*, Washington, DC. p1091.

115. Thommes, M., and Kleinebudde, P. (2008) The behavior of different carrageenans in pelletization by extrusion/spheronization, *Pharm. Dev. Technol. 13*, 27-35.

116. Thommes, M., and Kleinebudde, P. (2007) Properties of pellets manufactured by wet extrusion/spheronisation process using kappa-carrageenan: Effect of process parameters,, *AAPS PharmSciTech 8*, article 95.

117. Tho, I., Anderssen, E., Dyrstad, K., Kleinebudde, P., and Sande, S. A. (2002) Quantum chemical descriptors in the formulation of pectin pellets produced by extrusion/spheronisation, *Eur. J. Pharm. Sci 16*, 143-149.

118. Tho, I., Arne Sande, S., and Kleinebudde, P. (2005) Cross-linking of amidated low-methoxylated pectin with calcium during extrusion/spheronisation: Effect on particle size and shape, *Chem. Eng. Sci. 60*, 3899-3907.

119. Kumar, V., and Yang, T. (2002) HNO_3/H_3PO_4-$NaNO_2$ mediated oxidation of cellulose -- preparation and characterization of bioabsorbable oxidized celluloses in high yields and with different levels of oxidation, *Carbohydr. Polym. 48*, 403-412.

120. (2007) *USP30/NF25 (United States Pharmacopoeia 30/National Formulary 25)*, Washington, DC.p1687.

121. Yang, T. (2002) Preparation, characterization and pharmaceutical uses of biodegradable oxidized cellulose and its adduct with chitosan, The University of Iowa, Iowa City, USA.

122. Li, T.-Q., Henriksson, U., Klason, T., and Ödberg, L. (1992) Water diffusion in wood pulp cellulose fibers studied by means of the pulsed gradient spin-echo method, *J. Colloid Interface Sci. 154*, 305-315.

123. Nakamura, K., Hatakeyama, T., and Hatakeyama, H. (1983) Relationship between hydrogen bonding and bound water in polyhydroxystyrene derivatives, *Polymer 24*, 871-876.

124. McCrystal, C. B., Ford, J. L., and Rajabi-Siahboomi, A. R. (1997) A study on the interaction of water and cellulose ethers using differential scanning calorimetry, *Thermochim. Acta 294*, 91-98.

125. Hatakeyama, H., and Hatakeyama, T. (1998) Interaction between water and hydrophilic polymers, *Thermochim. Acta 308*, 3-22.

126. Ratto, J., Hatakeyama, T., and Blumstein, R. B. (1995) Differential scanning calorimetry investigation of phase transitions in water/chitosan systems, *Polymer 36*, 2915-2919.

127. Zografi, G., and Kontny, M. (1986) The interactions of water with cellulose- and starch-derived pharmaceutical excipients, *Pharm. Res. 3*, 187-194.

128. Ford, J. L., and Mitchell, K. (1995) Thermal analysis of gels and matrix tablets containing cellulose ethers, *Thermochim Acta 248*, 329-345.

129. Quirijns, E. J., van Boxtel, A. J. B., van Loon, W. K. P., and van Straten, G. (2005) Sorption isotherms, GAB parameters and isosteric heat of sorption, *J. Sci. Food Agr. 85*, 1805-1814.

130. Zografi, G., Kontny, M. J., Yang, A. Y. S., and Brenner, G. S. (1984) Surface area and water vapor sorption of macrocrystalline cellulose, *Int. J. Pharm. 18*, 99-116.

131. Rueda, D. R., Secall, T., and Bayer, R. K. (1999) Differences in the interaction of water with starch and chitosan films as revealed by infrared spectroscopy and differential scanning calorimetry, *Carbohydr. Polym. 40*, 49-56.

132. Tual, C., Espuche, E., Escoubes, M., and Domard, A. (2000) Transport properties of chitosan membranes: Influence of crosslinking, *J. Polym. Sci. Part B: Polym. Phy. 38*, 1521-1529.

133. Namur, J. (2011) Embolization of hepatocellular carcinoma with drug-eluting beads: Doxorubicin tissue concentration and distribution in patient liver explants, *J. Hepatol. 55*, 1332-1338.

134. Dan Dimitrijevich, S., Tatarko, M., Gracy, R. W., Linsky, C. B., and Olsen, C. (1990) Biodegradation of oxidized regenerated cellulose, *Carbohydrate Res. 195*, 247-256.

135. Abaev Iu, K., Kaputskii, V. E., Adarchenko, A. A., and Sobeshchukh, O. P. (1986) Mechanism of the antibacterial action of monocarboxycellulose and other ion-exchange derivatives of cellulose, *Antibiot. Med. Biotekhnol. 31*, 624-628.

136. Tokunaga, Y., Kojima, T., Naruse, T. (1998) Antitumor effect of oxycellulose as a hemostatic during operation, *Cancer Biothe. Radiopharm. 13*, 437-445.

137. Otterlei, M., Espvik, T., Skjak-Braek, G., Smidsrod, O. (1992) Diequatorially bound beta-1,4 polyuronates and use of same of cytokine stimulation., *European Patent*, 506,326.

138. Finn, M. D., Schow, S. R., and Schneiderman, E. D. (1992) Osseous regeneration in the presence of four common hemostatic agents, *J. Oral. Maxillofac. Surg. 50*, 608-612.

139. Pollack, R. P., and Bouwsma, O. (1992) Applications of oxidized regenerated cellulose in periodontal therapy, part I., *Compendium 13*, 888.

140. Dol'berg, E. B., Shuteeva, L. N., Yasnitskii, B. G., Obolentseva, G. V., Khadzhai, Y. I., and Furmanov, Y. A. (1974) Interaction of oxidized cellulose with medicinal compounds. III. Synthesis and biological properties of the reaction product of oxidized cellulose with kanamycin sulfate, *Khim. Farm. Zh. 8*, 23-26.

141. Shuteeva, L. N., Sukhinima, T. V., Yasnitskii, B. G., and Dol'berg, E. B. (1985) Study of the the main characteristics of adsorption some organic compounds on monocarboxy cellulose., *Teor. Prakt. Sorbtsionnykh Protsessov 17*, 30-33.

142. Firsov, A. A., Nazarov, A. D., and Fomina, I. P. (1987) Biodegradable implants containing gentamicin - drug release and pharmacokinetics, *Drug Dev. Ind. Pharm. 13*, 1651-1674.

143. Kaputskii, F. N., Bychkovskii, P. M., Yurkshtovich, T. L., Butrim, S. M., Korolik, E. V., and Buslov, D. K. (1995) Study of photrin sorption by monocarboxycellulose, *Colloid. J. 57*, 42-45.

144. Kosterova, R. I., Yurkshtovich, T. L., Kaputskii, F. N., and Golib, N. V. (1993) Effect of the counterion and solvent composition on sorption of dimetpramide by carboxylated cellulose, *Vestn. Beloruss. Gos. Univ. Ser. 2*, 12-17.

145. Zimatkina, T., Yurkshtovich, T., Zimatkin, S., and Kaputsky, F. (1996) Antitumor activity of hydroxythiamine and methotrexate immobilized on monocarboxycellulose, *Pol. J. Pharmacol. 48*, 163-169.

146. Alinovskaya, V. A., Yurkshtovich, T. L., and Kaputskii, F. N. (1989) Sorption immobilization of proteolytic enzymes on cellulose oxidized with nitrogen (IV) oxide., *Kolloidn. Zh. 51*, 1169-1172.

147. Kumar, V., and Deshpande, G. S. (2001) Noncovalent immobilization of bovine serum albumin on oxidized cellulose, *Artif. Cells Blood Substit. Immobil. Biotechnol. 29*, 203-212.

148. (2007) *USP30/NF25(United States Pharmacopoeia 30/National Formulary 25)*, Washington, DC.p2613.

149. Amyot, F., Jurski, K., Dufaux, J., and Guiffant, G. (2002) An experimental and theoretical study of mass transfer from loaded embolisation microbeads: Possible optimisation, *International Communications in Heat and Mass Transfer 29*, 623-632.

150. Borovac, T., Pelage, J. P., Kasselouri, A., Prognon, P., Guiffant, G., and Laurent, A. (2006) Release of ibuprofen from beads for embolization: in vitro and in vivo studies, *J. Control. Release 115*, 266-274.

151. Guo, J. (2003) Carbopol® Polymers for Pharmaceutical Drug Delivery Applications, *Drug Dev. Deliv. 3*, 2.

152. Neau, S. H., Chow, M. Y., and Durrani, M. J. (1996) Fabrication and characterization of extruded and spheronized beads containing Carbopol® 974P, NF resin, *Int. J. Pharm. 131*, 47-55.

153. Kriwet, B., and Kissel, T. (1996) Interactions between bioadhesive poly(acrylic acid) and calciumions, *Int. J. Pharm. 127*, 135-145.

154. Bommareddy, G. S., Paker-Leggs, S., Saripella, K. K., and Neau, S. H. (2006) Extruded and spheronized beads containing Carbopol® 974P to deliver nonelectrolytes and salts of weakly basic drugs, *Int. J. Pharm. 321*, 62-71.

155. Lu, G., and Jun, H. W. (1998) Diffusion studies of methotrexate in Carbopol and Poloxamer gels, *Int. J. Pharm. 160*, 1-9.

156. Zhou, C., Cui, D., Zhang, Y., Yuan, H., and Fan, T. (2012) Preparation and characterization of ketoprofen-loaded microspheres for embolization, *J. Mater. Sci. Mater. Med. 23*, 409-418.

157. Amyot, F., Boudy, V., Jurski, K., Counord, J. L., Guiffant, G., Dufaux, J., and Chaumeil, J. C. (2002) A new experimental method for the evaluation of the release profiles of drug-loaded microbeads designed for embolisation, *ITBM-RBM 23*, 285-289.

158. Yousefi, G., Foroutan, S. M., Zarghi, A., and Shafaati, A. (2010) Synthesis and characterization of methotrexate polyethylene glycol esters as a drug delivery system, *Chem. Pharm. Bull. 58*, 147-153.

159. Dan Dimitrijevich, S., Tatarko, M., Gracy, R. W., Linsky, C. B., and Olsen, C. (1990) Biodegradation of oxidized regenerated cellulose, *Carbohydr. Res. 195,* 247-256.

160. Heller, J. (1980) Controlled release of biologically active compounds from bioerodible polymers, *Biomaterials 1*, 51-57.